



PhD thesis

Morten Langer Andersen

Surface melt, dynamics and seismicity at Helheim Glacier, East Greenland

Centre for Ice and Climate, Niels Bohr Institute, University of Copenhagen
Copenhagen Global Change Initiative (COGCI)
Geological Survey of Denmark and Greenland (GEUS)



Academic advisor: Professor Dorthe Dahl-Jensen
Co-advisors: Tine B. Larsen, Andreas P. Ahlstrøm
Submitted: 04/10/2010

Acknowledgments

This thesis is the result of work carried out at the Geological Survey of Denmark and Greenland (GEUS), and Center for Ice and Climate, Niels Bohr Institute (NBI), University of Copenhagen. The PhD project was financed by the Copenhagen Global Change Initiative, GEUS and University of Copenhagen. Financial support for the field work was provided through grants from Kommissionen for Videnskabelige Undersøgelser i Grønland (KVUG).

I owe thanks to many people, who have helped me one way or another during the past three years.

First, I would like to thank my supervisors on the project: Tine B. Larsen, Andreas P. Ahlstrøm, both from GEUS, and Dorthe Dahl-Jensen at NBI. I have enjoyed the discussions we have had and you have prioritized my work in your busy schedules, which I have really appreciated.

I would also like to thank the international project group that formed the Helheim Project which is the academic basis for this work: Gordon Hamilton, Leigh Stearns, Pedro Elósegui, Julia de Juan, Lars Stenseng, Abbas Kahn, Jim Davis, René Forsberg, and Göran Ekström. During the many trips to East Greenland we have gotten to know each other quite well. It has been great and inspiring company, and I can truly say it has been a pleasure working with you! A special thanks to Meredith Nettles, Columbia University, for being available at all times for feedback and discussions of big and small issues, and for hosting me in New York in 2009. You have an amazing capability of keeping many balls in the air!

Through the daily work in the glaciology group at GEUS, I have gotten to know many very nice people, who I now consider as much friends as colleagues. I would like to thank them for making it enjoyable to come work every day: Dirk van As, Faezeh Nick, Robert Fausto, Kaarina Weckström, Michele Citterio, Horst Machguth, Signe B. Andersen, Francisca Staines, and Camilla S. Andresen. When I have been much too late with a technical or logistical problem, Søren Nielsen has made it happen anyway, which is very much appreciated. Thanks also to Peter Voss for saving me a lot of very valuable time

by helping with seismological data management, scripts, etc.

Thanks to Marco and Katharina for letting me use their wonderful summerhouse by the west coast during the final intense weeks of writing. I got a lot of work done between the runs at the beach. Also thanks to my family and friends for tolerating my absence – or absent-mindedness – during the project.

And finally, the biggest thanks to my girlfriend Signe for being more patient and understanding than what could reasonably be expected of anyone!

I have learned a lot and it has definitely been an interesting journey so far.

Abstract

Understanding the processes that govern the flow of the large outlet glaciers draining the Greenland Ice Sheet is critical for assessing the impact of climate change on sea-level rise. These processes include calving of icebergs and subsurface melt in the fjords, but drainage of surface runoff to the glacier bed also plays a role. How melt water affects the flow of fast outlet glaciers is poorly understood and is the main aim of the three interdisciplinary studies comprising this thesis. First, the extent of melt-water-induced flow speed variability is investigated. An energy balance model is developed for the surface of Helheim Glacier, East Greenland, in order to estimate runoff from surface melt. Melt variations during the summer seasons are compared to GPS observations of surface velocity. Significant correlations are found, with a 12–36 hours delay of velocity relative to melt. Next, the glacier's sensitivity to variations in melt-water input is quantified and found to decrease approximately exponentially with distance from the calving front. Sensitivity to melt generally increases over the melt season. The time-varying sensitivity is interpreted to result from changes in subglacial hydraulic routing caused by the changing volume of melt-water input. Finally, seismic signals associated with calving and ice rupture are considered. Large seismic events are found at Helheim Glacier to be preceded by long-duration rumblings with a characteristic frequency content. A detection algorithm is developed to automatically detect rumblings recorded at a seismic station located close to the glacier. The analysis shows a seasonal variation in the occurrence of rumblings with a peak in mid-September coinciding with the end of the melt season. Further research into understanding the flow dynamics of the fast outlet glaciers of Greenland is crucial in order to accurately predict the increasing contribution of iceberg-calving to sea-level rise.

Summary

Understanding the behavior of large outlet glaciers draining the Greenland Ice Sheet is critical for assessing the impact of climate change on sea-level rise. The flow of marine-terminating outlet glaciers is partly governed by calving-related processes taking place at the terminus, but is also influenced by the drainage of surface runoff to the glacier bed through moulins, cracks, and other pathways. On alpine glaciers, this has been shown to influence glacier flow speed when the volume of water is sufficient to increase basal fluid pressure and hence basal lubrication. However, the relative importance of these factors is poorly understood and little is known about the influence of surface melting on the large, marine-terminating outlet glaciers that drain the Greenland ice sheet. This thesis is based on three interdisciplinary studies carried out at Helheim Glacier, East Greenland during 2007 and 2008. Techniques employed include geodesy, glaciology, seismology, oceanography, and meteorology. In the first study, the extent of melt-water-induced flow speed variability is investigated. A distributed surface energy balance model (SEB) is developed for Helheim Glacier, East Greenland, to calculate surface melt and thereby estimate runoff. The model is driven by data from an automatic weather station (AWS) operated on the glacier surface during two summer seasons, and calibrated with independent measurements of ablation. Estimated melt variations during the summer seasons are compared to estimates of surface velocity derived from GPS surveys. Near the terminus, significant correlations ($>95\%$ levels) are found, with a 12–36 hours delay of velocity relative to melt. Relative changes in glacier speed due to melt-water input are small, but of similar absolute magnitude to those observed at smaller glaciers and on the ice-sheet margin. The findings suggest that the flow speed of Helheim Glacier is sensitive to changes in runoff. In the second study, the sensitivity of glacier flow speed to changes in surface melt is quantified. The glacier's sensitivity to variations in melt-water input decreases approximately exponentially with distance from the calving front. Sensitivity to melt generally increases as the melt season progresses. The time-varying sensitivity is interpreted to result from changes in subglacial hydraulic routing caused by the changing volume of melt-water input. Finally, in the third study, seismic signals associated with calving and ice rupture are considered. Teleseismically detected glacial earthquakes are found at Helheim Glacier to be preceded by long duration rumblings with a characteristic frequency content distinctively different from both tectonic earthquakes and the background noise. These rumblings have an average duration of 28–29 minutes and contain both high-frequency and low-frequency signals. A frequency-domain-based detection algorithm is developed to automatically detect rumblings recorded at a broad-band station ISO, located ~ 100 km from the glacier. The seismic detector is calibrated with observations of calving from a time-lapse camera near the glacier front. The analysis shows a seasonal variation in the occurrence of rumblings with a peak in mid-September coinciding with the end of the melt season. While these studies represent a new contribution to the understanding of Greenland outlet-glacier flow, further research is crucial in order to accurately predict the increasing contribution of iceberg-calving to sea-level rise.

Sammenfatning

For at kunne belyse klimaforandrings effekt på havniveaustigninger, er det nødvendigt at forstå mekanismerne der kontrollerer flydehastigheden af de store udløbsgletschere, der dræner den grønlandske indlandsis. Flydningen af udløbsgletscherne er til dels påvirket af kælvnings-relaterede processer ved gletscherfronten, men også af smeltevand fra overfladen der dræner til bunden af gletscheren. På alpine gletschere er der demonstreret en stærk påvirkning af flydehastigheden, når det tilførte smeltevandsvolumen er stort nok til forøge vandtrykket ved bunden af gletscheren. Hvordan disse faktorer influerer på flydningen af de store grønlandske udløbsgletschere er ikke velbeskrevet i litteraturen. Denne ph.d.-afhandling er bygget på tre multi-disciplinære studier udført på og omkring Helheim Gletscher i Østgrønland i 2007 og 2008. Der benyttes teknikker fra felterne geodæsi, glaciologi, seismologi, oceanografi og meteorologi. I det første studie undersøges i hvor vid udstrækning flydehastighed varierer som følge af smeltevandspåvirkning. En distribueret energibalancemodell for Helheim Gletscher konstrueres med henblik på at estimere afstrømning som følge af overfladesmeltning. Input-data til modellen er klima-data fra en automatisk vejstation (AWS) opstillet på gletscheren i de to smeltesæsoner. Modellen kalibreres med en uafhængig måling af overfladesænkning. Estimerede variationer i afsmeltning bliver sammenlignet med GPS-baserede observationer af hastighed foretaget på gletscheren. Ved gletscherfronten ses signifikante korrelationer (>95%) mellem afsmeltning og flydehastighed, med en forsinkelse af hastighedssignalet på 12–36 timer. Relativt er de smeltevandsbetingede accelerationer små, men i absolutte værdier sammenlignelige med observationer fra mindre gletschere og isranden. Resultaterne indikerer, at flydehastigheden er sensitiv overfor variationer i afstrømning. I andet studie undersøges sensitiviteten. Det ses, at denne aftager eksponentielt med afstanden fra gletscherfronten og øges henover sæsonen. Dette tolkes som et tegn på forandringer i det subglaciale dræningssystem. I det sidste studie undersøges seismiske signaler forbundet med kælving og sprækkedannelse. Seismisk aktivitet af 28–29 minutters varighed (rumlen), vises i dette studie at være forløbere for teleseismiske detektioner af glacielle jordskælv. Rumle-aktiviteten indeholder både høj- og lavfrekvente signaler, og har spektra der er tydeligt forskellige fra tektoniske jordskælv og baggrundsstøj. En frekvensdomæne-baseret detektionsalgoritme bliver derfor konstrueret og benyttet sammen med data fra den opsatte station ISO, ca. 100 km fra Helheim gletscheren. Detektoren kalibreres med tids-serie fotos af kælvinger fra fronten og det ses at forekomsten af rumlen er tydeligt sæsonbetinget, med det maksimale antal detektioner i det tidlige efterår, begge år. Disse tre studier repræsenterer et bidrag til forståelsen af de store udløbsgletscheres flydedynamik. Yderligere forskning er afgørende for at kunne danne realistiske modeller for massetabets betydning for stigninger i havniveauet.

Contents

1	Objectives	1
2	Background and theory	3
2.1	Terminology	3
2.2	Introduction	4
2.3	Glacier flow by deformation	4
2.4	Glacier hydrology	8
2.5	Surface energy balance models	17
2.6	Glacier seismology	19
3	Greenland – ice sheet and outlet glaciers	21
3.1	The Ice Sheet	21
3.2	Outlet glaciers	23
4	Observations	27
4.1	Automatic Weather Station	27
4.2	GPS	32
4.3	Tide gauge	32
4.4	Time-lapse camera	32
4.5	Seismic station	32

4.6	Data processing	34
5	Conclusions and outlook	39
5.1	Overview of results	39
5.2	Outlook	41
	Bibliography	43
	Manuscripts	53
	Paper I	53
	Paper II	89
	Paper III	112
	Appendices	133
A	Co-author statements, Paper I	135
B	Co-author statements, Paper II	151
C	Co-author statements, Paper III	157

Chapter 1

Objectives

The Greenland Ice Sheet is gaining and losing mass at the same time but in different places and at different rates. Mass-gain happens via precipitation while the mass loss occurs through surface melt, basal melt, dynamic thinning, and solid ice-loss at the termini of outlet glaciers (calving). The sum of these components comprise the total mass-balance of the Greenland Ice Sheet which has become increasingly negative during the last decade, reaching a loss of 267 ± 38 Gt/yr in 2007 (Rignot et al., 2008). An average of the years 2003–2008 is, according to Van den Broeke et al. (2009), 237 ± 20 Gt/yr, which is consistent with other studies. Drainage of the Greenland ice sheet occurs through a number of outlet glaciers flowing from the ice sheet into the ocean. While these are numerous, about 44% of the total ice discharge occurs through just 10 large glaciers around the coast (Rignot and Kanagaratnam, 2006). Measured by mass-flux, the largest of these outlet glaciers are found in West Greenland (Jakobshavn Isbræ) and South East Greenland (Helheim and Kangerdlugssuaq Glaciers). Since 2003, especially the South East Greenland outlet glaciers have accelerated, thinned and retreated significantly (Rignot and Kanagaratnam, 2006; Stearns and Hamilton, 2007; Howat et al., 2008a; Thomas et al., 2009). The ice loss in the form of solid mass comprises approximately half of the negative total mass balance; a fraction that has increased dramatically in the recent decade (Van den Broeke et al., 2009). As a consequence, the contribution to sea level rise from the Greenland Ice Sheet has doubled in the past 7-8 years (e.g., Chen et al., 2006; Velicogna and Wahr, 2006).

The root cause of the observed strong thinning and retreat is likely to be found in changes of the conditions at the terminus of the large outlet glaciers, changing the longitudinal stress field, a change brought about by a feedback effect of increased calving and the bed topography beneath the retreating glacier front (Stearns and Hamilton, 2007; Howat et al., 2008a; Nick et al., 2009). However, the controlling physics of these multiple coupled systems remain poorly understood (Alley et al., 2008).

Mass loss, and gain, from surface melt and precipitation is monitored by remote sensing methods (e.g., Shepherd and Wingham, 2007; Quincey and Luckman, 2009), validated with in-situ measurements by climate stations across the ice sheet (Steffen and Abdalati, 1996; Ahlstrøm et al., 2008), and thus reasonably well constrained. However, current modeling capabilities for predicting changes in flux through the outlet glaciers is much poorer than for the melt component, due to lack of knowledge of the mechanisms underlying the changes observed. In the most recent IPCC report, model estimates of the mass balance of the Greenland Ice Sheet do not take the fact that the dynamic component can change rapidly into consideration, due to too large uncertainties associated with this (Intergovernmental Panel on Climate Change, 2007). IPCC suggests that addressing this issue must have priority, in order to accurately predict future sea level rise.

In a warming climate, it is expected that the volume of ice lost through calving and thinning at the margins will continue to increase. An understanding of the mechanisms governing these processes is therefore crucial in order to construct realistic models of future scenarios. Progress in several major areas of glaciology is required to further understand the flow behavior of the large Greenland outlet glaciers.

The primary aims of the investigations carried out in this thesis are to:

- *Quantify the amount of runoff generated by surface melt at a fast-flowing outlet glacier during the melt season.*

To achieve this, an algorithm for estimating the energy budget of the surface (a Surface Energy Balance Model) is developed. The model is driven by meteorological data collected on the glacier surface over the course of two melt seasons.

- *Analyze the influence of variations in melt on glacier dynamics*

The estimated melt pattern and variability is analyzed together with position records from a broad Global Positioning System (GPS) network deployed on the glacier surface during the two study years (2007 and 2008).

- *Analyze the seasonal calving pattern*

Using seismic data recorded at a settlement close to the study area, a detection algorithm is developed to automatically pick seismic signals associated with calving events.

The investigations are undertaken using Helheim Glacier, East Greenland, as field location. Although the work is done at Helheim Glacier, the results presented in this thesis are expected to apply to fast outlet glaciers in Greenland in general.

Chapter 2

Background and theory

This chapter will provide an introduction to the theoretical foundation of the thesis. First, terminology and assumptions will be presented. Then, the fundamentals of glacier flow and glacial hydrology will be introduced. After this, a review of the literature regarding the current state of investigations of melt-driven flow acceleration in Greenland will follow. Theory supporting the surface energy balance model developed will then be reviewed. Finally, the subject of glacial seismology will be discussed in the context of the contributions to this field in the thesis.

2.1 Terminology

Various classification systems of glaciers have been suggested in the past and are in use today. In the following text, *alpine / mountain / valley* glacier (term used interchangeably) is taken to mean a glacier not connected to an ice sheet. The term *marine-terminating / tide-water* glacier (term used interchangeably) is used when a glacier terminates in the ocean, regardless of type. The term *outlet glacier* is used when describing the large, tidewater glaciers in Greenland, draining the ice sheet. When describing the temperature distribution through glaciers, the terms *polar* (or *cold*, meaning sub-freezing temperatures throughout the ice column), *subpolar* (or *polythermal*, meaning temperatures at the pressure melting point in some, but not all of the ice column), or *temperate* (ice is at the pressure melting point throughout) are used. In the literature, the designation *ice stream* is sometimes used in the meaning of an outlet glacier, and sometimes as describing an area of an ice sheet flowing significantly faster than the surrounding ice. Due to this ambiguity, ice stream will not be used in this text.

2.2 Introduction

Approximately 50% of Greenland's negative mass budget arises from ice loss in the form of solid mass drained to the oceans through the outlet glaciers (Van den Broeke et al., 2009). While there are numerous large outlet glaciers draining the Greenland Ice Sheet (e.g., Rignot and Kanagaratnam, 2006; Joughin et al., 2010), a large part of the mass loss occurs at a few, very fast-flowing (up to 12 km/year, Joughin et al., 2008a), marine-terminating glaciers, the largest of which are Jakobshavn Isbræ in West Greenland, and Helheim and Kangerdlugssuaq Glaciers on the east coast (Figure 2.1). The combined discharge from these three glaciers comprise ~22% of the total discharge of the Greenland Ice Sheet (Rignot and Kanagaratnam, 2006).

Literature examining the large Greenland outlet glaciers is limited, making it necessary to, to a large extent, make use of the large body of existing literature on alpine glaciers, which are well studied. The summary of glacial hydrology in this chapter is primarily based on this material, of which Fountain and Walder (1998) presented a thorough review. While alpine glaciers can be large and marine-terminating (e.g., Columbia Glacier, Alaska) the thermal regime may be different from the fast Greenland outlet glaciers mentioned above, in that these are expected to be polythermal (Meier and Post, 1987). This was confirmed in the case of Jakobshavn Isbræ in a large, multi-purpose study by Iken et al. (1993). There, ice temperatures down to -22.1 °C were measured, but it was concluded that near the bed, the ice was temperate. With regard to morphology, the outlet glaciers share many properties with alpine glaciers, although typically larger. Thus, analogues to alpine and temperate tidewater glaciers can reasonably be invoked. In cases of relevant differences, these will be discussed specifically.

2.3 Glacier flow by deformation

Glacier flow is a combination of three velocity components contributing to the speed measurable on the surface: plastic deformation of the ice body, sliding at the bed, and deformation of the bed in cases where the glacier rests on a deformable bed (e.g., a soft layer of sediment). Since the main objective of this thesis is how surface melt affects sliding velocities, flow by internal and bed deformation will only be briefly discussed with a presentation of the fundamental equations. This section primarily follows the analyses presented in Paterson (1994).

At the bed of a parallel-sided block of ice of thickness h , resting on an inclined bed with slope α , the basal shear stress τ_b is given by:

$$\tau_b = \rho_i g h \sin \alpha \quad (2.1)$$

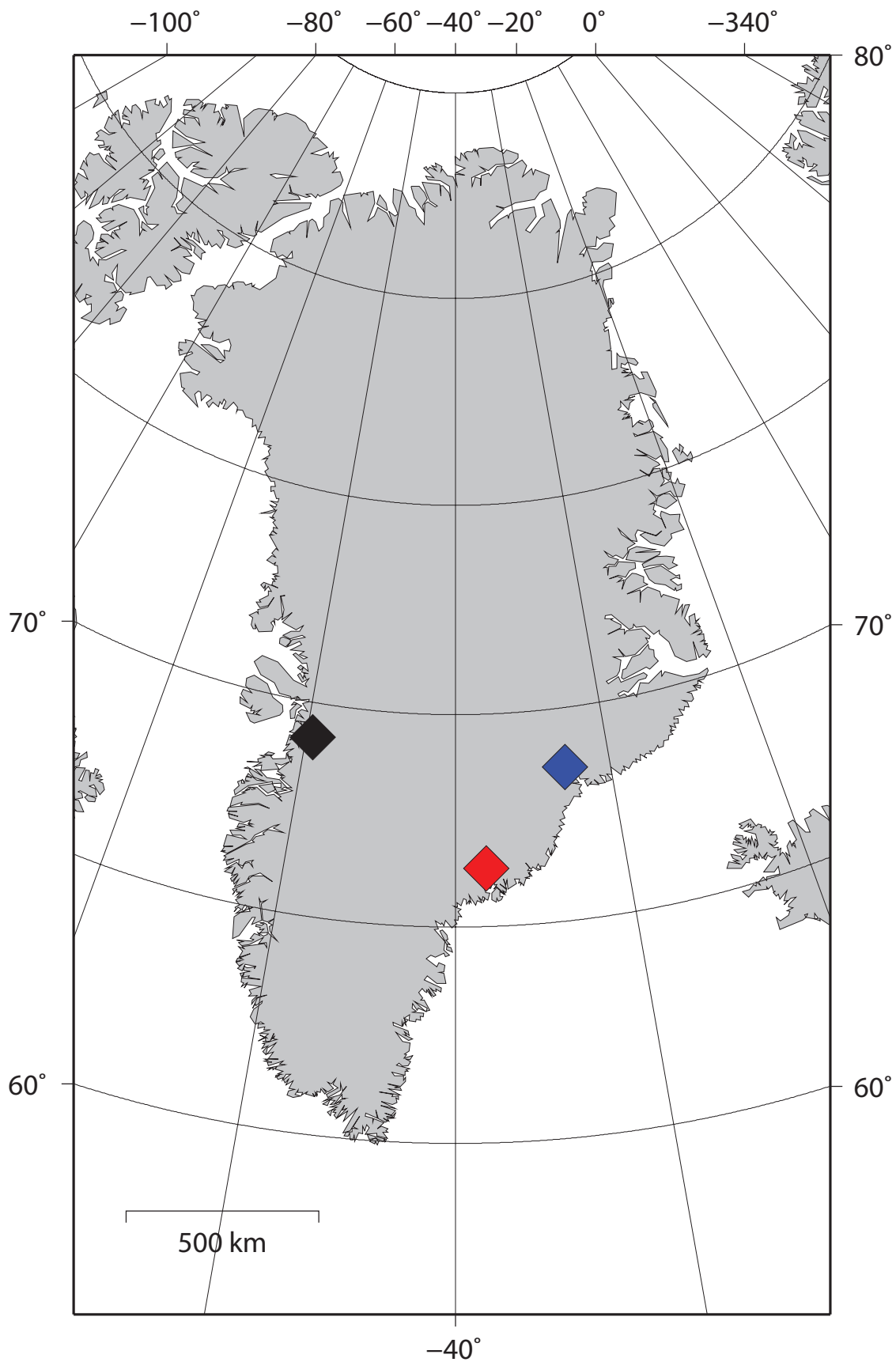


Figure 2.1: Map of Greenland with Jakobshavn (black), Helheim (red), and Kangerdlugssuaq (blue) glaciers marked.

where ρ_i is the density of ice and g is the gravitational acceleration. The basal shear stress, τ_b , is equal to the driving stress in a balanced system. The implication for small surface slopes is a direct proportionality between surface slope α and driving stress, in that $\sin \alpha \cong \alpha$ for small values of α , i.e., $\tau_b = \rho_i g h \alpha$. Similarly, the stress at height $(z - h)$ in the block can be described as:

$$\tau_{xz} = \rho_i g (h - z) \sin \alpha \quad (2.2)$$

when the coordinate system is oriented so that the x -axis is along-flow, parallel to the bed, the y -axis is transverse to the flow, parallel to the bed, and z -axis is perpendicular to the bed.

Ice deforms under its own weight (i.e., it flows) and in the context of flow, it is considered to have the rheological properties of a mixture of a Newtonian and a perfectly plastic material. That is, when stress is applied, it first deforms elastically and then, if the stress is continuously applied, creep (permanent strain) occurs (Paterson, 1994). The rate of deformation, strain rate $\dot{\epsilon}$, is an important quantity when evaluating flow of ice. Of special interest is typically the along-flow (or longitudinal) strain rate $\dot{\epsilon}_{xz}$ which, at the surface, readily is observed using surveying techniques. Commonly referred to as Glen's flow law, the fundamental relationship between applied stress and the corresponding shear strain rate of the ice is:

$$\dot{\epsilon}_{xz} = A \tau_{xz}^n \quad (2.3)$$

where $\dot{\epsilon}_{xz}$ is the strain rate in the xz -plane (along-flow), τ_{xz} is the shear stress in the xz -plane (Eq. 2.2), A is the flow law parameter which has different values depending on ice temperature, crystal orientation, impurity content, etc. (Table 5.1, Paterson, 1994), and n is the flow law exponent, typically set to ~ 3 .

The shear strain rate can also be approximated as $\dot{\epsilon}_{xz} = 1/2(du/dz + dw/dx)$ where u is the flow speed in direction x and w is the flow speed in direction z . Assuming simple shear, parallel to the bed (laminar flow), dw/dx is zero and thus $\dot{\epsilon}_{xz} = 1/2(du/dz)$. By integration of $1/2(du/dz) = A \tau_{xz}^n$ (Eq. 2.3) with τ_{xz} inserted from Eq. 2.2, the along-flow velocity, u , as a function of height, z , in a parallel-sided slab of ice can be described as (Paterson, 1994)

$$u(z) = -\frac{2A}{n+1} (\rho_i g \sin \alpha)^n [(h-z)^{n+1} + h^{n+1}] \quad (2.4)$$

A schematic of the profile is shown in Figure 2.2 (Basal sliding is ignored in this context, but will be discussed in section 2.4.4).

The longitudinal strain rate $\dot{\epsilon}_{xx}$ is in the common notation positive for extensive deformation while negative strain rates signify compressional deformation. The down stream trunk of a valley glacier is typically exposed to positive longitudinal strain rates, indicating extension towards the terminus. This can be realized by considering the continuity

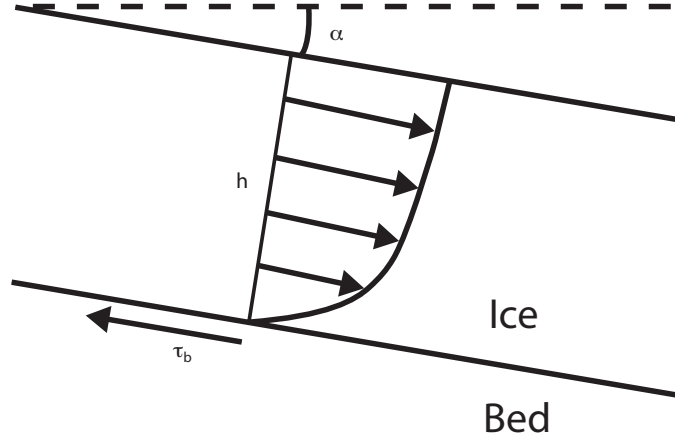


Figure 2.2: Schematic of along-flow section showing the velocity profile of internal deformation by laminar flow.

equation, describing the change of density of a control volume per unit time:

$$-\frac{\partial \rho}{\partial t} = \frac{\partial(\rho u)}{\partial x} + \frac{\partial(\rho v)}{\partial y} + \frac{\partial(\rho w)}{\partial z} = \frac{\partial q_x}{\partial x} + \frac{\partial q_y}{\partial y} + \frac{\partial q_z}{\partial z} \quad (2.5)$$

where ρ is density, t is the time, u , v , w are the flow velocities, and q_x , q_y , q_z are the mass fluxes through the sides of the control volume in directions x , y and z . In this context ice is considered incompressible, why the density change over time is zero. The equation therefore simplifies to:

$$\frac{\partial u}{\partial x} + \frac{\partial v}{\partial y} + \frac{\partial w}{\partial z} = 0 \quad (2.6)$$

The continuity equation can be applied to a vertical column of ice of thickness h . Mass change of the column per unit time must then be equal to the changes in mass by accumulation/ablation (b), changes in mass at the bed (b') and differences in mass flowing in and out through the sides of the column (q_x and q_y):

$$\frac{\partial h}{\partial t} = b + b' - \frac{\partial q_x}{\partial x} - \frac{\partial q_y}{\partial y} \quad (2.7)$$

Thus, the rate of change in thickness equals the sum of the surface and bed mass fluxes and the changes in fluxes flowing in/out from the column in along-flow direction x and transverse direction y . The density is still assumed constant, which is why the fluxes q_x and q_y reduce to $\int_B^S u dz$ and $\int_B^S v dz$, respectively, where S is the surface height and B is the bed height.

Introducing \bar{u} and \bar{v} as values for flow velocity averaged over the ice thickness in directions x and y , the fluxes q_x and q_y are:

$$q_x = h\bar{u} \quad (2.8)$$

$$q_y = h\bar{v} \quad (2.9)$$

which by differentiation leads to:

$$\frac{\partial q_x}{\partial x} = \frac{\partial(h\bar{u})}{\partial x} = \bar{u} \frac{\partial h}{\partial x} + h \frac{\partial \bar{u}}{\partial x} \quad (2.10)$$

$$\frac{\partial q_y}{\partial y} = \frac{\partial(h\bar{v})}{\partial y} = \bar{v} \frac{\partial h}{\partial y} + h \frac{\partial \bar{v}}{\partial y} \quad (2.11)$$

By inserting these differentiated fluxes in Eq. 2.7, and assuming steady state ($\partial h/\partial t = 0$) and no transverse flow ($\bar{v} = 0$), it can be realized that the longitudinal strain rate, $\partial \bar{u}/\partial x$, is dependent on accumulation/ablation, ice thinning, and the constriction/extension of the flow path, e.g., the ice flowing into a valley or trough (Paterson, 1994):

$$h \left(\frac{\partial \bar{u}}{\partial x} \right) = b + b' - \bar{u} \left(\frac{\partial h}{\partial x} \right) - h \left(\frac{\partial \bar{v}}{\partial y} \right) \quad (2.12)$$

In the ablation zone ($b < 0$) of a fast flowing glacier (\bar{u} high) experiencing, e.g., dynamic thinning ($\partial h/\partial x < 0$), and flowing into a narrowing channel ($\partial \bar{v}/\partial y < 0$) these terms all contribute to a positive strain rate. b' is typically negligible compared to the other terms. This analytical conclusion is relevant since it supports what is measured in the field (see discussion of observed strain rates in Paper II in Appendix B).

2.4 Glacier hydrology

The various elements of glacial hydrology have been studied extensively through the last four to five decades. In this context, the term covers three systems: surface, englacial and basal hydrology. A review of all three elements is given by Fountain and Walder (1998) and this will be the foundation for the following presentation.

Much of the theory of englacial and subglacial drainage (see below) is developed for steady state conditions (e.g., $dv/dt = 0$ where v is the flow speed of water). These may not be fulfilled during times of high melt output in the melt season which can lead to the subglacial system undergoing changes in configuration. However, a full treatment of subglacial hydrology in non-steady conditions will be outside the scope of this text.

2.4.1 Surface hydrology

The surface represents the top of the system and supplies water to the englacial hydraulic system. Surface water is primarily produced by surface melt or precipitation in the form of rain water.

The main across-glacier difference in supraglacial hydrology is the presence of a firn layer in the accumulation zone. This layer modulates the flow off the surface and thus

influences the temporal pattern of the water supply to the ice body below. In a temperate glacier, the bottom part of the firn layer above the ice-firn interface in the accumulation zone can be water saturated. From here, the water flows down stream until it reaches entrances into the englacial system, e.g., crevasses. The saturated firn layer has a hydraulic conductivity, and thus acts as a reservoir, not unlike a groundwater aquifer, delaying the delivery of water to the englacial system. The hydraulic conductivity of firn has been shown to be approximately $1\text{--}5\cdot 10^{-5}$ m/s (e.g., Fountain, 1989). With its ability to change storage capacity it also smoothes out diurnal variations (Fountain and Walder, 1998). Considerable amounts of water can be stored in the firn layer. For some alpine glaciers studied, up to 44% of the total seasonal water storage was determined to be held in the firn layer in the accumulation zone (Schneider, 2000). Water flow through this layer is slow compared to the drainage seen in the ablation zone; Fountain and Walder (1998) reported transit times of $\sim 10\text{--}160$ hrs for surface water to percolate to the saturated zone and from there reach an open drainage channel by flow through this zone. Complications arise when considering polar glaciers and ice sheets. Refreezing/retention of melt water in these environments can be significant, and presents major challenges in the understanding and modeling of these processes (Bøggild et al., 2005; Bøggild, 2007).

In the ablation zone, a seasonal snowpack may exist which can cause a delay in the water delivery, similar to that of the firn layer in the accumulation zone. However, this effect vanishes in the spring when the snow melts, exposing the bare ice surface. On the bare ice, water flows freely in melt water streams gaining rapid access to moulins and crevasses, i.e., pathways to the englacial hydraulic system.

Transient storage of water can occur on the surface in form of supra-glacial melt water lakes. These can drain rapidly when an ice dam breaks near the bottom and a connection to the englacial drainage system is established (e.g., Boon and Sharp, 2003). In case there are no established conduits beneath the lake, the water can expand cracks by pressure ("hydrofracturing", e.g., Van der Veen, 2007; Krawczynski et al., 2009), and thereby drain englacially (e.g., Das et al., 2008). Melt water lakes tend to form in the same locations in consecutive melt seasons (Echelmeyer et al., 1991; Luthje et al., 2006; Sneed and Hamilton, 2007; Georgiou et al., 2009), likely influenced by topography.

2.4.2 Englacial hydraulic system

The englacial hydraulic system is the system of pathways transporting water from the surface to the bed of the glacier. While still not completely understood, and likely to have significant variation between glaciers, theories have been developed which have been supported by field studies.

Water enters the ice-body through moulines (an opening in the ice developed from a crevasse now connected to the englacial drainage system) and crevasses that may or may not be hydraulically connected to each other. Classical theories of the drainage system developed by Shreve (1972) prescribe that it is constructed from a three-dimensional network of channels, plunging steeply into the ice body from the surface, joining in progressively fewer and larger channels with depth, i.e., an “arborescent” network (Figure 2.3). The conduits are formed following the steepest water pressure potential gradient. An analytical expression for the water pressure potential, ϕ , the gradient of which determines the direction of the flow within the glacier body is (Paterson, 1994):

$$\phi = \phi_0 + p_w + \rho_w g z \quad (2.13)$$

where ϕ_0 is a constant, p_w is the water pressure, ρ_w is the density of water, z is the elevation in the ice, and g is the gravitational acceleration. Assuming equilibrium between water and ice pressure, the water pressure is then given by:

$$p_w = \rho_i g (z_s - z) \quad (2.14)$$

where ρ_i is the density of ice, and z_s is the elevation of the surface. Substituting Eq. 2.14 in Eq. 2.13 leads to the expression for the water pressure potential:

$$\phi = \phi_0 + \rho_i g z_s + g(\rho_w - \rho_i)z \quad (2.15)$$

The direction of the englacial conduit will be perpendicular to the zero-gradient surfaces of ϕ , which by differentiation are seen to have the shape (in 2-D):

$$\frac{dz}{dx} = \left(\frac{-\rho_i}{\rho_w - \rho_i} \right) \frac{dz_s}{dx} \quad (2.16)$$

that is, a slope of ~ 11 times the surface slope and of opposite direction as illustrated in Figure 2.3. The size of these conduits is determined primarily by the flow of water through them averaged over a weekly timescale. It is only smaller channels that follow the steepest gradient – moulines tend to retain their orientation largely based on the orientation of the crevasse from which it develops (Paterson, 1994)

In addition to these steeply plunging channels, the englacial drainage system is believed to consist of smaller, near-horizontal channels connecting the larger ones (Fountain and Walder, 1998). Field studies by Harper and Humphrey (1995) using borehole cameras confirmed the existence of these. Moreover, in a similar, recent study by Fountain et al. (2005) at Storglaciären, Sweden, it was shown that *cracks* were prevalent as internal drainage features, rather than tubular channels. As for these smaller-diameter, near-horizontal englacial conduits, Fountain and Walder (1998) suggested that they are formed as water flows along the bottom of a crevasse, cutting deeper into the bottom of the crevasse. At a point in time, ice deformation (creep closing) will then close off the roof of the channel, isolating it from the crevasse.

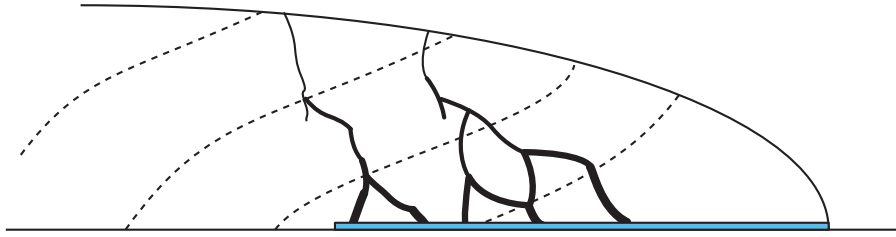


Figure 2.3: Schematic illustration of the englacial drainage system as described by Shreve (1972) with a subglacial channel at the bed. Dashed lines indicate the zero-gradient surfaces in the ice body. Modified from Paterson (1994).

2.4.3 Basal hydraulic system

When the water has passed through the englacial system it reaches the subglacial drainage system. Two key types of subglacial drainage can now be introduced: “channelized” (fast drainage) or “distributed” (slow drainage). Which type of drainage is active at which time, depends on several factors, the most important of which are the supply of water to the bed and the flow velocity of the ice. Fundamentally, the difference between the two is how the channels draining water from the base are arranged. In the channelized system the water is transported quickly through few, large tunnels at low pressure. In the distributed drainage system, many smaller channels drain the water slowly over a larger area of the bed, typically through cavities formed when the ice separates from the bed when sliding over bumps (Figure 2.4). Which configuration that is effective in a given case can have a profound effect on the glacier’s sliding behavior (Section 2.4.4).

In general, the water pressure potential gradient determining the direction of flow in the subglacial drainage system is primarily dependent on the surface slope, as can be realized from the following equation (Paterson, 1994):

$$\nabla\phi = \rho_i g (\nabla z_s + 0.09 \nabla z_b) \quad (2.17)$$

where ∇z_s is the gradient of the surface and ∇z_b is the gradient of the bed. The implication of this is, that the direction of water flow at the bed will be dominated by surface slope, rather than bed slope. This, in turn, means that in an overdeepening in the bed, basal water can be forced uphill if the surface slope is sufficiently steep.

2.4.3.1 Channelized flow

The channelized flow was described by Röthlisberger (1972). In his analysis he derived the fundamental differential equations that govern steady flow of water in an ice tunnel. Central in the analysis is the assumption of equilibrium between the closing rate of a channel due to creep and the expansion of the channel caused by the heat transported by

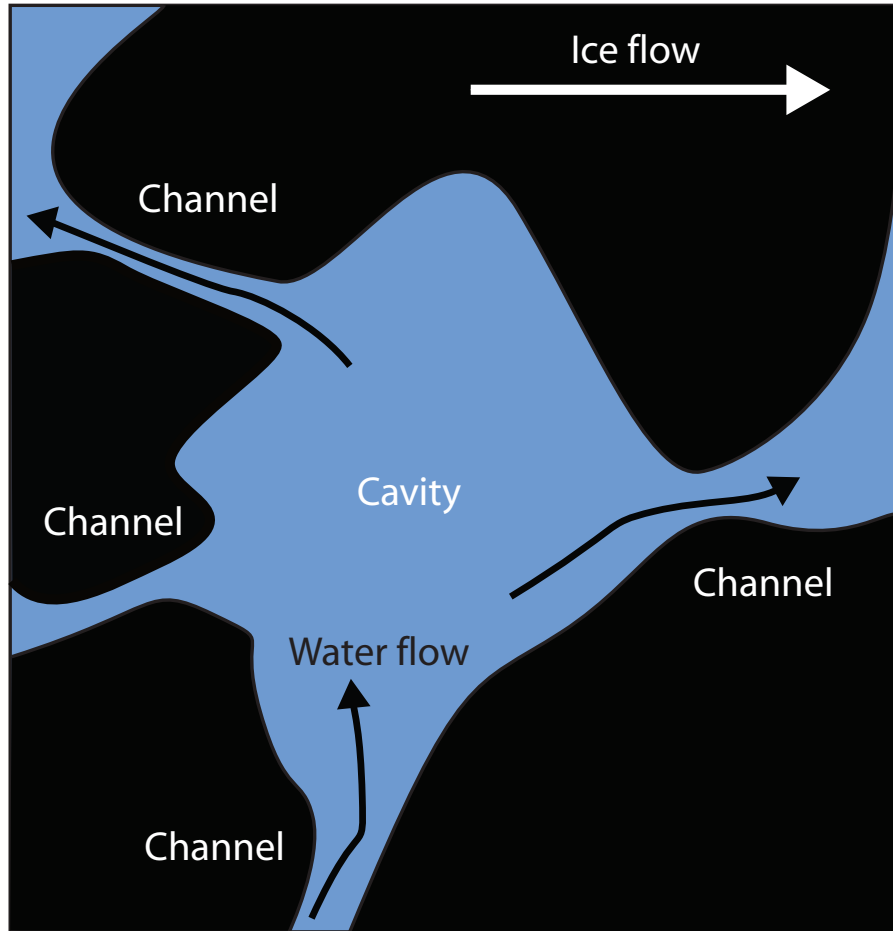


Figure 2.4: Schematic of a subglacial cavity with water flowing to and from the cavity via narrow channels. Black areas illustrate areas with contact between ice and bed. After Paterson (1994).

the flowing water. The channels are termed “Röthlisberger-channels” (or “R-channels”) and, using the notation in Fountain and Walder (1998), the central differential equation describing the pressure gradient in such a channel is:

$$\left(\frac{d\phi}{ds}\right)^{p+1} - \alpha \left(\frac{d\phi}{ds}\right)^p \frac{dp_w}{ds} = \beta Q^{-q} p_e^n \quad (2.18)$$

where $d\phi/ds$ is the change in pressure potential ϕ over distance ds ; α , β , p , q , and n are constants. ρ_w is the density of water, Q is the discharge through the channel, and p_e is the effective pressure (which equals the difference between water pressure and overburden pressure).

In the simple case of a horizontal channel, there is no gravitational component to the pressure potential and Eq. 2.13 simplifies to:

$$\phi = p_w \quad (2.19)$$

Eq. 2.18 thus becomes (Fountain and Walder, 1998):

$$\frac{dp_w}{dx} = \left(\frac{\beta}{1-\alpha} \right)^{1/(p+1)} Q^{-q/(1+p)} p_e^{n/(1+p)} \quad (2.20)$$

What can be realized from this expression is that there is an inverse proportionality between discharge in the channel, Q , and pressure gradient. That is, the water pressure in a channel carrying high discharge will be low. Thus, channels with high discharge will grow on the expense of smaller channels due to the lower pressure in the high-discharge channel (Röthlisberger, 1972). Fast flow in what was inferred to be a channelized drainage system on Variegated Glacier, Alaska, has been demonstrated with dye-tracer experiments by Kamb et al. (1985).

2.4.3.2 Distributed flow

The other main form of subglacial drainage that will be described here is distributed drainage. The slow, distributed drainage system consists of cavities forming when the glacier slides over bumps, separating the sole of the glacier from the bedrock (Walder, 1986; Kamb, 1987). The cavities are connected by narrow passageways that control the flow of water between the cavities (Figure 2.4). The passageways can be channels carved into the bed (Nye-channels) or R-channels as described above, or a combination of the two (Paterson, 1994). The network is distributed over a large area and is non-arborescent. With this type of drainage, the water has a much longer travel path and injected tracers are expected to show up later and more dispersed than in an R-channel configuration. This is also consistent with observations from Variegated Glacier, Alaska, by Kamb et al. (1985), who observed flow speeds (by proxy of tracer concentrations) of 0.7 m/s and 0.02 m/s, in what was expected to be a channelized and a distributed system, respectively. Steady state flow in this type of linked-cavity system was analyzed theoretically by Walder (1986) and Kamb (1987). It was there demonstrated that sliding exerts a stronger control over cavity formation and sustainability than melt. The equation describing the discharge flux, Q , in a linked cavity system is (in the notation from Fountain and Walder, 1998):

$$Q \sim u_b^m \left(\frac{d\phi}{ds} \right)^{(1/2)} p_e^{-3} \quad (2.21)$$

where u_b is the sliding speed of the glacier, and m is a constant with the value 0.5-1. It is clear from Eq. 2.21 that the inverse relationship between pressure and discharge seen with the R-channels does not apply to the cavities. Therefore, water in a linked-cavity system will not tend to collect in few, large streams.

When discussing slow drainage, another element must also be considered, namely the softness of the bed. In the analyses of cavity formation and evolution by Walder (1986)

and Kamb (1987) a hard bed is assumed. However, in a layer of sediment, a Darcian flow can occur which will discharge melt water. Subglacial sediments have been shown theoretically not to be able to transfer significant amounts of water compared to the discharge flux of a melt season (e.g., Fountain and Walder, 1998). Thus, beneath a soft-bedded glacier which is exposed to water fluxes of the magnitude corresponding to surface melt, water flows primarily between the top of the sediment layer and the ice. This adds some complexity: in channels in the top of the sediment layer, the water melts the roof and also erodes the sediment walls of the channel. An opposing effect to this is the creep closure of the ice and of the sediment. The possible configurations of a drainage system in a soft bedded setting was analyzed by Walder and Fowler (1994). They concluded that a soft bedded glacier could be drained with two types of drainage: a channelized system with R-channels (as described above) or a wide-spread system of broad, shallow channels (termed “canals”). They describe the flux in the latter case as (notation from Paterson, 1994):

$$Q = B(\sin \alpha)^2 h^3 (P - p_c)^{-n} \quad (2.22)$$

where B is a constant depending on the properties of the ice, P is the overburden pressure, α is the surface slope, h is the depth of the canal, p_c is the water pressure in the canal, and n is a flow parameter (typically ~ 3). Again, as in the case of the linked-cavity system, it is an important point that a high water flux corresponds to a high water pressure, p_c . That is, there is no tendency for the high-flux canals to attract discharge from nearby lower-pressure ones. The pressure gradient in the canal is related to the surface slope as discussed above (see Eq. 2.17).

Of the three types of drainage described above (channelized or distributed in linked-cavities or canals) it is reasonable to believe that a glacier is not completely drained by just one, but rather a combination of the three, possibly with one dominating depending on the supply of melt water from the surface or the time of year.

2.4.4 Seasonal evolution and the effect on sliding

The subglacial drainage system undergoes a change over the year. During winter, creep closes off larger R-channels, leaving a linked-cavity system upheld by the ongoing sliding. The sudden occurrence of large volumes of melt water when the snow has melted in the ablation zone enlarges the constrictions between the cavities (Figure 2.4) and if the rate of increase is high, unstable cavitation can ensue (Iken et al., 1983; Kamb, 1987; Bingham et al., 2003), and a channelized drainage system may form. The higher flux and the channelized configuration causes the mean pressure to drop (Eq. 2.18). This change from distributed to channelized drainage may not be the case for the entire bed – local

changes in drainage modes have been observed (e.g., Mair et al., 2002). The efficient R-channel dominated drainage system can endure for the remains of the melt season.

However, in addition to the seasonally-dependent increase of melt water flux in the spring, other sudden, large influxes of melt water following a supra- or englacial lake drainage, a period of intense melt, or strong rain fall can cause the system to switch between the two types of drainage systems in the same manner (e.g., Kamb et al., 1985; Iken and Bindschadler, 1986; Björnsson, 1998). Walder (1986) discussed the theoretical implications of very low effective pressure, i.e., water pressure close to the overburden pressure, causing unstable cavity growth when the cavity closing rate becomes smaller than the opening rate. In Walder (1986), a number of scenarios of drainage system development in the case of unstable cavity growth were discussed. Indications of the temporal evolution of the drainage system over the season have been observed and supported by dye-tracer experiments by several workers, e.g., Bingham et al. (2003) and Mair et al. (2002).

It has been established by many authors that the configuration and evolution of the subglacial drainage system over the season is intimately connected with sliding speed (e.g., Iken et al., 1983; Kamb et al., 1985; Iken and Bindschadler, 1986; Walters and Dunlap, 1987; Anderson et al., 2004; Howat et al., 2008b). When considering the case of no influence of melt water (i.e., sliding of the parts of the bed not covered by channels or cavities carrying melt water) it was demonstrated by Weertman (1957) that sliding occurs by regelation. While this has been established, it primarily applies to the case of channelized drainage, in that large parts of the sole is in contact with the bed in this configuration. When melt water is present between the ice and the bed, either as a sheet thicker than in regelation processes, or in cavities, “basal lubrication” becomes relevant. The mechanism is that increasing flow of water in the subglacial drainage system increases the basal water pressure (thus decreasing the effective pressure) at the bed, which causes the sole of the glacier to separate from the bed. The reduction in contact area between the ice and the bed with increasing cavity area, causes less drag, which in turn increases sliding velocity (Lliboutry, 1968). The speed-up of the surface as a result of this can occur on short timescales (e.g., Iken and Bindschadler, 1986; Jansson, 1995; Anderson et al., 2004) and on widely different thicknesses of ice, from an ice sheet (Das et al., 2008) to smaller, thinner alpine glaciers (Bartholomew et al., 2008). The concept of bed separation by low effective pressure (“hydraulic jacking”) has become an established explanation when describing uplift and rapid motion of glaciers and ice sheets as a consequence of a pressurized drainage system (e.g., Iken and Bindschadler, 1986; Warburton and Fenn, 1994; Bartholomew et al., 2010).

Following Iken (1981), Paterson (1994) presented an analytical examination of a glacier sliding over an idealized, model bed (the “tilted staircase”). Iken (1981) discussed the

effects of low effective pressures and introduced the concept of a separation pressure p_s , i.e., the pressure at which cavitation would begin. The analysis provided two main conclusions; one being that bed separation depends on the effective pressure, not the water pressure. The other conclusion drawn from Iken (1981) is that sliding velocity depends on the state of growth of the cavities. When the growth rate is highest, sliding velocity is also highest.

The considerations regarding low effective pressure are relevant, in that the linked-cavity configuration inherently have much higher water pressure than the channelized system (Kamb, 1987) and therefore lower effective pressure in general.

Empirical expressions of the relationship between basal pressure and sliding velocity on a smooth, undulating bed were reviewed in Paterson (1994). There, the sliding velocity u as a function of effective pressure N (overburden pressure minus water pressure) is given as:

$$u = k\tau^p N^{-q} \quad (2.23)$$

where p and q are positive integers with values 1-3 and 1, respectively (Budd et al., 1979); k is a constant and τ is the basal shear stress. Eq. 2.23 yields very high sliding velocities in case of, e.g., an outlet glacier close to flotation (low effective pressure and high basal shear stress). For glaciers terminating in water (tidewater or lakes), the effective pressure N can be calculated as:

$$N = \rho_i g h' \quad (2.24)$$

where ρ_i is the density of ice, g is the gravitational acceleration, and h' is the height above buoyancy.

Experimental studies of the mechanics of the link between water flow at the bed and surface acceleration have been conducted by several authors, and typically fall into two groups: studies indicating that subglacial water *storage* or studies indicating that subglacial water *pressure* is the controlling parameter. At Columbia Glacier, Alaska, Meier et al. (1994) and Kamb et al. (1994) found that increased melt water input correlated well with changes in water storage and less so with measurements of subglacial water pressure. This is consistent with the results of Bartholomaeus et al. (2008) (Kennicott Glacier, Alaska) and Vieli et al. (2004) (Hansbreen, Svalbard). Conversely, Iken et al. (1983) measured a significant uplift (0.4 m) at Unteraargletscher, Switzerland, and found that the rate of uplift correlated well with increases in horizontal velocity at the beginning of the melt season, suggesting that pressure, rather than storage, was the primary parameter controlling changes in sliding velocity. Iken and Bindshadler (1986) also found a strong correlation between pressure variations and variations in velocity, suggesting that effective pressure is the controlling parameter. Support for this was found by Fudge et al. (2009) on Bench Glacier, Alaska. However, those workers also encountered ambiguities,

in that variations in sliding and pressure were not always consistently linked, indicating a more complex relationship between basal pressure and sliding.

2.5 Surface energy balance models

Surface ablation can be estimated using the established correlation between times of above-zero mean air-temperatures and melt (e.g., Reeh, 1991; Braithwaite, 1995). This method requires little input data and is therefore useful when modeling ablation from large areas or at long time scales. In Hanna et al. (2005), this method is applied to estimate the runoff of the Greenland ice sheet at 5×5 km resolution.

Another approach is based on estimates of the energy-fluxes to and from the surface and the balance of these; the surface energy balance (SEB) model. A review of this method is given in Hock (2005). SEB-type models require more observational data which poses difficulties when considering, e.g., large areas. Van De Wal and Oerlemans (1994) used an energy balance model for the entire Greenland ice sheet driven by data from the margins and then interpolated to grid-cells where no observations existed. Ettema et al. (2009) describes model runs over the Greenland Ice Sheet with a regional climate mode, bounded by an surface energy balance model at the ice/atmosphere interface.

The energy budget at the surface is described by:

$$Q_M = Q_H + Q_E + Q_G + L_{SW} + L_{LW} + Q_R \quad (2.25)$$

where Q_M is the energy available for melt and equal to the sum of the sensible heat flux (Q_H), the latent heat flux (Q_E), the subsurface heat flux (Q_G), and the net long and short wave radiative components (L_{SW} and L_{LW}), and the energy added to the surface through rain fall (Q_R). In cases of $Q_M > 0$, melt will occur.

Over a melting ice surface, the bulk aerodynamic method is typically used, assuming surface temperature of zero degrees, and a vapor pressure of 6.11 hPa. Thereby, only one measurement above the surface is necessary to determine the heat and vapor gradient in the near-surface layer (Hock, 2005). The bulk aerodynamic method also assumes that Q_H is a function of the air temperature gradient, and Q_E a function of the humidity gradient. In addition, both fluxes are proportional to wind speed. The turbulent fluxes (Q_H and Q_E) can be approximated assuming Monin-Obukhov similarity:

$$Q_H = \rho c_p u_* \theta_* \quad (2.26)$$

$$Q_E = \rho L_v u_* q_* \quad (2.27)$$

where ρ is the air density, c_p is the specific heat capacity of air, and L_v is the latent heat of sublimation.

The friction velocity, u_* , in Eqs. 2.26 and 2.27 is given as:

$$u_* = \frac{ku_{z_w}}{\ln\left(\frac{z_w}{z_0}\right) - \psi_{m2} + \psi_{m1}} \quad (2.28)$$

where k is Von Karman's constant, u_{z_w} is measured wind speed at height z_w , and z_0 is the roughness length scale for momentum. ψ_{m1} and ψ_{m2} are momentum stability correction functions.

The virtual potential temperature scale, θ_* , in Eq. 2.26 is:

$$\theta_* = \frac{k(\theta_v - T_s)}{\ln\left(\frac{z_{tmp}}{z_t}\right) - \psi_{h2} + \psi_{h1}} \quad (2.29)$$

where z_{tmp} is the height at which temperature is measured, z_t is the roughness scale for temperature, θ_v is the virtual temperature and T_s is the surface temperature. ψ_{h1} and ψ_{h2} are temperature stability correction functions.

The turbulent scale of humidity, q_* , in Eq. 2.27 is given by:

$$q_* = \frac{k(q(z_{hum}) - q(0))}{\ln\left(\frac{z_{hum}}{z_q}\right) - \psi_{q2} + \psi_{q1}} \quad (2.30)$$

where z_{hum} is the height at which humidity is measured and z_q is the roughness length scale for humidity. ψ_{q1} and ψ_{q2} are humidity stability correction functions.

The stability-correction functions ψ_{m1} , ψ_{m2} , ψ_{h1} , ψ_{h2} , ψ_{q1} , and ψ_{q2} in equations 2.28, 2.29, and 2.30 are adopted from Paulson (1970) and Holtslag and De Bruin (1988) for stable and unstable conditions, respectively.

The subsurface heat flux, Q_G , can be computed numerically using a one-dimensional finite-difference solution of the heat equation. The subsurface is divided into a number of horizontal layers and the temperature gradient between each layer is determined in discrete time steps. The energy flux to the surface, Q_G will then be proportional to the temperature difference between the top layer and the layer below it, at that time. Boundary conditions can be stipulated so that the bottom layer has the same temperature as the layer immediately above it and the top layer has the temperature of the surface. The bottom boundary condition implies that heat exchange to and from the ice column through the bottom layer is not considered.

Some subsurface melting will occur as a consequence of short-wave penetration into the ice. This is potentially a significant contribution and must be quantified (e.g., Van den Broeke et al., 2008). The amount of radiation absorbed by the ice can be estimated using Beer's law with an extinction coefficient of 1.4 for ice (Greuell and Konzelmann, 1994).

In numerical models of the SEB, an iterative approach is used to determine the surface temperature, which is the only remaining unknown, assuming that the energy budget

is balanced. If the surface temperature T_s is required to be $>0^\circ\text{C}$ in order to balance the budget, energy will be available for melt. In the subsequent iteration, T_s will be set to zero, and the excess energy flux will then be converted to melt for the time step.

With the quantities in the energy budget determined, the corresponding surface ablation rate, M , (in m s^{-1}) is:

$$M = \frac{Q_M}{\lambda \rho_{ice}} \quad (2.31)$$

where λ is the latent heat of fusion ($3.35 \cdot 10^5 \text{ J kg}^{-1}$) and ρ_{ice} is the density of ice.

In this thesis, a distributed SEB model was developed using the software package Matlab v7. The SEB was estimated at $\sim 11,000$ gridpoints across a model grid with gridcells of size $500\text{m} \times 500\text{m}$, comprising $\sim 550 \text{ km}^2$. Elevations were described by an ASTER-derived DEM. Parameterizations were implemented in order to estimate temperature, wind speed and incoming short wave radiation (shading from the surrounding topography was accounted for). For the reflected short wave component, albedo values were determined using the MODIS MOD10A1 Daily Snow Albedo Product. Further details can be seen in Andersen et al. (2010) (Paper I in Appendix A).

2.6 Glacier seismology

The seismogenic nature of glaciers has been known for decades. Early studies established a link between glacier motion and emission of seismic signals in both terrestrial and tidewater-type alpine glaciers (e.g., Neave and Savage, 1970; VanWormer and Berg, 1973). Recently, a new class of glacially related seismic events has been discovered, termed *Glacial Earthquakes* (Ekström et al., 2003). These events are detectable on the Global Seismic Network (GSN), and have magnitudes $M \sim 4-5$. They exhibit a different frequency content than that of normal, tectonic earthquakes of similar magnitude, in being dominated by low-frequency energy and lacking the high-frequency content of tectonic earthquakes. They also display a seasonal variability (Ekström et al., 2006) and analysis of the source locations (Tsai and Ekstrom, 2007) places a large number of them at or close to the large Greenland outlet glaciers. Various source mechanisms have been suggested, including stick-slip behavior induced by changes of subglacial hydraulics, or rapid sliding following the loss of buttressing resistance associated with calving (Joughin, 2006; Tsai et al., 2008). By comparing teleseismic detections and GPS-based observations of surface velocity at Helheim Glacier, Nettles et al. (2008) found that occurrences of glacial earthquakes coincided in time with large ice-loss events at the terminus, while Joughin et al. (2008b) noted an association between calving activity observed from satellite images and teleseismic detections. It has thus been established that the glacial earthquakes as first described by Ekström et al. (2003) are associated

with calving. Nettles and Ekström (2010) discussed possible source mechanisms, including that of a capsizing iceberg pushing against the front of the glacier during rotation, thereby transferring momentum. Calculations have shown this to be a plausible hypothesis for explaining the observed seismic response.

In Greenland, field-based studies of glacially-related seismicity are few and mainly concentrated on the west coast (e.g., Amundson et al., 2008; Rial et al., 2009; Amundson et al., 2010). At Jakobshavn Isbræ, Amundson et al. (2008) observed glacially-related seismicity, coincident with visually observed calving activity. Rial et al. (2009) used a network of high-frequency seismometers on the ice sheet margin north of the fast-flowing part of Jakobshavn Isbræ to detect glacially-related seismic events. Rial et al. (2009) identified and described intermittent seismicity occurring between larger events as “rumblings”; gradually onsetting tremors of $\sim 10\text{--}40$ min. duration. The source locations of the rumblings were 10–20 km upstream from the calving front and those authors posited upstream fracture propagation initiated by a calving event at the front as a possible explanation for the locations.

As an analogue to the large Greenland outlet glaciers, O’Neel et al. (2007) and O’Neel and Pfeffer (2007) conducted studies involving automatic detection of calving-related seismic events at Columbia Glacier, Alaska, using a temporary network of seismic stations on the rock walls bordering the glacier. Those workers assembled a large data set and concluded that the calving-related seismicity to a large degree was monochromatic, indicating a common source mechanism. In a recent study also from Columbia Glacier, Walter et al. (2010) monitored calving in the same band as O’Neel et al. (2007) (1–3 Hz), but also at higher frequencies, 10–20 Hz, where seismicity arising from fracturing and crevassing can be recorded. The study focused on a comparison of the characteristic type of seismicity occurring before and after Columbia Glacier became ungrounded in 2007. Walter et al. (2010) noted a transition in seismically detectable calving style: prior to flotation, the calving was frequent and in smaller volumes. After flotation, fewer events occurred, but at a much larger scale.

In Iceland, Jonsdottir et al. (2009) found increasing seismicity in the 1–4 Hz band over the period 1991–2007 and located the sources to be at an outlet glacier from the Mýrdalsjökull glacier. It was concluded that the seismicity arose from falling seracs, calving over the edge of a plateau. The study by Jonsdottir et al. (2009) also found a strong seasonal signal, indicating a climatic control. The temporal pattern of seismicity correlated well with occurrence of intense rainstorms in the autumn. The authors suggested that rain water affected the basal conditions in a way which caused enhanced sliding and subsequent increased calving.

Chapter 3

Greenland – ice sheet and outlet glaciers

Different techniques have been applied in order to study the flow speeds at the margins of the Greenland Ice Sheet, including the large outlet glaciers, and how it is affected by melt water. One group of methods used is remote-sensing type techniques, which provide good spatial coverage, but typically have monthly to yearly time resolutions. Another group of studies is the field-based, in-situ types, of which there are few from the surface of outlet glaciers. In terms of sample rate, these often have much higher temporal resolution, but lack the spatial coverage of the remote-sensing methods.

This chapter contains a review of the existing knowledge of the physical properties of the fast-flowing outlet glaciers and the influence of melt water on the flow of these and the ice sheet.

3.1 The Ice Sheet

The remote-sensing based studies include works that provide overviews of large parts of the ice sheet and the ice sheet margin (e.g., Rignot and Kanagaratnam, 2006; Joughin et al., 2008a), and also of specific locations (e.g., Luckman and Murray, 2005; Luckman et al., 2006; Howat et al., 2007; Stearns and Hamilton, 2007).

Joughin et al. (2008a) presented a study of the West Greenland Ice Sheet and a number of outlet glaciers in that region, using three years of data. The investigation was combined of remote sensing (InSAR) and some field measurements (Global Positioning System, GPS). Joughin et al. (2008a) found that during summer the ice sheet sped up considerably (50–100%), while the outlet glaciers appeared less sensitive (speedups of 9–14%).

Due to the exceptionally high flow speed of the outlet glaciers, the absolute numbers are in fact comparable, with the ice sheet speed-up corresponding to 36–71 m/yr and the outlet glaciers 51–77 m/yr, respectively. Joughin et al. (2008a) reached the conclusion that the spring onset of melt had a significant effect on the flow speed of the ice sheet, but not on the outlet glaciers covered in their study. This is consistent with the work of Echelmeyer and Harrison (1990) who found no effect of melt water on flow speed at Jakobshavn Isbræ.

Several ground-based studies have provided evidence for the effect of melt water enhanced sliding on the ice sheet. One of the first studies to suggest a connection between melt water production and associated acceleration of flow was Zwally et al. (2002). These authors observed a ~30% increase in the flow speed of the ice sheet near Swiss Camp, West Greenland correlating well with periods of intense melt. Further south, at the *K-transect*, Shepherd et al., 2009 found an increase in flow speed of 35% per positive degree day. In the same area, Van de Wal et al., 2008 noted up to 30% variation in ice sheet flow speed associated with melt.

That fractures can propagate to the bottom of glaciers and the ice sheet near the margin has been shown theoretically by Van der Veen (2007) in which the so-called “hydrofracturing” is modeled numerically. It was there demonstrated that, provided there is sufficient water supply from the surface, cracks can propagate all the way to the bed of the ice sheet. Field studies confirm the results of Van der Veen (2007) in, e.g., Das et al. (2008). Das et al. (2008) monitored the rapid drainage of a melt water lake and the subsequent rapid (<2 hours) uplift and speed-up of the ice sheet in the area where the thickness is ~980 m.

Deductions about the drainage system of the ice sheet have been made from the observations mentioned above. Joughin et al. (2008a) interpreted the spatial uniformity of the accelerated sliding of the ice sheet they observed as indications of distributed drainage (see Chapter 2). Supporting this are the in-situ observations of vertical displacement of the ice surface during large melt or precipitative water fluxes made in several studies, both on alpine glaciers (e.g., Iken et al., 1983; Iken and Bindschadler, 1986) and also on the Greenland Ice Sheet margin (Shepherd et al., 2009; Bartholomew et al., 2010). In alpine studies, with concomitant alternative observations of the drainage system, the uplift has been associated with bed separation in a distributed, high pressure drainage system (e.g., Iken and Bindschadler, 1986; Kamb et al., 1985).

3.2 Outlet glaciers

3.2.1 Physical characteristics

The fast outlet glaciers in Greenland are characterized by high driving stresses and thus high flow speeds (up to 12 km/yr, Joughin et al., 2008a), which can be inferred from surface observations (Iken et al., 1983). Of the fast-flowing Greenland outlet glaciers, Jakobshavn Isbræ, West Greenland, has been the subject of multi-decadal research campaigns and remains the most studied. This has involved a wide variety of geophysical methods like drilling and instrumentation of boreholes (e.g., Iken et al., 1993; Funk et al., 1994; Luthi et al., 2002), geodetic surveying (e.g., Amundson et al., 2010; Dietrich et al., 2007), and seismic investigations (e.g., Clarke and Echelmeyer, 1996; Amundson et al., 2008).

The geometry of Jakobshavn Isbræ has successfully been investigated by Clarke and Echelmeyer (1996) using active-source seismic methods. These workers observed a deep subglacial trough and found ice thicknesses of ~2800-1800 m along the center line, decreasing down stream. The up stream surrounding ice sheet was ~1000 m thick. These thicknesses have later been confirmed by recent ice-penetrating radar-studies (e.g., Braaten et al., 2002; Legarsky and Huang, 2006; Li, 2010).

A combination of works by Iken et al. (1993), Funk et al. (1994), and Luthi et al. (2002) forms a comprehensive field-based contribution. There, a large drilling campaign was conducted approximately 50 km up stream from the location of the terminus at that time. A number of boreholes were made, in some cases reaching the bed near the edges of the fast flow zone. Temperatures in the boreholes were measured and evidence of the existence of a temperate layer of ice near the bed was found, caused by the strong deformation occurring when the ice enters the deep, narrow channel (Funk et al., 1994). This temperate layer was thicker near the middle of the stream and is in general suspected to have a large influence on the flow dynamics, by way of its lower viscosity. In the study reported on by Luthi et al. (2002), the amount of basal motion was inferred to be 60% of the total surface velocity in the area adjacent to the deep channel. However, Luthi et al. (2002) suggests that within the actual trunk, the amount of deformation will be significantly larger where the temperate ice layer is up to an order of magnitude thicker. A main conclusion of the investigations conducted is thus the confirmed observation of a thick temperate ice layer near the bed which suggests that the fast flow of Jakobshavn Isbræ is primarily a result of strong deformation of this basal temperate layer and less so the result of basal sliding. In a recent observation Luthi et al. (2009) discussed the visual observation of a layer of ice expected to be the temperate layer, observed in a recently calved-off iceberg.

Our knowledge of the subglacial hydraulic system of the fast outlet glaciers is limited and mainly based on inferences from surface observations. While alpine glaciers have been investigated using dye-tracers, this has not been feasible at the much larger Greenland outlet glaciers. In a study of surface velocities of Jakobshavn Isbræ by Echelmeyer and Harrison (1990), a lack of seasonal variability was observed. This remains somewhat puzzling considering the large amounts of melt water generated in the melt season. Echelmeyer and Harrison (1990) suggested that the lack of seasonally-based velocity fluctuations could be explained by the melt water traveling englacially almost to the grounding line, where it connects to the bed. It is also conceivable that the amount of sliding that does occur at the bed generates heat that by dissipation maintains a layer of water at the base. An already existing layer of water will possibly have a dampening effect on the response to added melt-water.

3.2.2 The effect of melt on flow speed

The factors governing the flow speeds of outlet glaciers are not very well constrained. In recent years, this has been the subject of several investigations. It has been demonstrated that ice-loss from the terminus varies over the year (Sohn et al., 1998) and that calving exerts a modulating effect on outlet glacier flow speed (e.g., Nettles et al., 2008; Joughin et al., 2008b; Amundson et al., 2008; Howat et al., 2008c, Nick et al., 2009). Additionally, recent investigations of the oceanographic conditions in the fjords where the tidewater glaciers terminate suggest that warm ocean water causes subsurface melt, and that this may play a role in the thinning and accelerations of outlet glacier flow (e.g., Bindshadler, 2006; Holland et al., 2008; Straneo et al., 2010).

The effect of surface melt or rain water accelerating sliding speed by way of increasing the basal water pressure is well established on alpine glaciers (e.g., Iken and Bindshadler, 1986; Anderson et al., 2004; Bartholomaus et al., 2008) and tidewater glaciers outside Greenland (Meier et al., 1994; Kamb et al., 1994). However, less is known about how variations in melt water supply affect the flow speed of large Greenland outlet glaciers. When considering ocean-terminating glaciers, added complexity must be expected. Second-order effects may exist, for example in the form of enhanced calving due to crevasses filling with surface melt water (Benn et al., 2007), then leading to increased discharge.

As demonstrated in Andersen et al. (2010), variations in melt water production at Helheim Glacier, East Greenland, correlate well with variations in flow speed as observed at the surface. Although the fractional increase in speed ascribed to melt in Andersen et al. (2010) is moderate (up to $\sim 5\%$), the absolute amount of extra discharge is large (e.g., a speedup of $\sim 4\%$ above the 2007 summer mean of 25 m/d equals an extra discharge

from Helheim of ~ 1.3 Gt/yr). If the conclusions drawn in Andersen et al. (2010) apply to the outlet glaciers in general as suggested, it is argued that this can be a significant contribution to ice discharge across Greenland.

Few field-based studies of seasonal variation of outlet glacier drainage exist. Especially studies elucidating winter time drainage are sparse. This is likely to be caused by the practical and logistical difficulties associated with instrumenting a fast flowing outlet glacier throughout a full year. In one study, Echelmeyer and Harrison (1990) measured year-round surface velocity of Jakobshavn Isbræ and found no change between summer and winter speeds. They interpreted this to be indicative of englacial drainage accommodating the surface melt with no hydraulic connection to the bed. This is consistent with the low sensitivity of the outlet glaciers found by Joughin et al. (2008a), but contrasts with a recent study of the seasonal evolution of the subglacial drainage system of West Greenland outlet glacier Russell Glacier by Bartholomew et al. (2010). These authors found strong speed-ups (up to 220% increases relative to the 100 m/yr background flow speed) to coincide with the onset of melt in late May. It should be noted, though, that Russell glacier – while an outlet from the ice sheet – is land-terminating and much slower than the fast flowing, marine-terminating outlet glaciers, why it velocity-wise resembles the ice sheet more than the fast outlet glaciers.

On an Icelandic outlet glacier draining Vatnajökull Ice Cap, Howat et al. (2008b) also inferred distributed drainage during periods of intense melt and rain, accompanied by uplift. However, this glacier was significantly slower than the Greenland outlet glaciers (peak sliding speed reported in Howat et al. (2008b) was ~ 750 m/yr).

The fast flow of the Greenland outlet glaciers may play an important role in the behavior of the subglacial drainage system. As noted by Iken et al. (1993) on Jakobshavn Isbræ, the thick temperate layer possibly caused by strain heating is a direct consequence of the high driving stresses not seen in the alpine examples. Directly related to the flow speed is also the amount of heat generated by friction at the ice-bedrock interface. The relationship is described by the equation: $Q_{base} = \tau_{base}u_{base}$ where Q_{base} is the heat flux, τ_{base} is the basal shear stress, and u_{base} is the sliding velocity at the bed (Paterson, 1994). For a relatively steep, fast-flowing ($u_{surface} = 7500$ m/yr), 1200 m thick glacier with a surface slope of 1.7° and assuming $u_{base} = 0.3u_{surface}$, the heatflux generated by frictional heating, Q_{base} is ~ 23 W/m². This is significant compared to, e.g., geothermal heat fluxes, which range from 0.046 to 0.077 W/m² (Paterson, 1994).

In general, it is expected that the conclusions drawn from the work conducted at Jakobshavn Isbræ are applicable in a broad sense to the other large outlets of Greenland (e.g., Helheim and Kangerdlugssuaq Glaciers), possibly with some modifications. While there are other outlet glaciers which drain considerable amounts of ice (e.g., Petermann Glacier in North West Greenland which drains $\sim 3\%$, Rignot and Kanagaratnam, 2006),

these are slower-flowing and located in a colder surrounding climate. It is therefore not necessarily justified to extrapolate information inferred about the subglacial conditions Jakobshavn Isbræ to these.

Chapter 4

Observations

In this thesis, several types of data have been used in conjunction, all collected at or near Helheim Glacier, East Greenland (Figure 4.1). The data sets include meteorological data, geodetic data, hydrographic data, photographic data, and seismic data. In this chapter, the technical specifications of the equipment used, the locations and the periods of operation will be presented. A section on the post-collection data processing techniques used is also included.

4.1 Automatic Weather Station

An Automatic Weather Station (AWS) was used to collect meteorological data from the surface of Helheim Glacier during the melt seasons of 2007 and 2008 (Figures 4.2). The horizontal position of the AWS was approximately 66.42N, 38.44W, 640 m. above sea level (Figure 4.5). The AWS was deployed in approximately the same position both years, the horizontal difference in position being ~ 650 m.

Data was recorded for 27 full days in 2007 (days of year 208 to 235) and 49 full days in 2008 (days of year 183-231).

4.1.1 Tripod

Sensors were mounted on a collapsible aluminum tripod, the height of which was approximately 3.10 m. The triangular footprint was approximately 3.7 m^2 . The tripod was of a type developed at the Geological Survey of Denmark and Greenland (GEUS), constructed from aluminum tubing ($\text{\O}48$ mm, mast; $\text{\O}33$ mm, feet). Wires were threaded between the ends of the legs and as guy-wires to an anchor-point on the mast. One guy-

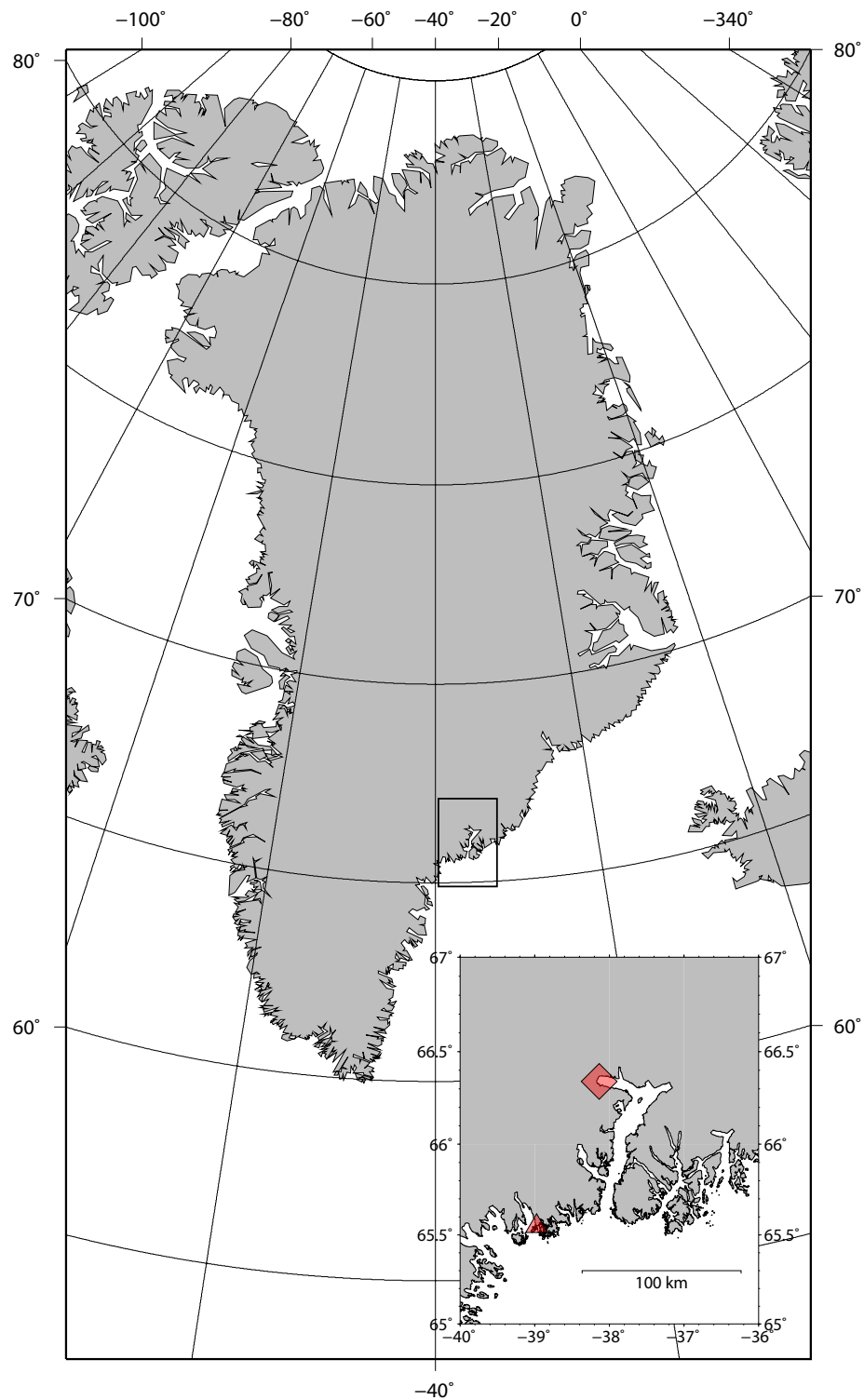


Figure 4.1: Greenland and study area, Helheim Glacier, South East Greenland (inset). The red diamond indicates Helheim Glacier, the red triangle marks the settlement of Isortoq.

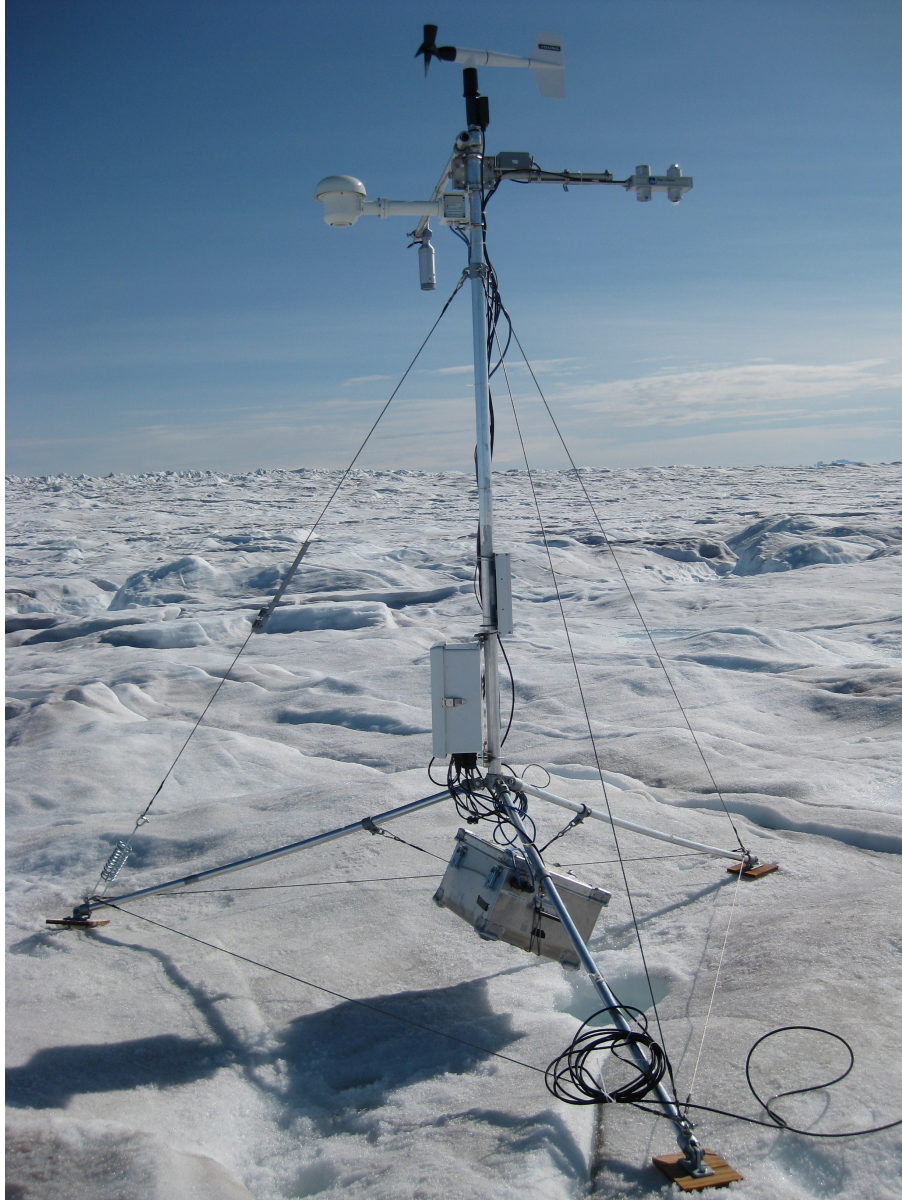


Figure 4.2: Automatic Weather Station (AWS) deployed in the field at Helheim Glacier.

wire was spring-loaded, allowing for adjustment of the wire tension in the tripod. The sensors were mounted at heights 2.8–3.2 m (the wind sensor was mounted at the top end of the mast, thus exceeding the ~ 3.10 m height of the station).

4.1.2 Power supply

Power to the station was provided by four 12 V batteries installed in a water-tight aluminum case suspended from the feet of the AWS, thereby lowering the centre of gravity and providing an anchor for the AWS (Figure 4.2). Charging of the batteries was by way of a south-facing solar panel attached to the mast, outputting 10W when completely illuminated.

4.1.3 Data

The AWS recorded standard meteorological parameters: Aspirated near-surface air temperature, relative humidity, incoming and outgoing long- and short-wave radiation, wind speed and direction, station inclination, and distance to ice surface using a separate tripod (Figure 4.3 and Section 4.1.4). All values were measured and logged once per hour except wind speed, which was logged as the average of values measured during the preceding hour, sampled at each execution of the logging program (~ 10 seconds). Due to technical constraints on the logging device, barometric pressure was not measured at the AWS. Barometric pressure data was acquired from the Danish Meteorological Institute station in Tasiilaq (<http://www.dmi.dk/dmi/index/gronland/vejrkarkiv-gl.htm>) and extrapolated to Helheim Glacier during data processing (Section 4.6.1).

The sensors used for the data collection are listed in Table 4.1 along with their accuracies as specified by the manufacturers. All data were logged to a Campbell CR10X data logger.

4.1.4 Ablation measurement

To provide an independent check value for ablation modeling, a separate ablation measurement was conducted close to the AWS. Aluminum stakes were drilled into a depth of >5 m to avoid further self-drilling and the sonic ranger distance-sensor was mounted on a crossbar (Figure 4.3).

Table 4.1: Types of the sensors used on the AWS and their accuracies.

Measurement	Instrument type	Accuracy
Aspirated temperature		
Instrument house w/ fan	Rotronics	-
Temperature, temp. probe	Rotronics PT100	± 0.1 K
Relative humidity	Rotronics S3 hygroclip	$\pm 1\%$
Radiation	Kipp & Zonen CNR1	
Long wave	CG3 (in CNR1)	$\pm 10\%$ (dail. tot.)
Short wave	CM3 (in CNR1)	$\pm 10\%$ (dail. tot.)
Ablation	Campbell SR50	± 0.01 m
Wind speed/direction	Young 05103-5	
Wind speed		± 0.3 m/s
Wind direction		$\pm 3^\circ$
Station inclination	NS-25/E2	$\pm 0.6\%$ of ang.

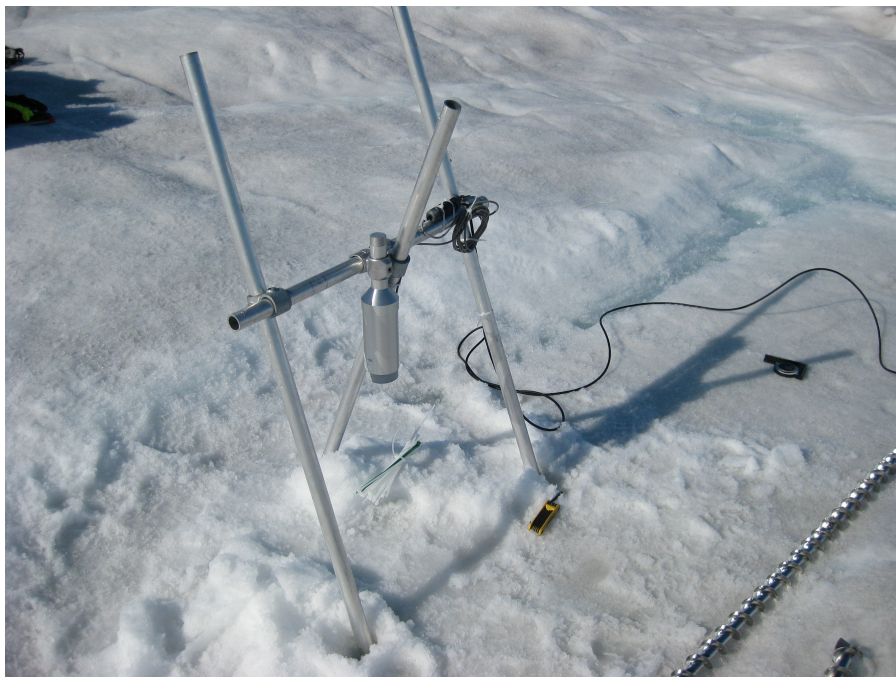


Figure 4.3: Separate ablation measurement, Helheim Glacier, located 3–4 m from the AWS (outside frame of photo). The ablation measurement is logged by the AWS.

4.2 GPS

Position data were collected using 12–22 continuously recording Differential GPS receivers of the type Trimble netRS, Trimble 5700, and Trimble R7, deployed across the surface of Helheim Glacier. The receivers were enclosed in weather proof Pelican boxes and powered by internal batteries charged by a solar panel mounted on the side of the box. The networks extended from within a few km of the calving front to 25 km up stream. Maps of the GPS deployments for 2007 and 2008 are shown in Figure 4.5. The receivers recorded positions at rates of 1–5 samples per second, operating throughout the periods marked in Figure 4.6.

4.3 Tide gauge

A tide gauge was installed at an island in Helheim Fjord, ~25 km from the calving front during the summer of 2008 (position 66.24N, 37.60W). The sensor was of type Global Water WL16-U and monitored variations in water level, sampling at one-minute intervals. Calving of icebergs from the glacier terminus causes short-period ($P \sim 10$ min.) disturbances of the water level, which were captured by the tide-gauge, thus providing a constraint on the calving activity.

The tide-gauge was operating from day 185 to day 201 and again from day 214 to 234, 2008.

4.4 Time-lapse camera

In the summer of 2008, a digital SLR camera was mounted in a weather-proof enclosure on the northern fjord wall of Helheim Fjord. The camera was directed at the calving front and configured to record images automatically every four minutes. The time-lapse record provides visual identification of the times of major calving events.

4.5 Seismic station

An STS-2 broad-band seismometer was installed in the small settlement of Isertoq, approximately 100 km from Helheim Glacier (Figure 4.1). Data was logged to a RefTek 130 data logger, sampling at a rate of 20 samples/second. The instrument was installed in the basement of a building, which allowed for mains power supply (Figure 4.7). Instrument orientation was carried out using a handheld GPS and a compass. The maximum

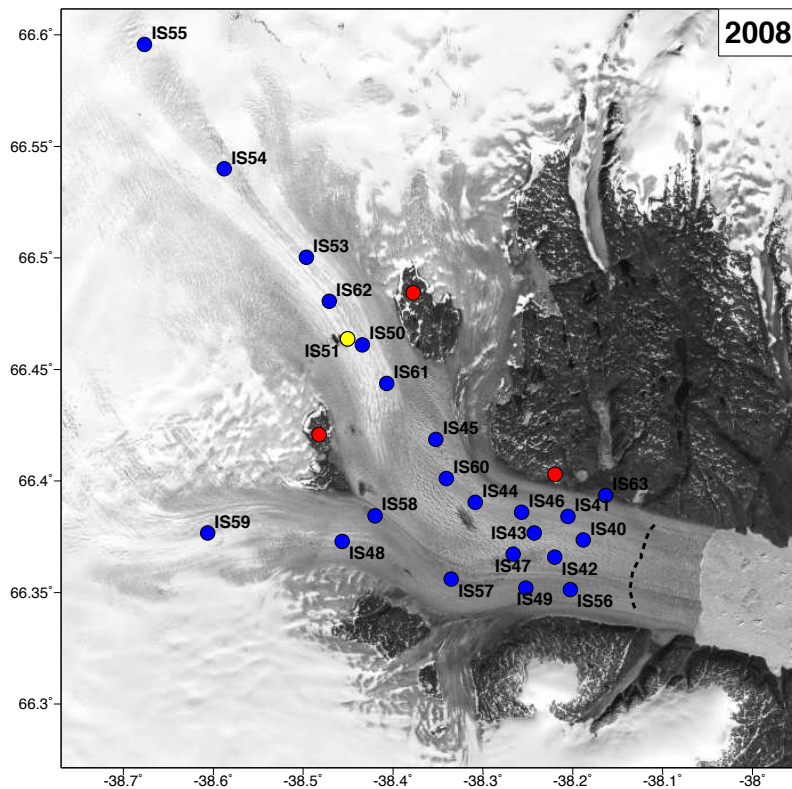
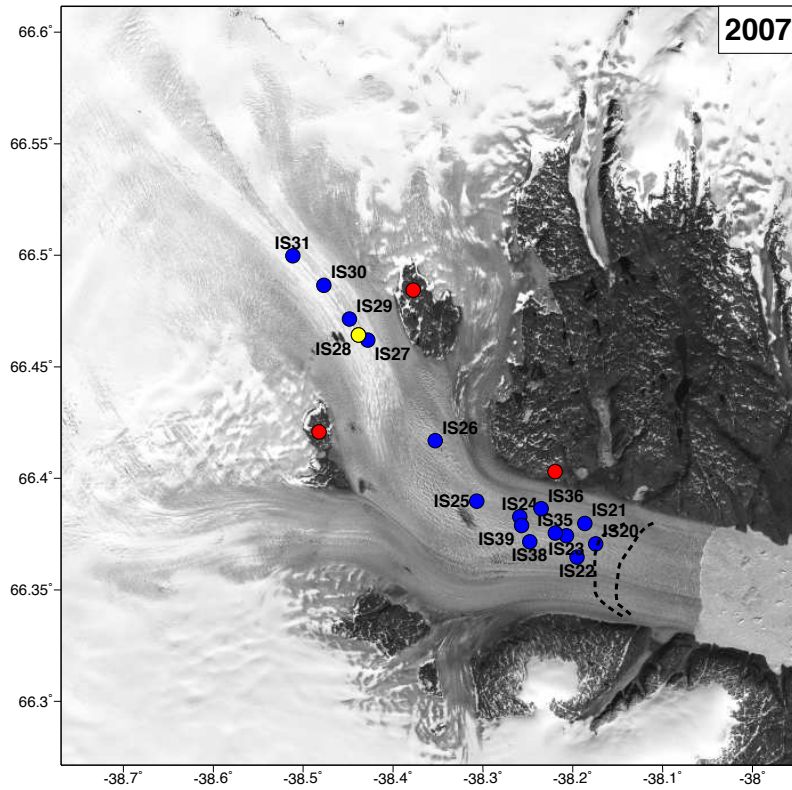


Figure 4.4: Maps of the 2007 and 2008 GPS and AWS deployment sites. Blue dots indicate locations of GPS receivers, yellow dot indicates position of AWS, and red dots indicate reference sites placed on the rock outcrops. Map produced by M. Nettles, Columbia University, for use in this work.



Figure 4.5: GPS receiver deployed in the field (black box circled), Helheim Glacier.

expected misalignment during this procedure is $\sim 5^\circ$. Following installation and orientation, the sensor was covered with foam insulation material to reduce long-period thermal effects.

The station, designated ISO, operated from July 2007 to February 2009, with intermittent data gaps due to lack of storage capacity.

4.6 Data processing

4.6.1 AWS

In order to use the AWS data for further studies, erroneous measurements, data gaps and other unnatural irregularities in the raw data record were mitigated.

4.6.1.1 Radiation

Central in such a correction scheme is the incoming short wave radiation. The short wave radiative flux is a large component in the energy budget (van de Wal et al., 2005). The sensor used, Kipp & Zonen CM3, is sensitive to tilt (van den Broeke et al., 2004), thus requiring careful correction.

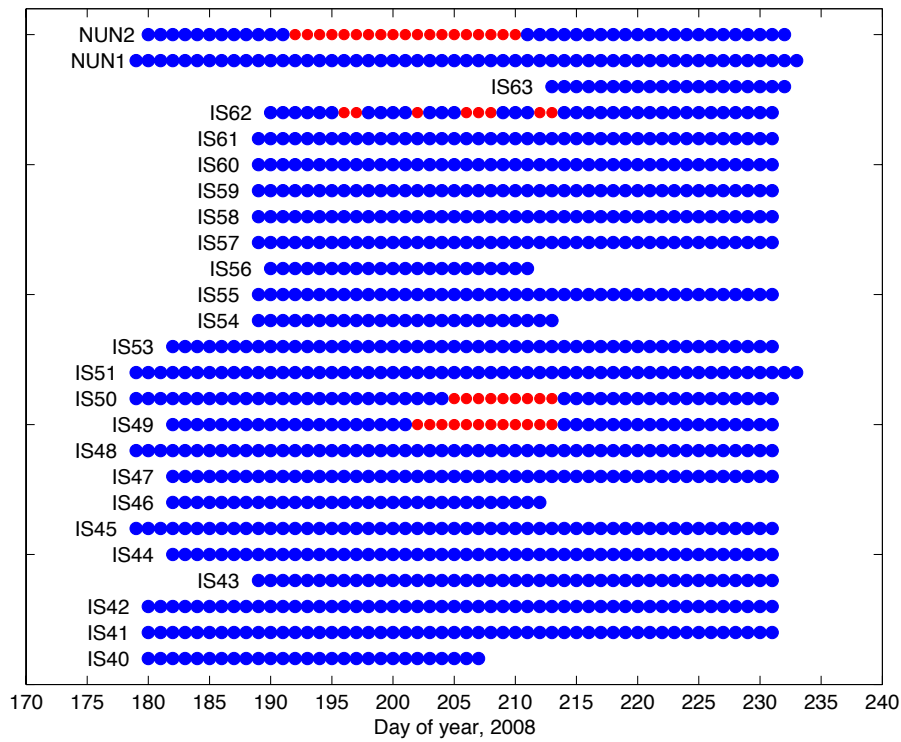
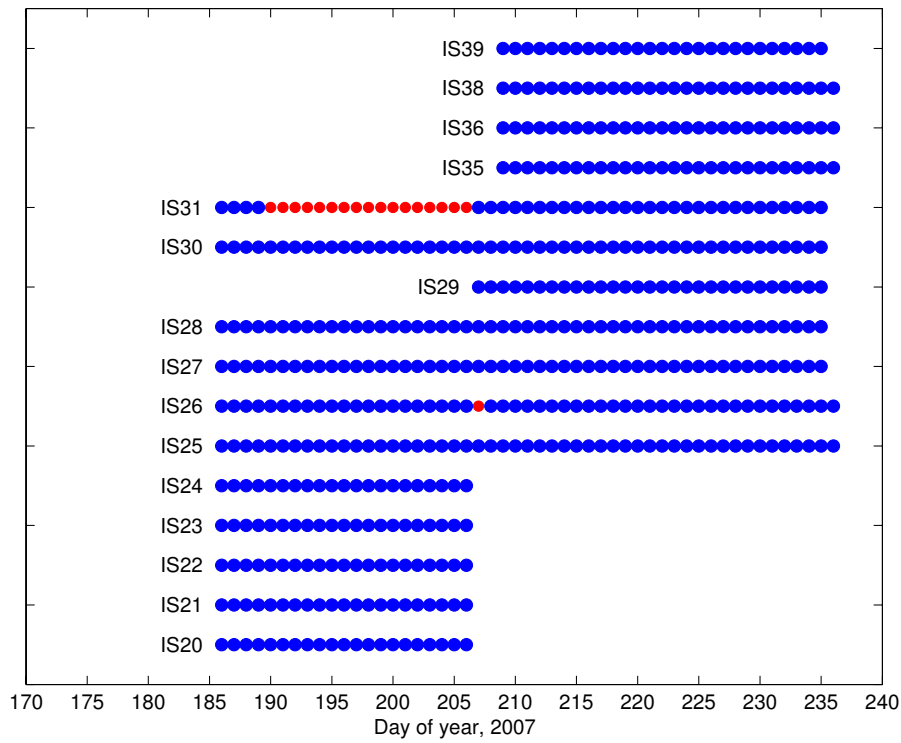


Figure 4.6: Days of recorded GPS data in (top) 2007 and (bottom) 2008.



Figure 4.7: Installation of the seismometer in the settlement of Isertoq.

Global radiation G is defined as $G = I + D$ where I is the direct component and D is the diffuse component. The direct component I of the global radiation is the fraction sensitive to the tilt that occurs as the season progresses and the AWS changes position. To correct only I , it is necessary to know the distribution of the global radiation on the two components, i.e., the diffuse fraction (DF). DF is assumed to be governed by the cloud fraction and has the value of 0.2 as cloud-free limit and 1 as fully overcast. Cloud fraction is determined by the relationship of air temperature (T) to incoming long-wave radiation LR_{in} , where two polynomials describe the boundaries corresponding to $DF = 0.2$ and $DF = 1$. For a set of (T, LR_{in}) -values DF is found by interpolating between the two bounding polynomials. With DF known, the direct component $I = (1 - DF)G$ can be corrected with a factor k described by (MacWhorter and Weller, 1991):

$$k = \frac{\cos \theta_z}{\cos \beta \cos \theta_z + \sin \beta \sin \theta_z \cos(\Psi - \gamma)} \quad (4.1)$$

where β is the surface slope, θ_z is the zenith angle, Ψ is the solar azimuth, and γ is the surface azimuth. Unrealistically high radiation values caused by instrument glitches, unnatural reflections from, e.g., the aluminum tripod of the AWS were set to 80% of the calculated top-of-atmosphere radiation at the specific time of measurement.

The measured long wave radiative flux is affected by the temperature of the instrument casing. The casing temperature was measured and the energy contribution from this was quantified using the Stefan-Boltzman law, assuming black body radiative properties.

4.6.1.2 Barometric pressure

Daily values of barometric pressure measured at sea-level in the nearby town of Tasiilaq (~100 km from Helheim Glacier) are available from the Danish Meteorological Institute. These were interpolated to hourly values and then extrapolated vertically to the station altitude of 640 m above sea level using the barometric equation. Where the record from DMI was incomplete, missing values were set to mean values of the past 5 years of the day in question.

4.6.1.3 Temperature

Due to an instrument malfunction in the AWS when deployed in 2007, measurements of near-surface air temperature and ablation were not acquired. The temperature was therefore reconstructed using the casing temperature from the CNR1 net radiometer which was successfully logged. A simple model equation relating observed aspirated air temperature, T_{asp} , to casing temperature T_{CNR1} , shortwave radiation SW_{in} and wind speed U was constructed:

$$T_{asp} = a T_{CNR1} + b SW_{in} + c U + d \quad (4.2)$$

Using the 2008 data, a least squares solution to equation 4.2 was found. The solution yielded coefficients a , b , c , and d which could then be used to synthesize an aspirated temperature record for 2007. Applying the equation to the 2008 data (when measured temperature existed providing a validation of the model) yielded a RMS residual of ~1 K and a correlation coefficient of $r = 0.65$. This was deemed sufficiently good to use the 2007 data for analysis.

4.6.1.4 Sonic ranger

Distance measurement by way of ultrasonic pulses must be corrected for the difference in travel times incurred by variations in the air temperature. A simple equation was used for correction of distance:

$$D_{corr} = D_{meas} \sqrt{\frac{T_{asp}}{273.15}} \quad (4.3)$$

where D_{corr} is the corrected distance, D_{meas} is the raw distance value logged, and T_{asp} is the aspirated air temperature measured by the AWS.

4.6.2 GPS

Daily average velocities were made available to the studies in this thesis. The daily velocities were calculated by fitting a linear model to position estimates determined kinematically at 15 s intervals, as described in Nettles et al. (2008). The velocity estimates have uncertainties of approximately 0.1 m/d.

4.6.3 Seismic data

The 15 min. data files logged in the RefTek 130 data logger were merged into coherent SAC files. Prior to analysis, the instrument response was deconvolved using the GSAC software package.

Chapter 5

Conclusions and outlook

The recent acceleration in mass loss from the Greenland Ice Sheet has predominantly been driven by increases in iceberg-calving and dynamic thinning from the outlet glaciers draining the ice sheet. In this thesis, investigations into the effect of surface melt on the flow speed of the fast Greenland outlet glaciers have been carried out. This chapter will provide a short review of the results from the three studies conducted in the thesis and compare them to conclusions reached by other authors. In general, the literature to which the current results can be compared and discussed with is limited due to the lack of studies conducted on fast-flowing Greenland outlet glaciers. Suggested future research efforts are then discussed. Discussions of the results in details and in a broader perspective are provided in the manuscripts.

5.1 Overview of results

The first study seeks to understand to which extent variations in melt water affects the flow of outlet glaciers. The melt-induced flow-speed variations are isolated by removing calving events known to be associated with changes in velocity (Nettles et al., 2008). A distributed surface energy balance model is developed and validated against field observations of ablation. The model is used for quantification of the surface-melt production across Helheim Glacier. It is demonstrated that there are significant correlations between the GPS observed velocity signals and the estimated melt variation from the model. This is tested spatially by comparing locally estimated melt signals with the GPS observations from the same point. It is noted that the correlations are stronger near the front, than upstream. However, all correlations except one were statistically significant >90% levels. The correlation is peaked at a delay of the velocity signal, relative to the melt signal, of 12–36 hours. Speed variations of up to ~4% relative to mean, believed to

be attributable to melt are observed. While the fractional speed-up is moderate, the absolute amount of additional ice flux due to melt-water input is similar to that observed by other authors on the land-terminating portions of the ice-sheet margin, due to the high background flow speed of Helheim Glacier. The conclusions contradict the results of previous studies of the effect of melt water on fast outlet glacier flow (Echelmeyer and Harrison, 1990) but is consistent with Joughin et al. (2008a) who found a modest, seasonally dependant speed-up in relative terms.

The second study builds on the first one, in that the objective is to explore the spatial and temporal variation – if any – of the association between melt and speed changes demonstrated in the first study. It is shown that there is spatial and temporal variability in the glacier's sensitivity to melt-water input. It is seen that the sensitivity of the glacier to melt decays exponentially with distance from the calving front, suggesting spatial differences in the configuration of the basal hydraulic drainage system. Moreover, early in the season the glacier is less sensitive to melt than later (the fraction of the speed signal explained by melt in a statistical sense increases from close to zero to 80% as the melt season progresses). As the residual variances drop over the season, the sensitivity to melt also increases, coincident with a week-long speed anomaly of 3–4% above the mean near the calving front. Many authors have made observations on alpine glaciers suggesting a change in the basal hydraulic system over the season (e.g., Bingham et al., 2003; Howat et al., 2008b), caused by increasing melt or precipitation. However, the inferences about the subglacial conditions in these cases are not necessarily transferable to a fast outlet glacier where flow velocities can be up to several orders of magnitude higher. Some indications of an effect of strain conditions in the ice modulating the melt-water response are also found. In areas where calculated strain rates indicate compressional strain, the velocity data less well explained by the melt signal. The observations suggest a region of high basal water pressure near the calving front of Helheim Glacier, perhaps associated with near-flotation conditions and a distributed subglacial drainage system.

The final study is based on automatic detection of ice-loss events occurring at Helheim Glacier by way of seismic data recorded at a distance of ~ 100 km from the glacier. The link between calving and the emission of seismic energy in certain frequency bands has been shown by O'Neel et al. (2007), Jonsdottir et al. (2009), Rial et al. (2009) and Nettles et al. (2008). A detection algorithm is therefore developed and calibrated against a number of calving events observed through teleseismic detections or by time-lapse photography. Time and frequency domain analysis of the signals reveal similarities with those of Rial et al. (2009) and O'Neel et al. (2007). A seasonal pattern is established, with a clear peak in calving-related seismicity in the early autumn. This is consistent with the studies of Ekström et al. (2006), who found a seasonal signal in teleseismically detected glacial earthquakes. It also agrees with the results of Jonsdottir et al. (2009), who also noted a peak in calving-related seismicity during the autumn months in Iceland. It is

therefore suggested that there is a climatic control on the amount of calving occurring at the large outlet glaciers, possibly through melt-water-enhanced calving. A drop in seismicity from 2007 to 2008 with 33% more detections per day in 2007 than in 2008 is noticed, consistent with the drop in teleseismically detected events between the two years. The teleseismically detected events have been shown to coincide with large scale calving events (Nettles et al., 2008), why this is therefore interpreted as indicative of a decrease in ice loss.

In a warming climate, it is likely that the conclusions of all three studies will remain valid. Moreover, it is likely, that the effect of melt-water input to the glacier will result in a closer association (stronger correlation, stronger speed-up and higher sensitivity), as well as a longer period of increased calving activity.

5.2 Outlook

In a broader perspective, it has in recent years been clearly demonstrated that a key to understanding the increasing ice discharge from the Greenland ice sheet lies in an increased understanding of the flow dynamics of the large outlet glaciers. The understanding of the association between flow and calving as well as the role played by warm ocean currents reaching into the fjords is still at a rudimentary level. Different approaches can be taken in future efforts to understand the dynamics of the large tidewater glaciers. One avenue of investigation that is currently being pursued is instrumentation of multiple glacial fjords with oceanographic instruments, attempting to link terminus behavior to hydrographic conditions. The investigations are economically and logistically demanding, but the data sets and information will be invaluable and needed to gain insight into the heat exchange at the ice/ocean interface.

An alternative is to instrument fewer outlet glaciers more thoroughly. Much of the knowledge existing today about the mechanisms of outlet glacier flow has been gained by in-situ investigations of, e.g., Jakobshavn Isbræ. These field-based investigations are typically one or two decades old, and the technological advances made since then merits that similar studies be repeated today. Given the difficulties in quantifying the components of the hydrological budget of the outlet glaciers, a large unknown is the amount of basal water and the pressure conditions at the ice-bedrock interface. While remote-sensing methods can now accurately map the thickness and internal structuring of the outlet glaciers, near-terminus basal hydrology – and geology – is still left to be inferred from surface measurements of displacement. Although the instrumentation of the fjords will provide us with subsurface conditions at the terminus, drilling campaigns on the actual glacier trunk could yield valuable constraints on the amount of frictional heat generated, basal water pressure, strain conditions and ice temperature. Given the high

strain rates observed on these highly dynamic glaciers, drilling will be challenging and the development of new techniques may be necessary.

The need for several, parallel research strategies underscores the necessity of interdisciplinary collaborations. The coupled processes that together govern the flow of the Greenland outlet glaciers are complicated and knowledge from multiple fields such as geodesy, glaciology, oceanography, meteorology, and seismology must be combined to gain insight into these. This thesis is a product of one such cross-disciplinary effort.

In a warming climate, one concern is that the glaciers enter into a feedback cycle with mass loss at the front incurring faster flow by loss of buttressing resistance, again increasing mass loss. In order to build models that accurately predict this behavior, it is crucial to gain insight into the balance and robustness of the large outlet glaciers in a scenario of increasing calving and/or surface melt-water production.

Bibliography

- Ahlstrøm, A., S. Andersen, D. van As, M. Citterio, R. Fausto, S. Nielsen, H. Jepsen, S. Kristensen, E. Christensen, L. Stenseng, R. Forsberg, S. Hanson, and D. Petersen (2008), A new programme for monitoring the greenland ice sheet mass loss, *GEUS Bulletin Series: Review of Survey Activities*.
- Alley, R. B., M. Fahnestock, and I. Joughin (2008), CLIMATE CHANGE Understanding Glacier Flow in Changing Times, *Science*, 322(5904), 1061–1062, doi:{10.1126/science.1166366}.
- Amundson, J. M., M. Truffer, M. P. Luethi, M. Fahnestock, M. West, and R. J. Motyka (2008), Glacier, fjord, and seismic response to recent large calving events, Jakobshavn Isbrae, Greenland, *Geophysical Research Letters*, 35(22), L22501, doi:{10.1029/2008GL035281}.
- Amundson, J. M., M. Fahnestock, M. Truffer, J. Brown, M. P. Luethi, and R. J. Motyka (2010), Ice melange dynamics and implications for terminus stability, Jakobshavn Isbrae Greenland, *Journal of Geophysical Research, Earth Surface*, 115, doi:{10.1029/2009JF001405}.
- Andersen, M. L., T. Larsen, M. Nettles, P. Elosegui, D. van As, G. S. Hamilton, L. A. Stearns, J. L. Davis, A. P. Ahlstrøm, J. de Juan, G. Ekström, L. Stenseng, S. A. Khan, R. Forsberg, and D. Dahl-Jensen (2010), Spatial and temporal melt variability at Helheim Glacier, East Greenland, and its effect on ice dynamics, *Journal of Geophysical Research, Earth Surface* (in press).
- Anderson, R. S., S. P. Anderson, K. R. MacGregor, E. D. Waddington, S. O'Neel, C. A. Riihimaki, and M. G. Loso (2004), Strong feedbacks between hydrology and sliding of a small alpine glacier, *Journal of Geophysical Research*, 109, doi:{10.1029/2004JF000120}.
- Bartholomaus, T. C., R. S. Anderson, and S. P. Anderson (2008), Response of glacier basal motion to transient water storage, *Nature Geoscience*, 1(1), 33–37, doi:{10.1038/ngeo.2007.52}.

Bibliography

- Bartholomew, I., P. Nienow, D. Mair, A. Hubbard, M. A. King, and A. Sole (2010), Seasonal evolution of subglacial drainage and acceleration in a Greenland outlet glacier, *Nature Geoscience*, 3(6), 408–411, doi:{10.1038/NGEO863}.
- Benn, D. I., C. R. Warren, and R. H. Mottram (2007), Calving processes and the dynamics of calving glaciers, *Earth-science Reviews*, 82(3-4), 143–179, doi:{10.1016/j.earscirev.2007.02.002}.
- Bindschadler, R. (2006), Climate change - Hitting the ice sheets where it hurts, *Science*, 311(5768), 1720–1721, doi:{10.1126/science.1125226}.
- Bingham, R. G., P. W. Nienow, and M. J. Sharp (2003), Intra-annual and intra-seasonal flow dynamics of a High Arctic polythermal valley glacier, *Annals of Glaciology*, 37, 181–188.
- Björnsson, H. (1998), Hydrological characteristics of the drainage system beneath a surging glacier, *Nature*, 395(6704), 771–774.
- Bøggild, C. (2007), Simulation and parameterization of superimposed ice formation, *Hydrological Processes*, 21(12), 1561–1566, doi:{10.1002/hyp.6718}.
- Bøggild, C., R. Forsberg, and N. Reeh (2005), Meltwater retention in a transect across the Greenland ice sheet, in *Annals of glaciology, Annals of Glaciology*, vol. 40, edited by MacAyeal, DR, pp. 169–173.
- Boon, S., and M. Sharp (2003), The role of hydrologically-driven ice fracture in drainage system evolution on an Arctic glacier, *Geophysical Research Letters*, 30(18), doi:{10.1029/2003GL018034}.
- Braaten, D., S. Gogineni, D. Tammana, S. Namburi, J. Paden, and K. Gurumoorthy (2002), Improvement of radar ice-thickness measurements of Greenland outlet glaciers using SAR processing, in *Annals of Glaciology, vol. 35, Annals of Glaciology*, vol. 35, edited by Wolff, EW, pp. 73–78.
- Braithwaite, R. (1995), Positive degree-day factors for ablation on the Greenland Ice-sheet studied by energy-balance modeling, *Journal of Glaciology*, 41(137), 153–160.
- Budd, W. F., P. L. Keage, and N. A. Blundy (1979), Empirical studies of ice sliding, *Journal of Glaciology*, 23(89), 157–170.
- Chen, J. L., C. R. Wilson, and B. D. Tapley (2006), Satellite gravity measurements confirm accelerated melting of Greenland ice sheet, *Science*, 313(5795), 1958–1960, doi:{10.1126/science.1129007}.
- Clarke, T., and K. Echelmeyer (1996), Seismic-reflection evidence for a deep subglacial trough beneath Jakobshavns Isbrae, West Greenland, *Journal of Glaciology*, 42(141), 219–232.

- Das, S. B., I. Joughin, M. D. Behn, I. M. Howat, M. A. King, D. Lizarralde, and M. P. Bhatia (2008), Fracture propagation to the base of the Greenland Ice Sheet during supraglacial lake drainage, *Science*, 320(5877), 778–781, doi:{10.1126/science.1153360}.
- Dietrich, R., H.-G. Maas, M. Baessler, A. Ruelke, A. Richter, E. Schwalbe, and P. Westfeld (2007), Jakobshavn Isbrae, West Greenland: Flow velocities and tidal interaction of the front area from 2004 field observations, *Journal of Geophysical Research, Earth Surface*, 112(F3), doi:{10.1029/2006JF000601}.
- Echelmeyer, K., and W. D. Harrison (1990), Jakobshavn Isbræ, West Greenland: Seasonal variations in velocity – or lack thereof, *Journal of Glaciology*, 36(122), 82–88.
- Echelmeyer, K., T. S. Clarke, and W. D. Harrison (1991), Surficial glaciology of Jakobshavn Isbræ, West Greenland. Part I. Surface morphology, *Journal of Glaciology*, 37(127), 368–382.
- Ekström, G., M. Nettles, and G. Abers (2003), Glacial earthquakes, *Science*, 302, 622–624.
- Ekström, G., M. Nettles, and V. Tsai (2006), Seasonality and Increasing Frequency of Greenland Glacial Earthquakes, *Science*, 311, 1756–1758, doi:{DOI:10.1126/science.1122112}.
- Ettema, J., M. R. Van den Broeke, E. van Meijgaard, W. J. van de Berg, J. L. Bamber, J. E. Box, and R. C. Bales (2009), Higher surface mass balance of the Greenland ice sheet revealed by high-resolution climate modeling, *Geophysical Research Letters*, 36, L12501, doi:{10.1029/2009GL038110}.
- Fountain, A. (1989), The storage of water in, and hydraulic characteristics of, the firn of South Cascade Glacier, Washington State U.S.A., *Annals of Glaciology*, 13, 69–75.
- Fountain, A., and J. Walder (1998), Water flow through temperate glaciers, *Reviews of Geophysics*, 36(3), 299–328.
- Fountain, A. G., R. W. Jacobel, R. Schlichting, and P. Jansson (2005), Fractures as the main pathways of water flow in temperate glaciers, *Nature*, 433, 618–621.
- Fudge, T. J., J. T. Harper, N. F. Humphrey, and W. T. Pfeffer (2009), Rapid glacier sliding, reverse ice motion and subglacial water pressure during an autumn rainstorm, *Annals of Glaciology*, 50(52), 101–108.
- Funk, M., K. Echelmeyer, and A. Iken (1994), Mechanisms of fast flow in Jakobshavn Isbræ, West Greenland: Part II. Modeling of englacial temperatures, *Journal of Glaciology*, 40(136), 569–585.
- Georgiou, S., A. Shepherd, M. McMillan, and P. Nienow (2009), Seasonal evolution of supraglacial lake volume from ASTER imagery, *Annals of Glaciology*, 50(52), 95–100.

Bibliography

- Greuell, W., and T. Konzelmann (1994), Numerical Modeling of the energy balance and the englacial temperature of the Greenland Ice-sheet - calculations for the ETH-Camp location (West Greenland, 1155 m asl), *Global and Planetary Change*, 9(1-2), 91–114.
- Hanna, E., P. Huybrechts, I. Janssens, J. Cappelen, K. Steffen, and A. Stephens (2005), Runoff and mass balance of the Greenland ice sheet: 1958-2003, *Journal of Geophysical Research - Atmospheres*, 110(D13), D13108, doi:{10.1029/2004JD005641}.
- Harper, J. T., and N. F. Humphrey (1995), Borehole video analysis of a temperate glacier's englacial and subglacial structure: Implications for glacier flow models, *Geology*, 23(10), 901–904.
- Hock, R. (2005), Glacier melt: a review of processes and their modelling, *Progress in Physical Geography*, 29(3), 362–391.
- Holland, D. M., R. H. Thomas, B. De Young, M. H. Ribergaard, and B. Lyberth (2008), Acceleration of Jakobshavn Isbrae triggered by warm subsurface ocean waters, *Nature Geoscience*, 1(10), 659–664, doi:{10.1038/ngeo316}.
- Holtslag, A. A. M., and H. A. R. De Bruin (1988), Applied modeling of the nighttime surface-energy balance over land, *Journal of Applied Meteorology*, 27(6), 689–704.
- Howat, I. M., I. Joughin, and T. A. Scambos (2007), Rapid changes in ice discharge from Greenland outlet glaciers, *Science*, 315(5818), 1559–1561, doi:{10.1126/science.1138478}.
- Howat, I. M., B. E. Smith, I. Joughin, and T. A. Scambos (2008a), Rates of southeast Greenland ice volume loss from combined ICESat and ASTER observations, *Geophysical Research Letters*, 35(17), doi:{10.1029/2008GL034496}.
- Howat, I. M., S. Tulaczyk, E. Waddington, and H. Björnsson (2008b), Dynamic controls on glacier basal motion inferred from surface ice motion, *Journal of Geophysical Research*, 113, doi:{10.1029/2007JF000925}.
- Howat, I. M., I. Joughin, M. Fahnestock, B. E. Smith, and T. A. Scambos (2008c), Synchronous retreat and acceleration of southeast Greenland outlet glaciers 2000-06: ice dynamics and coupling to climate, *Journal of Glaciology*, 54(187), 646–660.
- Iken, A. (1981), The effect of the subglacial water pressure on the sliding velocity of a glacier in an idealized numerical model, *Journal of Glaciology*, 27(97), 407–421.
- Iken, A., and R. A. Bindschadler (1986), Combined measurement of subglacial water-pressure and surface velocity of Findelengletscher, Switzerland - conclusions about drainage system and sliding mechanism, *Journal of Glaciology*, 32(110), 101–119.

- Iken, A., H. Röthlisberger, A. Flotron, and W. Haerberli (1983), The uplift of Unteraar-gletscher at the beginning of the melt season - A consequence of water storage at the bed, *Journal of Glaciology*, 29(101), 28–47.
- Iken, A., K. Echelmeyer, W. Harrison, and M. Funk (1993), Mechanisms of fast flow in Jakobshavn Isbræ, West Greenland: Part I. Measurements of temperature and water-level in deep boreholes, *Journal of Glaciology*, 39(131), 15–25.
- Intergovernmental Panel on Climate Change (2007), *Fourth Assessment Report: Climate Change 2007: The Physical Science Basis*, Cambridge: Cambridge University Press.
- Jansson, P. (1995), Water-pressure and basal sliding on Storeglaciären, Northern Sweden, *Journal of Glaciology*, 41(138), 232–240.
- Jonsdottir, K., R. Roberts, V. Pohjola, B. Lund, Z. H. Shomali, A. Tryggvason, and R. Boovarsson (2009), Glacial long period seismic events at Katla volcano, Iceland, *Geophysical Research Letters*, 36, doi:{10.1029/2009GL038234}.
- Joughin, I. (2006), Climate change - Greenland rumbles louder as glaciers accelerate, *Science*, 311(5768), 1719–1720, doi:{10.1126/science.1124496}.
- Joughin, I., S. B. Das, M. A. King, B. E. Smith, I. M. Howat, and T. Moon (2008a), Seasonal speedup along the western flank of the Greenland Ice Sheet, *Science*, 320(5877), 781–783, doi:10.1126/science.1153288.
- Joughin, I., I. Howat, R. B. Alley, G. Ekstrom, M. Fahnestock, T. Moon, M. Nettles, M. Truffer, and V. C. Tsai (2008b), Ice-front variation and tidewater behavior on Helheim and Kangerdlugssuaq Glaciers, Greenland, *Journal of Geophysical Research - Earth Surface*, 113(F1), F01004, doi:10.1029/2007JF000837.
- Joughin, I., B. E. Smith, I. M. Howat, T. Scambos, and T. Moon (2010), Greenland flow variability from ice-sheet-wide velocity mapping, *Journal of Glaciology*, 56(197), 415–430.
- Kamb, B. (1987), Glacier surge mechanism based on linked cavity configuration of the basal water conduit system, *Journal of Geophysical Research - Solid earth and planets*, 92(B9), 9083–9100.
- Kamb, B., C. Raymond, W. Harrison, H. Engelhardt, K. Echelmeyer, N. Humphrey, M. Brugmann, and T. Pfeffer (1985), Glacier surge mechanism - 1982-1983 surge of Variegated Glacier, Alaska, *Science*, 227(4686), 469–479.
- Kamb, B., H. Engelhardt, M. A. Fahnestock, N. Humphrey, M. Meier, and D. Stone (1994), Mechanical and hydrologic basis for the rapid motion of a large tidewater glacier. 2. Interpretation, *Journal of Geophysical Research - Solid Earth*, 99(B8), 15,231–15,244.

Bibliography

- Krawczynski, M. J., M. D. Behn, S. B. Das, and I. Joughin (2009), Constraints on the lake volume required for hydro-fracture through ice sheets, *Geophysical Research Letters*, 36, doi:{10.1029/2008GL036765}.
- Legarsky, J., and H. Huang (2006), Detection of main channel thickness from radar data at Jakobshavn Isbrae, Greenland, *Journal of Glaciology*, 52(177), 315–317.
- Li, J. (2010), Mapping of ice sheet deep layers and fast outlet glaciers with multi-channel-high-sensitivity radar, (145), 201.
- Lliboutry, L. (1968), General theory of subglacial cavitation and sliding of temperate glaciers, *Journal of Glaciology*, 49, 21–58, doi:{}.
- Luckman, A., and T. Murray (2005), Seasonal variation in velocity before retreat of Jakobshavn Isbrae, Greenland, *Geophysical Research Letters*, 32(8), doi:{10.1029/2005GL022519}.
- Luckman, A., T. Murray, R. de Lange, and E. Hanna (2006), Rapid and synchronous ice-dynamic changes in East Greenland, *Geophysical Research Letters*, 33(3), L03503, doi:{10.1059/2005GL025048}.
- Luthi, M., M. Funk, A. Iken, S. Gogineni, and M. Truffer (2002), Mechanisms of fast flow in Jakobshavn Isbræ, West Greenland: Part III. Measurements of ice deformation, temperature and cross-borehole conductivity in boreholes to the bedrock, *Journal of Glaciology*, 48(162), 369–385.
- Luthi, M. P., M. Fahnestock, and M. Truffer (2009), Calving icebergs indicate a thick layer of temperate ice at the base of Jakobshavn Isbræ, Greenland, *Journal of Glaciology*, 55(191), 563–566.
- Luthje, M., L. T. Pedersen, N. Reeh, and W. Greuell (2006), Modelling the evolution of supraglacial lakes on the West Greenland ice-sheet margin, *Journal of Glaciology*, 52(179), 608–618.
- MacWhorter, M., and R. Weller (1991), Error in measurements of incoming shortwave radiation made from ships and buoys, *Journal of Atmospheric and Oceanic Technology*, 8(1), 108–117.
- Mair, D., P. Nienow, M. Sharp, T. Wohlleben, and I. Willis (2002), Influence of subglacial drainage system evolution on glacier surface motion: Haut Glacier d’Arolla, Switzerland, *Journal of Geophysical Research - Solid Earth*, 107(B8), doi:{10.1029/2001JB000514}.
- Meier, M., S. Lundstrom, D. Stone, B. Kamb, H. Engelhardt, W. W. Dunlap, M. Fahnestock, R. M. Krimmel, and R. Walters (1994), Mechanical and hydrologic basis for the rapid motion of a large tidewater glacier. 1. Observations, *Journal of Geophysical Research, Solid Earth*, 99(B8), 15,219–15,229.

- Meier, M. F., and A. Post (1987), Fast tidewater glaciers, *Journal of Geophysical Research - Solid Earth and Planets*, 92(B9), 9051–9058.
- Neave, K., and J. Savage (1970), Icequakes on Athabasca Glacier, *Journal of Geophysical Research*, 75(8), 1351–1362.
- Nettles, M., and G. Ekström (2010), Glacial Earthquakes in Greenland and Antarctica, *Annual Reviews of Earth and Planetary Science*, 38, 467–491, doi:{10.1146/annurev-earth-040809-152414}.
- Nettles, M., T. B. Larsen, P. Elósegui, G. S. Hamilton, L. A. Stearns, A. P. Ahlstrøm, J. L. Davis, M. L. Andersen, J. de Juan, S. A. Khan, L. Stenseng, G. Ekström, and R. Forsberg (2008), Step-wise changes in glacier flow speed coincide with calving and glacial earthquakes at Helheim Glacier, Greenland, *Geophysical Research Letters*, 35, L24503, doi:{10.1029/2008GL036127}.
- Nick, F. M., A. Vieli, I. Howat, and I. Joughin (2009), Large-scale changes in Greenland outlet glacier dynamics triggered at the terminus, *Nature Geoscience*, 2, 110–114, doi:{doi:10.1038/ngeo394}.
- O'Neel, S., and W. T. Pfeffer (2007), Source mechanisms for monochromatic icequakes produced during iceberg calving at Columbia Glacier, AK, *Geophysical Research Letters*, 34, doi:{doi:10.1029/2007GL031370}.
- O'Neel, S., H. P. Marshall, D. E. McNamara, and W. T. Pfeffer (2007), Seismic detection and analysis of icequakes at Columbia Glacier, Alaska, *Journal of Geophysical Research*, 112, doi:{10.1029/2006JF000595}.
- Paterson, W. S. B. (1994), *The Physics of Glaciers*, 3rd ed., Butterworth Heinemann.
- Paulson, C. A. (1970), The Mathematical Representation of Wind Speed and Temperature Profiles in the Unstable Atmospheric Surface Layer, *Journal of Applied Meteorology*, 9(6), 851–856.
- Quincey, D. J., and A. Luckman (2009), Progress in satellite remote sensing of ice sheets, *Progress in Physical Geography*, 33(4), 547–567, doi:{10.1177/0309133309346883}.
- Reeh, N. (1991), Parameterization of melt rate and surface temperature, *Polarforschung*, 59(3), 113–128.
- Rial, J. A., T. C., and S. K (2009), Glacial rumblings from Jakobshavn ice stream, Greenland, *Journal of Glaciology*, 55(191), 389–399, doi:{}.
- Rignot, E., and P. Kanagaratnam (2006), Changes in the velocity structure of the Greenland ice sheet, *Science*, 311(5763), 986–990, doi:{10.1126/science.1121381}.

Bibliography

- Rignot, E., J. E. Box, E. Burgess, and E. Hanna (2008), Mass balance of the Greenland ice sheet from 1958 to 2007, *Geophysical Research Letters*, 35(20), doi:{10.1029/2008GL035417}.
- Röthlisberger, H. (1972), Water pressure in intra- and subglacial channels, *Journal of Glaciology*, 11(62), 177–203.
- Schneider, T. (2000), Hydrological processes in the wet-snow zone of a glacier: A review., *Z. Gletscherkd. Glazialgeol.*, 36(1), 89–105.
- Shepherd, A., and D. Wingham (2007), Recent sea-level contributions of the Antarctic and Greenland ice sheets, *Science*, 315(5818), 1529–1532, doi:{10.1126/science.1136776}.
- Shepherd, A., A. Hubbard, P. Nienow, M. King, M. McMillan, and I. Joughin (2009), Greenland ice sheet motion coupled with daily melting in late summer, *Geophysical Research Letters*, 36, L01501, doi:{10.1029/2008GL035758}.
- Shreve, R. L. (1972), Movement of water in glaciers, *Journal of Glaciology*, 62, 205–214.
- Sneed, W. A., and G. S. Hamilton (2007), Evolution of melt pond volume on the surface of the Greenland Ice Sheet, *Geophysical Research Letters*, 34(3), doi:{10.1029/2006GL028697}.
- Sohn, H., K. Jezek, and C. Van der Veen (1998), Jakobshavn Glacier, West Greenland: 30 years of spaceborne observations, *Geophysical Research Letters*, 25(14), 2699–2702.
- Stearns, L. A., and G. S. Hamilton (2007), Rapid volume loss from two East Greenland outlet glaciers quantified using repeat stereo satellite imagery, *Geophysical Research Letters*, 34(5), L05503, doi:{10.1029/2006GL028982}.
- Steffen, K., and W. Abdalati (1996), Greenland Climate Network: GC-Net, *CRREL Spec. Rep. 96-27*, pp. 98–103.
- Straneo, F., G. S. Hamilton, D. A. Sutherland, L. A. Stearns, F. Davidson, M. O. Hamill, G. B. Stenson, and A. Rosing-Asvid (2010), Rapid circulation of warm subtropical waters in a major glacial fjord in East Greenland, *Nature Geoscience*, 3(3), 182–186, doi:{10.1038/NGEO764}.
- Thomas, R., E. Frederick, W. Krabill, S. Manizade, and C. Martin (2009), Recent changes on Greenland outlet glaciers, *Journal of Glaciology*, 55(189), 147–162.
- Tsai, V. C., and G. Ekstrom (2007), Analysis of glacial earthquakes, *Journal of Geophysical Research - Earth Surface*, 112(F3), doi:{10.1029/2006JF000596}.

- Tsai, V. C., J. R. Rice, and M. Fahnestock (2008), Possible mechanisms for glacial earthquakes, *Journal of Geophysical Research - Earth Surface*, 113(F3), doi:{10.1029/2007JF000944}.
- Van De Wal, R., and J. Oerlemans (1994), An energy-balance model for the Greenland Ice-sheet, *Global and Planetary Change*, 9(1-2), 115–131.
- van de Wal, R. S. W., W. Greuell, M. R. van den Broeke, C. H. Reijmer, and J. Oerlemans (2005), Surface mass-balance observations and automatic weather station data along a transect near Kangerlussuaq, West Greenland, in *Annals of Glaciology*, Vol. 42, 2005, *Annals of Glaciology*, vol. 42, edited by Dowdeswell, J and Willis, IC, pp. 311–316.
- Van de Wal, R. S. W., W. Boot, M. R. Van den Broeke, C. J. P. P. Smeets, C. H. Reijmer, J. J. A. Donker, and J. Oerlemans (2008), Large and rapid melt-induced velocity changes in the ablation zone of the Greenland Ice Sheet, *Science*, 321(5885), 111–113, doi:{10.1126/science.1158540}.
- van den Broeke, M., D. van As, C. Reijmer, and R. van de Wal (2004), Assessing and improving the quality of unattended radiation observations in Antarctica, *Journal of Atmospheric and Oceanic Technology*, 21(9), 1417–1431.
- Van den Broeke, M., P. Smeets, J. Ettema, C. van der Veen, R. van der Wal, and J. Oerlemans (2008), Partitioning of melt energy and melt water fluxes in the ablation zone of the west Greenland ice sheet, *The Cryosphere*, 2, 179–189.
- Van den Broeke, M., J. Bamber, J. Ettema, E. Rignot, E. Schrama, and W. J. van den Berg (2009), Partitioning Recent Greenland Mass Loss, *Science*, 326, 984–986, doi:{}.
- Van der Veen, C. J. (2007), Fracture propagation as means of rapidly transferring surface meltwater to the base of glaciers, *Geophysical Research Letters*, 34(1), doi:{10.1029/2006GL028385}.
- VanWormer, D., and E. Berg (1973), Seismic Evidence for Glacier Motion, *Journal of Glaciology*, 12(65), 259–265.
- Velicogna, I., and J. Wahr (2006), Acceleration of Greenland ice mass loss in spring 2004, *Nature*, 443(7109), 329–331, doi:{10.1038/nature05168}.
- Vieli, A., J. Jania, H. Blatter, and M. Funk (2004), Short-term velocity variations on Hansbreen, a tidewater glacier in Spitsbergen, *Journal of Glaciology*, 50(170), 389–398.
- Walder, J. S. (1986), Hydraulics of subglacial cavities, *Journal of Glaciology*, 32(112), 439–445.
- Walder, J. S., and A. Fowler (1994), Channelized subglacial drainage over a deformable bed, *Journal of Glaciology*, 40(134), 3–15.

Bibliography

- Walter, F., S. O'Neel, D. McNamara, W. T. Pfeffer, J. N. Bassis, and H. A. Fricker (2010), Iceberg calving during transition from grounded to floating ice: Columbia Glacier, Alaska, *Geophysical Research Letters*, 37, doi:{10.1029/2010GL043201}.
- Walters, R. A., and W. W. Dunlap (1987), Analysis of time-series of glacier speed – Columbia Glacier, Alaska, *Journal of Geophysical Research - Solid Earth and Planets*, 92(B9), 8969–8975.
- Warburton, J., and C. R. Fenn (1994), Unusual flood events from an alpine glacier – observations and deductions on generating mechanisms, *Journal of glaciology*, 40(134), 176–186.
- Weertman, J. (1957), On the sliding of glaciers, *Journal of Glaciology*, 3(21), 33–38.
- Zwally, H., W. Abdalati, T. Herring, K. Larson, J. Saba, and K. Steffen (2002), Surface melt-induced acceleration of Greenland ice-sheet flow, *Science*, 297(5579), 218–222.

Spatial and temporal melt variability at Helheim Glacier, East Greenland, and its effect on ice dynamics

M. L. Andersen^{1,2}, T. B. Larsen¹, M. Nettles³, P. Elosegui⁴,
D. van As¹, G. S. Hamilton⁵, L. A. Stearns⁶,
J. L. Davis⁷, A. P. Ahlstrøm¹, J. de Juan⁴, G. Ekström³,
L. Stenseng⁸, S. A. Khan⁸, R. Forsberg⁸, D. Dahl-Jensen²

Journal of Geophysical Research - Earth Surface (*in press*)

¹Geological Survey of Denmark and Greenland (GEUS), Copenhagen DK-1350, Denmark

²Centre for Ice and Climate, Niels Bohr Institute, Univ. of Copenhagen, Copenhagen DK-2100, Denmark

³Lamont-Doherty Earth Observatory, Columbia University, Palisades, NY 10964, USA

⁴Institute for Space Sciences (ICE) and Marine Technology Unit (UTM), CSIC, Barcelona, Spain

⁵Climate Change Institute, University of Maine, Orono, ME 04469, USA

⁶Department of Geology, University of Kansas, Lawrence, KS 66045, USA

⁷Harvard-Smithsonian Center for Astrophysics, Cambridge, MA 02138, USA

⁸DTU-Space, Technical University of Denmark, Copenhagen DK-2100, Denmark

Abstract

Understanding the behavior of large outlet glaciers draining the Greenland Ice Sheet is critical for assessing the impact of climate change on sea-level rise. The flow of marine-terminating outlet glaciers is partly governed by calving-related processes taking place at the terminus, but is also influenced by the drainage of surface runoff to the bed through moulins, cracks, and other pathways. To investigate the extent of the latter effect, we develop a distributed surface energy balance model (SEB) for Helheim Glacier, East Greenland, to calculate surface melt and thereby estimate runoff. The model is driven by data from an automatic weather station (AWS) operated on the glacier during the summers of 2007 and 2008, and calibrated with independent measurements of ablation. Modeled melt varies over the deployment period by as much as 68% relative to the mean, with melt rates approximately 77% higher on the lower reaches of the glacier trunk than on the upper glacier. We compare melt variations during the summer season to estimates of surface velocity derived from Global Positioning System (GPS) surveys. Near the front of the glacier,

there is a significant correlation (on $>95\%$ levels) between variations in runoff (estimated from surface melt) and variations in velocity, with a one-day delay in velocity relative to melt. Although the velocity changes are small compared to accelerations previously observed following some calving events, our findings suggest that the flow speed of Helheim Glacier is sensitive to changes in runoff. The response is most significant in the heavily crevassed, fast-moving region near the calving front. The delay in the peak of the cross-correlation function implies a transit time of 12-36 hours for surface runoff to reach the bed.

1 Introduction

In assessing climate change and its impact on sea-level rise, understanding changes in the flow dynamics of large outlet glaciers and ice streams is crucial. Flow speed variations occur on a variety of time scales, from minutes (*Amundson et al.*, 2008; *Nettles et al.*, 2008) to months (e.g., *Luckman and Murray*, 2005; *Joughin et al.*, 2008b) to years (e.g., *Luckman et al.*, 2006; *Howat et al.*, 2007; *Joughin et al.*, 2008c) and longer. It has recently been established that variations in conditions at the glacier terminus exert an important influence on glacier flow speed in Greenland (e.g., *Amundson et al.*, 2008; *Howat et al.*, 2008a; *Joughin et al.*, 2008c; *Nettles et al.*, 2008; *Nick et al.*, 2009), but less is known about how variations in surface melting influence outlet glacier dynamics. During the annual melt season, a fraction of the melt water produced at the surface evaporates and a fraction may run off the glacier via supraglacial channels. Part of the melt water also drains from the surface into the englacial hydrological system through crevasses and moulins. This system is likely to supply water to the bed of the glacier. Changes in this supply may affect the flow of the glacier by increasing the basal water pressure and reducing the effective pressure, creating a lubricating effect at the ice–bedrock interface. Although this effect has been established on alpine glaciers (e.g., *Iken and Bindschadler*, 1986; *Bartholomaus et al.*, 2008), and within the ice sheet (e.g., *Zwally et al.*, 2002; *van de Wal et al.*, 2008), its magnitude on fast flowing outlet glaciers in Greenland has not been studied extensively. In this study, we focus on the effect of runoff on the flow of Helheim Glacier, a large outlet glacier in East Greenland.

Melt studies conducted on glaciers have used a variety of techniques, depending on the timescale and available data. A frequently used technique is the positive degree-day (PDD) model, which employs a correlation between melt and periods with above zero-mean air temperatures (e.g., *Reeh*, 1991; *Braithwaite*, 1995). PDD methods require minimal input data and are therefore suitable for large areas and long time scales since few parameterizations need be made. *Hanna et al.* (2005) applied this technique to calculate runoff for the entire Greenland Ice Sheet at 5×5 km resolution and *Huybrechts et al.*

(1991) used the PDD method to project runoff for future warming scenarios. An alternative, physically-based, approach is to calculate the surface energy balance (SEB) and thus quantify the energy available for melt at the surface (Hock, 2005). Due to the greater requirement for observational input data, energy balance models typically are run for short time scales and small areas, although *van De Wal and Oerlemans* (1994) constructed an energy balance model for the entire Greenland Ice Sheet at 20 km resolution. Recent work (modeling as well as in-situ observations) has increased the performance and resolution of large scale energy balance models through improvements of regional climate models. These models can include an energy balance model at the ice-atmosphere boundary, as in the case of *Ettema et al.* (2009), which describes model runs over the Greenland Ice Sheet with an 11 km resolution.

Most of what is known about the general velocity behavior of glaciers in Greenland comes from space-based remote sensing studies, either for the whole ice sheet perimeter (e.g., *Rignot and Kanagaratnam* (2006)) or specific glacier catchment basins (e.g., *Stearns et al.*, 2005; *Luckman et al.*, 2006; *Howat et al.*, 2007; *Howat et al.*, 2008a; *Joughin et al.*, 2008c). A limitation of this approach is the low temporal resolution of most remote sensing products.

Ground-based melt and velocity studies have been conducted in Greenland by several authors, although almost exclusively on the ice sheet, not on outlet glaciers. *Zwally et al.* (2002) found indications of an association between surface generated melt water and the velocity of the ice sheet near Swiss Camp, north of Jakobshavn Isbræ. Near Kangerlussuaq, South West Greenland, *van de Wal et al.* (2008) observed velocity variations of up to 30% along the *K-transect* during the 2005-2006 melt season. In the same area, *Shepherd et al.* (2009) found increases of ice-sheet flow speed of up to 35% per positive degree-day of melting. While ground-based methods typically have very high temporal resolution, they suffer from the lack of spatial coverage of space- or airborne remote sensing techniques.

Joughin et al. (2008b) combined field observations with remote sensing data and noted a large and widespread influence of surface melt water on ice-sheet velocity, with smaller variations in outlet glacier velocity resulting from melt water lubrication. Those authors observed seasonal velocity increases of 50–100% (36–71 m yr⁻¹) on the ice sheet and 9–14% (51–77 m yr⁻¹) on regions defined as outlet glaciers.

Little is known about short-term velocity variations in outlet-glacier flow. *Amundson et al.* (2008) and *Nettles et al.* (2008) established a correlation between calving events and glacier acceleration at Jakobshavn and Helheim glaciers. However, no comprehensive study has investigated the link between changes in melt rates and near-terminus velocity variations on fast outlet glaciers. As the climate warms, understanding the influence of melt water becomes increasingly important for estimates of sea-level rise. In addition to

the direct effect of added freshwater runoff into the oceans, indirect effects such as the influence of melt water on ice flow speed must be considered.

Here, we develop a surface energy balance model for Helheim Glacier in East Greenland, utilizing data recorded by an automatic weather station (AWS) deployed on the glacier. We compare the pattern of melt variability derived from the SEB model with a velocity record derived from Global Positioning System (GPS) observations to assess the influence of daily variations in melt volume on glacier flow speed.

2 Data and methods

This study combines an observational and a modeling approach to study the effect of glacier melt variability on glacier dynamics. The observational component includes data from an AWS we deployed on the trunk of Helheim Glacier during the summers of 2007 and 2008, a network of 12-22 continuously operating GPS receivers also deployed across Helheim Glacier during the summers of 2007 and 2008, and standard stake-based ablation point measurements made at the locations of the GPS stations during their deployment, servicing and retrieval (Figure 1). We use the AWS data to calibrate and drive a SEB model for the snow-free ablation area of Helheim Glacier, and use this model to predict melt variations across the glacier during the summer seasons of 2007 and 2008. We then perform a cross-correlation analysis with the GPS velocity records to assess the influence of melt variations on glacier speed.

2.1 Surface Energy Balance model

We construct a surface energy balance model for the snow-free ablation area of Helheim Glacier, first developing the SEB model for a single point, corresponding to the location of our AWS. We then distribute the model across the glacier as described in section 2.2 below.

We quantify melt by determining the budget of energy fluxes to and from the surface, following standard methods (e.g., *van De Wal and Oerlemans, 1994; Hock, 2005; Hock and Holmgren, 2005; van As et al., 2005; van den Broeke et al., 2008*). In our case, the energy flux available for melt, Q_M , is determined by the balance of terms of the energy flux budget at the surface:

$$Q_M = Q_H + Q_E + Q_G + L_{SW} + L_{LW} + Q_R \quad (1)$$

which is calculated in hourly time steps.

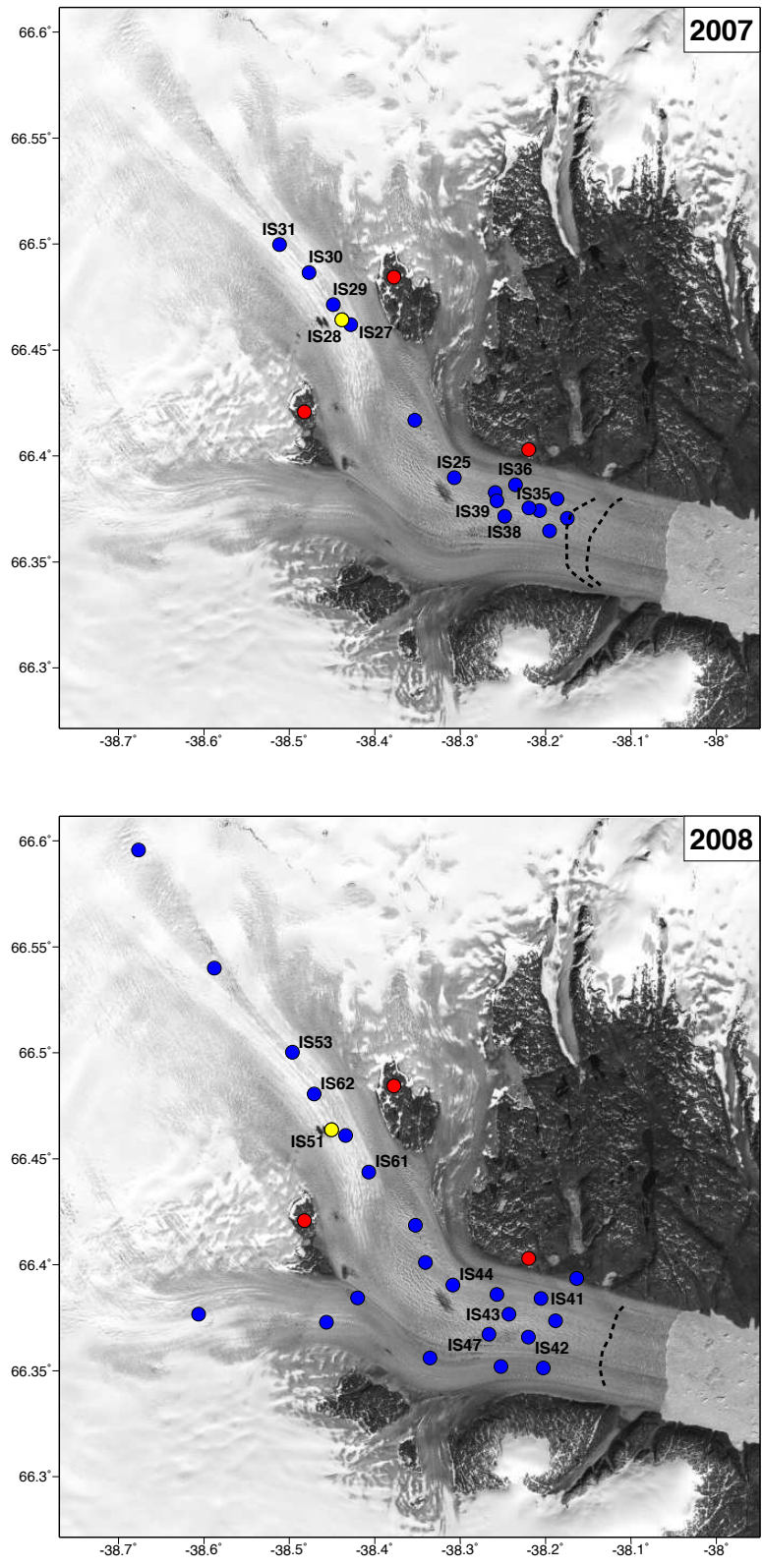


Figure 1: Map of AWS and GPS deployments 2007 (top) and 2008 (bottom) overlain on a 2001 LANDSAT image. Dots mark the position of (blue) GPS ice sites, (yellow) co-located AWS and GPS sites, and (red) GPS reference sites. GPS sites mentioned in the text are labelled. Dotted lines are calving front positions on (top) 4 July 2007 (westernmost) and 24 August 2007, both from MODIS 250-m images, and (bottom) 31 July 2008, from field observations.

The sensible heat flux, Q_H , is the turbulent transfer of heat resulting from a temperature difference between the surface and near-surface atmosphere. The latent heat flux, Q_E , is a function of the near-surface atmospheric vapor gradient and wind speed, giving the heat loss/gain caused by sublimation and evaporation.

Q_G is the subsurface heat flux, i.e., heat conducted to or from the surface through the ice column below. L_{SW} and L_{LW} are the net short wave and long wave radiative energy fluxes, respectively. Q_R is the energy added to the surface by rainfall, which in our case is set to zero, due to a lack of necessary data (see Section 2.1.2 below). The sign convention dictates that energy fluxes into the surface are positive, while fluxes directed away from the surface are negative.

The net short wave flux, L_{SW} , is the difference between the measured incoming short wave radiation at the AWS and the reflected short wave radiation found by applying an albedo value at each time step, as described below. The net long wave radiation, L_{LW} , is the difference between the incoming long wave radiation measured at the AWS and the outgoing long wave radiation calculated from the modeled surface temperature at each time step, assuming black-body properties.

The bulk aerodynamic method assumes that Q_H is a function of the air temperature gradient, and that Q_E is a function of the humidity gradient. In addition, both fluxes are proportional to wind speed. Assuming Monin-Obukhov similarity, the turbulent fluxes, Q_H and Q_E , can be approximated as:

$$Q_H = \rho c_p u_* \theta_* \quad (2)$$

$$Q_E = \rho L_v u_* q_* \quad (3)$$

where ρ is the air density, c_p is the specific heat capacity of air, and L_v is the latent heat of sublimation.

The friction velocity, u_* , in Eqs. 2 and 3 is given as:

$$u_* = \frac{k u_{z_w}}{\ln\left(\frac{z_w}{z_0}\right) - \psi_{m2} + \psi_{m1}} \quad (4)$$

where k is Von Karman's constant, u_{z_w} is measured wind speed at height z_w , and z_0 is the roughness length scale for momentum. ψ_{m1} and ψ_{m2} are momentum stability correction functions.

The virtual potential temperature scale, θ_* , in Eq. 2 is:

$$\theta_* = \frac{k(\theta_v - T_s)}{\ln\left(\frac{z_{tmp}}{z_t}\right) - \psi_{h2} + \psi_{h1}} \quad (5)$$

where z_{tmp} is the height at which temperature is measured, z_t is the roughness scale for temperature, θ_v is the virtual temperature and T_s is the surface temperature. ψ_{h1} and ψ_{h2} are temperature stability correction functions.

The turbulent scale of humidity, q_* , in Eq. 3 is given by:

$$q_* = \frac{k(q(z_{hum}) - q(0))}{\ln\left(\frac{z_{hum}}{z_q}\right) - \psi_{q2} + \psi_{q1}} \quad (6)$$

where z_{hum} is the height at which humidity is measured and z_q is the roughness length scale for humidity. ψ_{q1} and ψ_{q2} are humidity stability correction functions.

The stability-correction functions ψ_{m1} , ψ_{m2} , ψ_{h1} , ψ_{h2} , ψ_{q1} , and ψ_{q2} in equations 4, 5, and 6 are adopted from *Paulson (1970)* and *Holtslag and De Bruin (1988)* for stable and unstable conditions, respectively.

We calculate the subsurface heat flux, Q_G , using a one-dimensional finite-difference solution of the heat equation, such that the energy flux to the surface from the first layer below the surface is proportional to the temperature difference between the two layers. Q_G -energy fluxes are calculated at 15 minute intervals for 200 layers, each 0.05 m thick, i.e., for a 10 m deep ice column. The layer thickness is chosen to provide sufficient resolution to represent small vertical variations while the number of layers is chosen to ensure that the base of the column is only weakly affected by diurnal variations, and to keep calculations stable. The top layer in the ice column is fixed at the modeled surface temperature at each time step and the bottom layer has the temperature of the layer immediately above it. The bottom boundary condition implies that we only evaluate the effect of heat storage and release in the upper ice column. The net transfer to and from the lower glacier is not considered. The model is initialized using an observed summer temperature profile from the TAS-U station maintained by the Programme for Monitoring of the Greenland Ice Sheet (PROMICE; <http://www.promice.dk>) at a site ~ 100 km south of Helheim Glacier and at a similar altitude to our AWS. The effective conductivity is assumed constant in ice and set to $2.2 \text{ WK}^{-1}\text{m}^{-1}$. The ice density is set to 917 kg m^{-3} .

Short wave penetration into the ice causing subsurface heating, and possibly melt, cannot be ignored over a melting ice surface (e.g., *van den Broeke et al., 2008*). For the short wave fraction not reflected by the surface we therefore apply an exponential absorption for the flux in the ice column, according to Beer's law with an extinction coefficient of 1.4 for ice (*Greuell and Konzelmann, 1994*). The resulting contribution is added to the temperature profile used in the solution of the heat equation described above. In cases where the subsurface temperature reaches the melting point, we calculate melt from the excess energy flux and add this to the melt produced at the surface.

The surface temperature, T_s , is the only remaining unknown parameter. Following, e.g., *van den Broeke et al. (2008)*, we determine T_s by an iterative process in each timestep,

assuming balance in the energy budget. For solutions in which $T_s > 0^\circ\text{C}$, T_s is set to the melting point, leaving a residual energy flux available for melt (if $Q_M > 0$).

With the quantities in the energy budget determined, the corresponding surface ablation rate, M , (in m s^{-1}) is:

$$M = \frac{Q_M}{\lambda \rho_{ice}} \quad (7)$$

where λ is the latent heat of fusion ($3.35 \cdot 10^5 \text{ J kg}^{-1}$) and ρ_{ice} is the density of ice. The melt water generated by ablation in the model is assumed to run off the surface instantaneously.

2.1.1 AWS observations

We drive the surface energy balance model using meteorological measurements recorded at Helheim Glacier. We deployed an AWS on a relatively slow-moving section ($\sim 12 \text{ m d}^{-1}$) of the glacier trunk (Figure 1). The AWS collected continuous data (Figure 2) at a rate of one sample per hour for a total of 27 days in the summer of 2007, and 49 days in the summer of 2008. To facilitate inter-annual comparisons, we endeavored to occupy approximately the same glacier location with the AWS during both deployments. The station locations (approximately 66.42N , 38.44W , 640 m a.s.l.), were within 650 m distance and 20 m elevation of each other, with the second year lower than the first.

The AWS recorded standard meteorological parameters including wind speed and direction, aspirated air temperature, snow surface height, short and long wave radiative fluxes (incoming and reflected), station tilt, and surface ablation. Wind speed and direction were measured with a Young 05103-5 wind vane, aspirated temperature and relative humidity were measured using a combined fan ventilated Rotronic PT100 temperature probe and an S3 hygroclip, accurate to 0.1 K and 1% , respectively. Radiative fluxes were measured with a Kipp & Zonen CNR1 net radiometer with a specified accuracy of 10% on daily totals. Sensors were mounted on a tripod at heights of $2.8\text{--}3.2 \text{ m}$. The untethered AWS lowered with the ablating surface. The surface ablation measurement is crucial for evaluating the SEB model performance and was made on a separate rig with stakes drilled $>5 \text{ m}$ into the ice, to avoid self-drilling. Snow height and ablation were measured with two Campbell SR50 sonic rangers, each accurate to 1 cm .

The air density, ρ_{air} , a parameter in the turbulent flux calculations, depends in part on the barometric pressure. Barometric pressure was not measured at the AWS, but daily values measured in the nearby town of Tasiilaq ($\sim 100 \text{ km}$ from Helheim glacier) are available from the Danish Meteorological Institute (<http://www.dmi.dk/dmi/index/gronland/vejrkarkiv-gl.htm>). These measurements were interpolated linearly in time to obtain hourly values and were then spatially extrapolated to the station altitude using the baro-

metric equation. When the DMI record was incomplete, missing values were set to mean values of the past 5 years for the day in question.

Measurements of near-surface air temperature and ablation were not acquired in 2007 due to instrument malfunctions. The temperature record for 2007 was therefore reconstructed using the casing temperature from the CNR1 radiometer, which operated throughout the season. A simple equation relating observed aspirated air temperature, T_{asp} , to casing temperature T_{CNR1} , short wave radiation SW_{in} and windspeed U was used:

$$T_{asp} = a T_{CNR1} + b SW_{in} + c U + d \quad (8)$$

and a least squares solution was found using the 2008 data. The solution yielded coefficients a , b , c , and d which were then used to calculate an aspirated temperature record for 2007 (shown in Figure 2). For the 2008 record the postfit root-mean-square (RMS) residual was 1 K, approximately one order of magnitude larger than the quoted error of the PT100 temperature probe (0.1 K). This residual represents 13% of the range of the values measured (8.3 K). We adopt the value of 1 K as an estimate of the error for the reconstructed 2007 temperature record, and include this record in our analysis. Independent ablation measurements at the AWS also failed during almost all of 2007, leaving only one automatically measured value at the end of the time-series available for model validation. Hourly data values were successfully acquired for all other parameters.

Prior to implementation in the SEB model, the data are edited for gaps and outliers. Incoming short wave radiation measurements are sensitive to the tilt of the instrument and are therefore corrected based on tilt measurements using a standard algebraic transformation (e.g., *MacWhorter and Weller, 1991*). We also perform a number of other standard corrections, including correction of the sonic ranger ablation measurements for variations in the speed of sound with air temperature. The measured albedo at the AWS site is also smoothed with a running ± 12 hr average.

2.1.2 Perturbation analysis for SEB error assessment

Errors in the SEB model arise from measurement errors in the input data and inaccuracies in assumptions made in the model calculations. Following *van As et al. (2005)*, we use a simplified sensitivity analysis to characterize the effect of parameter perturbations on SEB model output. Specifically, we alter all measured values (relative humidity, net short wave flux, net long wave flux, aspirated temperature, wind speed and direction, and barometric pressure) with the quoted uncertainties from the instrument documentation, positive and negative, about the measured values. We do this with one parameter at a time while fixing all remaining parameters to unperturbed values, for all GPS station locations and the AWS site, and record the difference with respect to the unper-

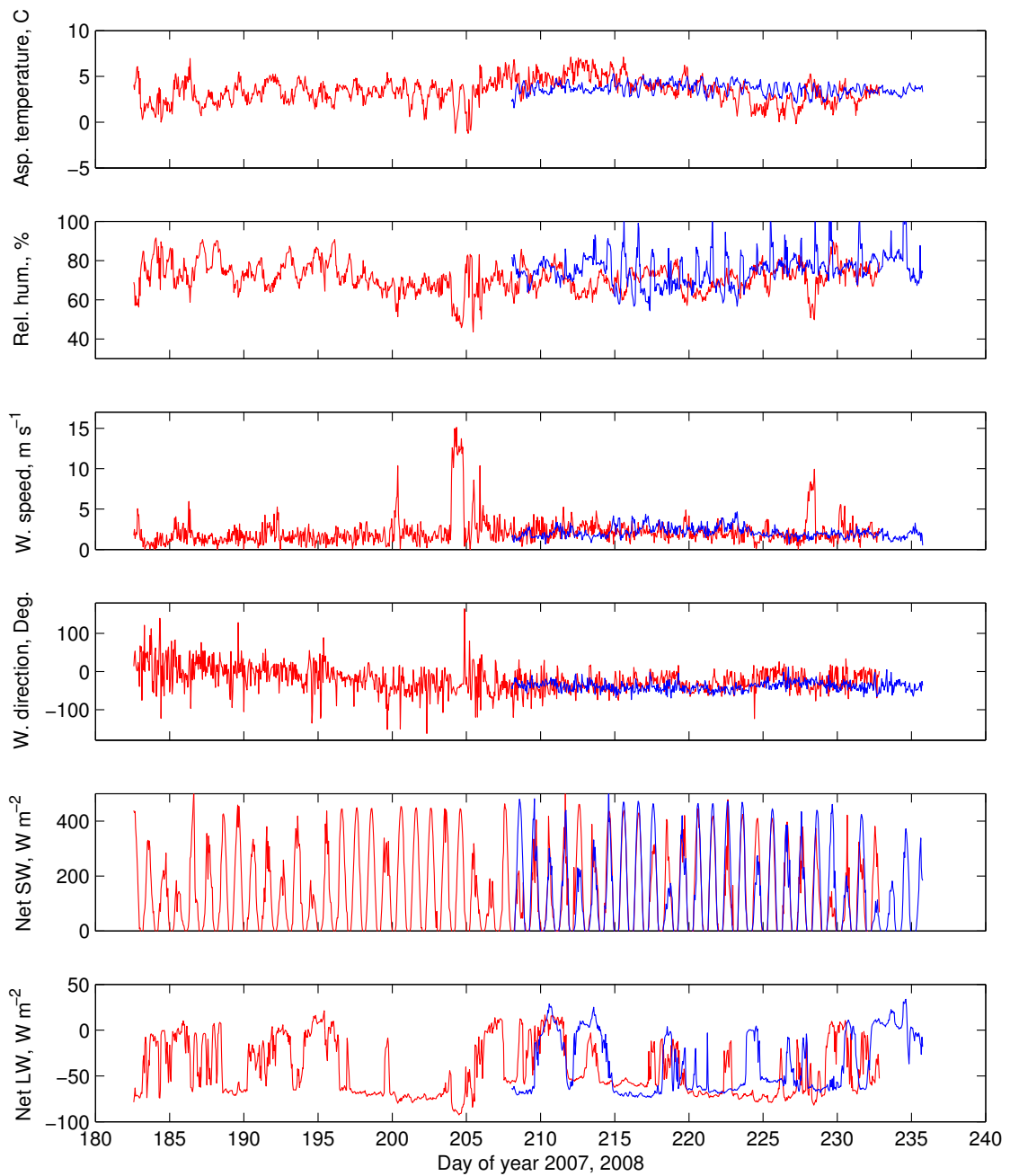


Figure 2: Time series of meteorological parameters measured by the AWS in (blue) 2007 and (red) 2008. Aspirated temperature is modeled for 2007 (see text). Wind direction is plotted in the interval $[-180, 180]$ degrees from N with positive values increasing clockwise.

turbed model solution. For each location, we thereby generate a set of 14 perturbed melt model outputs (i.e., two per each of the seven measurable parameters above), which we group into those yielding more melt than the unperturbed solution and those yielding less melt. Upper and lower error bounds on the melt are then calculated by forming, independently for each (positive and negative) group, the RMS of the residuals of the perturbed melt outputs relative to the unperturbed model melt solution. The resulting (positive and negative) errors thus calculated are not exactly symmetric because the SEB model is not linear on the perturbed parameters, the small-number statistics involved, or both. (A fully comprehensive error analysis such as in a Monte Carlo-type simulation is deemed unnecessary.)

In our analysis the net short wave component is perturbed with the $\pm 10\%$ value provided by Kipp & Zonen as the uncertainty for daily totals measured with the CNR1 net radiometer. However, *van den Broeke et al.* (2004), testing the same sensor, found the actual error value to be $<5\%$. The application of maximum perturbation values and the method of accumulating the errors in each time step leads to a conservative (i.e., large) error estimate for each time step and for the cumulative melt, with the maximum error always carried over from one time step to the next.

Energy added to the surface by rainfall is not included due to the lack of a precipitation record from Helheim Glacier. A sensitivity study using the Tasiilaq rain record was performed, and revealed very low energy fluxes (mean contribution to the energy budget was $\sim 0.25 \text{ W m}^{-2}$). We therefore do not include this effect, nor do we consider the added runoff caused by rain water. While the added runoff from rainfall has been shown to affect sliding velocity (e.g., *Howat et al.*, 2008b), applying the Tasiilaq precipitation record at Helheim Glacier is not justified. Anecdotal field observations show strongly changing weather conditions over the $\sim 100 \text{ km}$ between the locations.

2.2 Distributed Surface Energy Balance calculations

We distribute the SEB spatially by discretizing the glacier surface in $500 \text{ m} \times 500 \text{ m}$ model cells, and calculating the energy flux available for melt (Q_M) in each cell. The distributed SEB model is run for the full periods for which data are available for 2007 and 2008 (days of year 208-235 for 2007, days of year 182-232 for 2008). All cells within the model domain with altitudes above 1000 m a.s.l. , or located on rock outcrops, are masked to isolate the potential melt area. All cells are assumed snow-free, i.e., not contributing to runoff by way of snow melt. Field observations from early July 2008 (at the beginning of the data collection, which was earlier than in 2007) support this assumption.

2.2.1 Digital Elevation Model

Several of the input parameters for the SEB model are altitude dependent. We obtain altitudes for the model cells using a digital elevation model (DEM) of Helheim Glacier constructed using the method described in *Stearns and Hamilton* (2007). We use an ASTER image acquired on 30 August 2006 and smoothed to 500 m grid spacing, using nearest neighbor interpolation.

Geolocation information is derived from the satellite ephemeris information contained in the image header file and has an uncertainty of approximately 50 m. The DEM uncertainties are a combination of systematic errors and random errors due to satellite positioning, image acquisition geometry, and atmospheric conditions. Elevations from GPS point measurements on Helheim Glacier made at the time of the 30 August 2006 image acquisition are used to assess the accuracy of the ASTER DEM (*Stearns*, 2007). The absolute elevation error (RMS difference) of the 30 August 2006 DEM is 16.9 m, most of which is due to a systematic bias in the DEM. When this bias is removed, the RMS difference drops to 6.5 m.

2.2.2 Albedo

A large component of the total energy budget is the net short wave energy flux, L_{SW} , which is the sum of the incoming and the reflected short wave radiation. The incoming component was measured at the AWS and is assumed uniform across the model domain. The reflected component is determined from multiplication of the incoming component with the reflectivity (albedo). We acquire daily albedo values for all model cells in the grid using Moderate Resolution Imaging Spectroradiometer (MODIS) observations. For 2007 and 2008, 44 and 58 scenes are selected from the MOD10A1 Daily Snow Albedo product (*Hall et al.*, 2007; *Hall et al.*, 2008), respectively. To avoid extrapolation near the beginning and end of the experiment, scenes from outside the deployment periods are also included. The selected scenes are re-projected onto an equal-area regular grid for analysis. Daily values are thus acquired on a cell-by-cell basis. In the case of partly cloud-covered images, which cause occasional data gaps for one or more cells, values are linearly interpolated in time from the last known albedo value of the relevant cell. The longest data gaps are 4-5 consecutive days for the majority of the model domain. Helheim Glacier exhibits large spatial variations in albedo caused by highly crevassed areas and melt water lakes. By using the position-specific values from the MODIS pixels we capture this variation in the model to within a $500 \text{ m} \times 500 \text{ m}$ resolution.

Stroeve et al. (2006) evaluated the accuracy of the MOD10A1 albedo product. They found that in the accumulation zone there was a good correlation with field observations, while

in the ablation zone, the correlation was somewhat lower. In a few particular instances, we observe daily differences between MODIS and observed albedo of up to $\sim 20\%$ with the MODIS pixel having an unrealistically high value. However, an analysis of albedo for the cell containing the AWS reveals an average difference between measured and MODIS derived albedo of only $\sim 3\%$ for 2007 and $\sim 6\%$ for 2008 (Figure 3). A possible source of this offset is the difference in spatial averaging between the point measurement at the AWS and the $500\text{ m} \times 500\text{ m}$ MODIS tile. It is unclear why the higher MODIS values are most pronounced early in the season, although the changing solar angle during the measurement period may play a role, as discussed by *Stroeve et al.* (2006). The correlation between the MODIS albedo, interpolated to hourly values, and the ± 12 hours-smoothed albedo measured by the AWS is significant at $>95\%$ levels, indicating that the temporal variation in the signal is captured well.

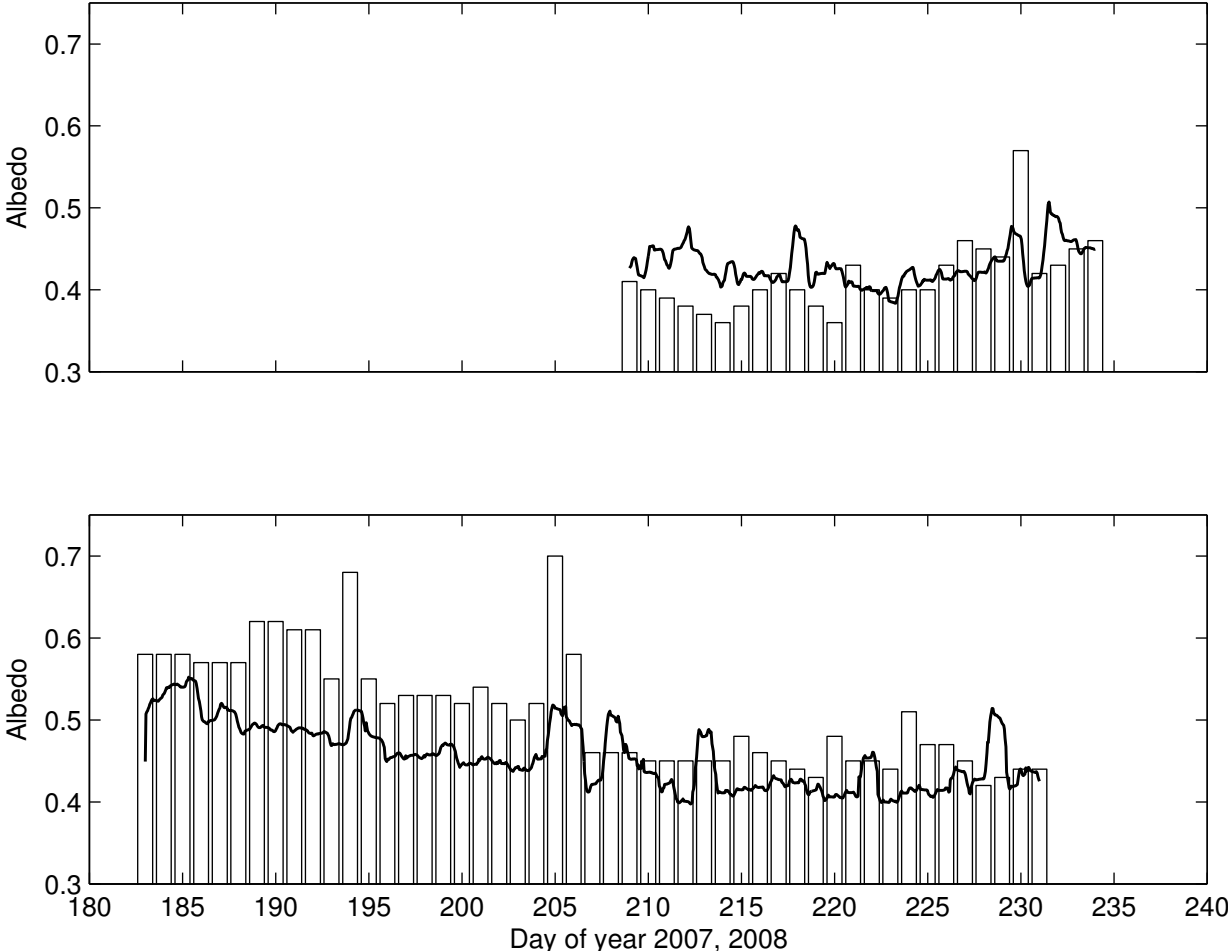


Figure 3: (bars) MODIS derived and (curve) measured albedos in (top) 2007 and (bottom) 2008 in the model cell where the AWS was deployed.

2.2.3 Other parameterizations

The DEM derived altitudes are used to parameterize values of aspirated near surface air temperature T_{asp} . We use an adiabatic lapse rate of 6.3 K km^{-1} based on an average of June, July and August lapse rates from eight transects along the Greenland Ice Sheet (Mernild *et al.*, 2008). Values for the roughness length for momentum, z_0 , have large variability in the literature. Brock *et al.* (2006) find values for z_0 in the range 0.92–5.47 mm for an alpine glacier while Munro (1989) finds a value of 2.44–2.48 mm for glacier ice. Meesters *et al.* (1997) determine a value of 0.3 mm for a melting Greenland ice surface, while Greuell and Konzelmann (1994) observe $z_0=3.2$ mm for the Swiss Camp location on the West Greenland ice sheet. We have no direct knowledge of the spatial or temporal variation of z_0 across Helheim Glacier so instead we calibrate z_0 to the value of 4 mm, which is consistent with cited values and matches the measured and modeled ablation at the AWS site (see Section 3.1.1).

As in Hock and Holmgren (2005), relative humidity, RH, is assumed homogenous across the glacier and set to the value measured at the AWS. Given the spatial scale of the glacier (the total modeled area is $\sim 515 \text{ km}^2$), and the common surface characteristics (melting ice) in all cells, this assumption should be reasonable. In addition, RH over a melting ice surface is expected to be close to saturation most of the time, counteracting large vertical gradients.

Incoming long and short wave radiation is also assumed to be uniform across the model domain. However, in each time step the incoming short wave radiation for all model cells is corrected for shading from surrounding topography and surface element azimuths facing away from the sun, again based on the DEM.

Wind speed in the model cells is affected by local topography, providing sheltered as well as exposed areas. Given the topographic variability within the model domain, and that we only have wind speed observations from one point on the glacier, we opt to apply a simple, slope- and curvature-dependent parameterization of wind speed as described in Liston and Elder (2006). The process adjusts the wind speed in each time step for all model cells, depending on the wind direction relative to the terrain slope, slope azimuth, and curvature.

2.3 Stake measurements

During the deployment of GPS receivers, we embedded aluminum stakes into the ice at each site. The stakes were drilled to a depth of 3 to minimize additional self-drilling. Exposed stake heights were measured during installation, during a mid-season servic-

ing visit, and during retrieval. These measurements yield average melt rates over the periods between observation. In most cases each site had two stakes installed for the main part of the deployment, providing two values, which we average here.

The accuracy of our observations is significantly lower than with usual stake experiments. This error arises from the field conditions, in particular the tendency of the hollow, non-capped aluminum stakes to melt into the hole walls and tilt, effectively lowering the observed melt rate. Moreover, the stake measurements are not from randomly chosen sites, and are not necessarily representative of the model cell in which they were placed. Field safety considerations dictated site selection, with the mostly flat, exposed surfaces contributing to the non-random nature of the stake sites. On a smaller scale, irregular surface conditions around the stakes also introduce a potential measurement error. In some cases measured heights for two stakes at the same site yielded melt rates up to 30% different. Therefore, while we make a quantitative comparison between stake heights and modeled melt rates, we also assign a relatively high uncertainty of 30% to the stake data.

2.4 Glacier surface velocity

We deployed a network of 12-22 continuously recording GPS receivers on Helheim Glacier during the summers of 2007 and 2008 for 54 days and 55 days, respectively. Dual-frequency Trimble 5700 and NetRS receivers collected data at sampling intervals of 1-5 seconds. Daily velocities were calculated by fitting a linear model to position estimates determined kinematically, as described in *Nettles et al.* (2008). Each season's network extended over the length of the glacier trunk, including locations within a few km of the calving front (Figure 1).

For this study, several processing steps are performed on the daily velocity time series for 2007 and 2008. The largest changes in daily glacier velocity are associated with glacial earthquakes (*Nettles et al.*, 2008), and appear in the record as step-like increases in velocity on the days of the earthquakes. In order to assess the influence of melt, we subtract this increase (i.e., the velocity difference between the day of the earthquake and the next) from all days following an earthquake in the GPS velocity record. We then remove the mean, and a single, best-fitting linear trend from the timeseries for each GPS station; the latter accounts approximately for the effects of advection of the station through the glacier flow field. While more sophisticated techniques could be employed for de-trending the data (e.g. *Amundson et al.*, 2008) this simple method is adequate for our current analysis.

For the dates on which maintenance visits occurred, we substitute the average speed

from the days before and after to avoid incorporating artificial antenna displacements. In cases of data gaps, we assign the mean station velocity of the season. Uncertainties for the velocity estimates are approximately 0.1 m d^{-1} (Nettles *et al.*, 2008).

To simplify our analysis, we distinguish between stations near the front (downstream) and those farther upstream. A cross correlation of daily velocity estimates between 2007 front stations IS25, IS35, IS36, IS38, and IS39 (see map in Figure 1a) demonstrates sufficient similarity between records that we can select one station record as representative of this area. An average correlation coefficient of 0.78 (significant at the 95% level or higher) is found when correlating IS25 with IS35, IS36, IS38, and IS39 respectively. Therefore, IS25 is picked as representative for the front stations, since it has the longest record. A similar spatial pattern is observed for 2008, where we find average correlation coefficients of 0.97 when correlating the front station IS41 with IS42, IS43, IS44, and IS47. Hence, IS41 is picked as representative for front velocity behavior for 2008.

Unlike the downstream stations, melt records from upstream stations (2007: IS27, IS28, IS29, IS30, IS31; 2008: IS51, IS53, IS61, IS62) are somewhat dissimilar (not shown), perhaps due to their larger altitude difference. Therefore, individual stations of interest are selected for comparison with the melt signal.

3 Results

3.1 Validation of SEB model

To evaluate the SEB model, in this section we first analyze the atmospheric conditions and melt at the AWS site, and then compare the SEB melt rates with in situ, stake-based measurements of ablation.

3.1.1 Meteorological conditions and melt at the AWS site

Values measured at the AWS show many similarities between 2007 and 2008, and some notable differences (Figure 2). The relative humidity measured in 2007 exhibits a daily cycle that is not evident in 2008, except in days 193-198 with a somewhat lower amplitude. The wind speed is comparable for the two years and aspirated temperatures are also similar for both years, even though the 2007 temperature record was synthesized, not observed, as described above in section 2.1.1. The net short wave radiation is slightly higher in 2007 than 2008, indicating more frequent clear skies. Measurements of net short wave radiation from both years follow the expected daily cycle. Amplitudes

of 2007 net long wave radiation resemble those observed in 2008.

In 2008 an anomaly occurs on day 204, lasting for 17 hours (0100-1800 UTC). During this period, the hourly averaged wind speed reaches $\sim 15 \text{ m s}^{-1}$. Low relative humidity values and the lowest aspirated air temperatures of the 2008 experiment were recorded during this time interval, indicating a katabatic wind event. The mean wind direction during this period is 315° , which is not an anomaly, but supports this interpretation. During this event, the large scale atmospheric forcing was most likely aligned with the common katabatic force, favoring stronger winds than usual within the period. No similar events were observed for 2007.

The average daily energy fluxes calculated from the SEB for the AWS site in 2008 are shown in Figure 4. The katabatic wind event on day 204 is clearly seen in the sensible and latent heat fluxes. There is a strong increase in sensible heat flux as a consequence of above average wind speed, and the latent heat flux drops due to the lower humidity gradient over the surface. In spite of high net short wave and sensible heat fluxes, melt is generally low during this event, since the positive fluxes are balanced by the strongly negative latent heat flux.

The net short wave flux is a large component in the flux budget (Figure 4) so it is not unexpected that the available melt energy flux Q_M is closely correlated with the net short wave radiative flux L_{SW} . Maximum melt in 2008 occurs on day 212 after a period of four days with increasing melt.

A total ablation of 1.59 m is modeled at the AWS site for 2008 over the ~ 50 days of observation. For 2007 the total modeled melt for the 27 day deployment is 0.89 m. Considering only the days of year where the two records overlap, this yields similar melt rates for the two years of $\sim 3.2 \text{ cm d}^{-1}$.

The SEB model's performance in the grid cell occupied by the AWS in 2008 is shown in Figure 5. The choice of $z_0 = 4 \text{ mm}$ described in section 2.2.3 minimizes the average difference between measured and modeled ablation, but does not change the shape of the melt curve. The shapes of the melt curves match well, indicating satisfactory performance in capturing changes in melt rates over the season. Panel (b) in Figure 5 shows the difference between modeled and measured melt throughout the 2008 deployment. The largest difference occurs on day 222, when the observed ablation was $\sim 4 \text{ cm}$ higher than the modeled amount. The average difference throughout the deployment is 0.5 cm.

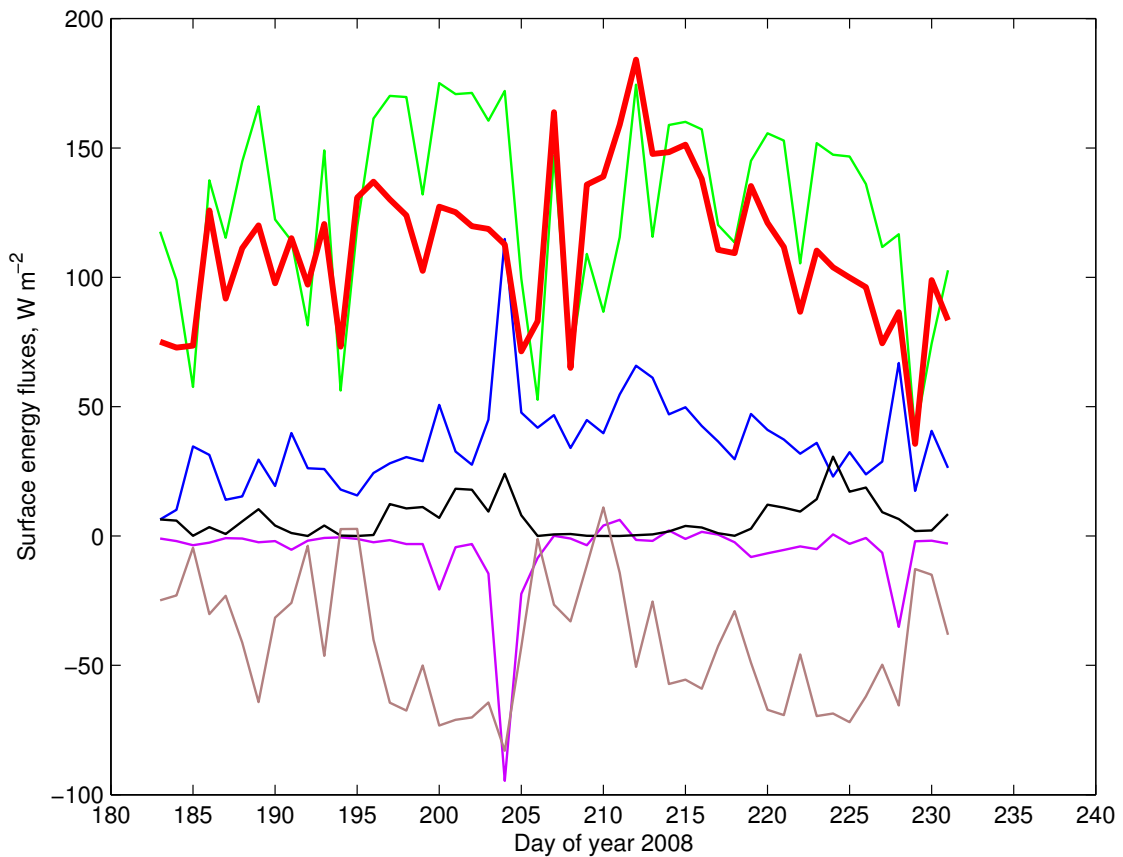


Figure 4: Daily average surface energy fluxes in 2008 at the AWS site for (blue) sensible heat, (purple) latent heat, (black) subsurface heat, (green) net short wave radiation, (brown) net long wave radiation, and (red, bold) total energy flux available for melt. (See Eq. 1).

3.1.2 Comparison between modeled melt and stake measurements

In 2007, the modeled melt is 0.89 m at the location of the AWS (Figure 5). To measure ablation over the same period, we combined two measurements of ice-surface height relative to the structure of the AWS. The first measurement is an estimate made from photographs of the AWS taken at the time of its deployment. The second is a distance measurement from the AWS sonic ranger obtained at the end of the occupation, on day of year 235 (i.e., 23 August 2007). Unfortunately, the sonic ranger record is missing, except for that day, due to instrument malfunction. Figure 5 shows that the measured ablation (0.85 ± 0.15 m) is consistent with the modeled ablation, 0.89 m. The large uncertainty quoted is due to having resorted to using photographs, which are of significantly lower precision than the sonic ranger. The 2008 sonic ranger record is complete and also plotted in Figure 5 together with one independent stake measurement, made on a field visit on day 213. Bias relative to the stake measurements in both years is consistent, i.e., positive but within the error bars.

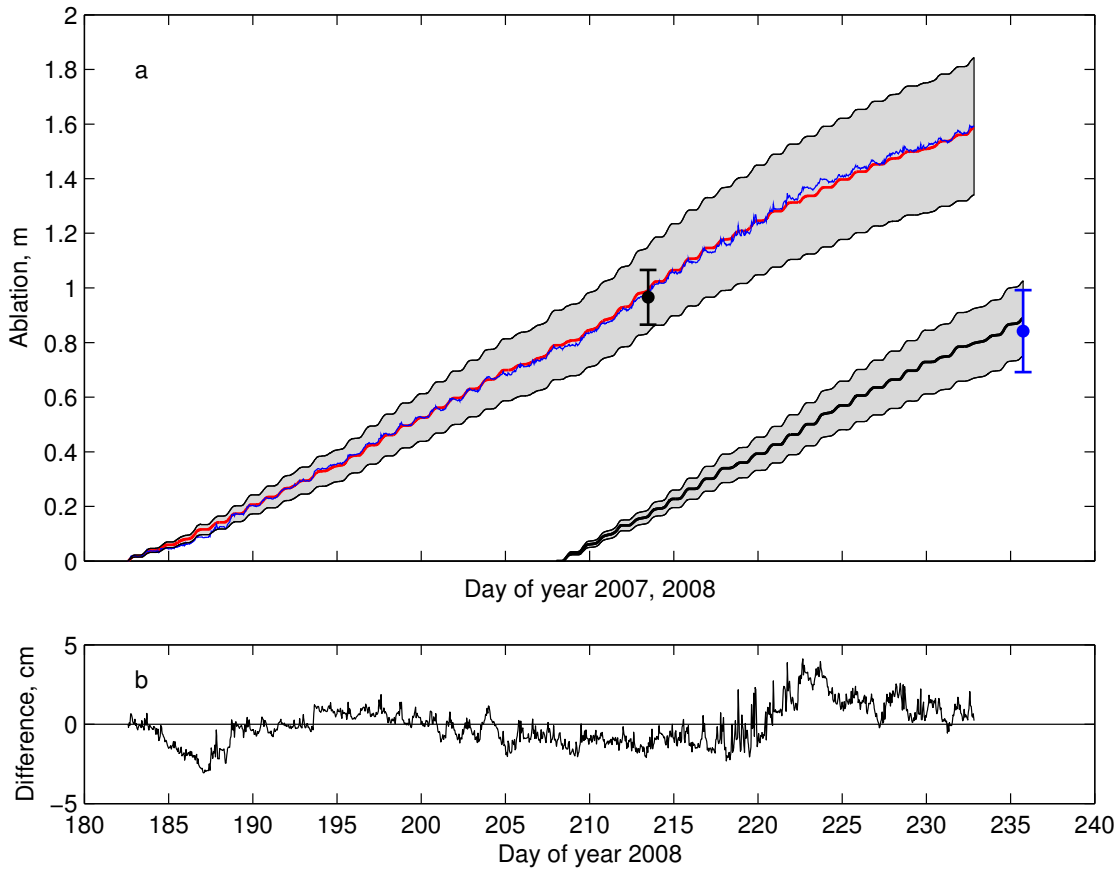


Figure 5: (a) Ablation at model cell corresponding to AWS location. Cumulative ablation for (red) 2008, as calculated by the model, (blue) ablation measured, 2008, by the sonic ranger. Curves are very similar and overlie each other. Black dot with ± 10 cm errorbar is an independent stake measurement of ablation made on a field visit on day 213, 2008. The jagged nature of the measured data plot around days 217-223, 2008, is suspected to result from thermal or wind effects on the sensor. Black curve is cumulative ablation for 2007 as calculated by the model. Blue dot with ± 15 cm error bar is the only existing automatic sonic ranger measurement. The error bar is the error on the initial mounting height of the sensor at deployment time, 2007, as estimated from photos of the AWS. Shaded area is propagated uncertainty determined by perturbing all measured parameters with uncertainty values provided by instrument manufacturers (see Section 2.1.2). (b) Difference between cumulative measured and modeled melt as a function of time, 2008. Note the change in scale.

We now evaluate the ability of the SEB model to capture spatial variation across Helheim Glacier by comparing modeled melt rates to stake measurements made at the sites occupied by GPS receivers. This comparison focuses on 19 GPS station locations of the 2008 data set, since the AWS record from that year is more complete than that from 2007. The average measured melt rate at the 19 locations is $3.3 \pm 1 \text{ cm d}^{-1}$. The relatively large uncertainty associated with the measured melt rates is discussed in section 2.3. Figure 6 shows the modeled and observed melt rates at the 19 sites. Of the 19 sites, observed melt rates at 11 sites are consistent with the modeled melt rates in the same locations within the assigned error. Interestingly, the remaining eight sites (plotted in red) are clustered at low elevation where we expect self-drilling to be most prevalent. The horizontal error bars (i.e., those associated with the modeled melt rates) show the mean of the daily errors calculated as per the error analysis described in Section 2.1.2. The errors on the modeled melt rates are within $\pm 13\%$ of the unperturbed model solution.

3.2 Spatial distribution of surface melt

To investigate the model's ability to capture local variations in melt, separate records are extracted for the grid cells within which the GPS data were recorded. The average positions of each GPS receiver during the deployment are used to identify these cells, which are located both up- and downstream of the AWS.

3.2.1 Integrated melt

Figure 7 shows the 2007 and 2008 results for the distributed grid, plotted as average melt rates in millimeters per day, water equivalent ($\text{mm d}^{-1} \text{ w.e.}$). Helheim Glacier exhibits a large altitudinal gradient in melt. Mean melt in the front area is $\sim 63\text{-}77\%$ higher than at the upper sites, with average melt rates of $39 \text{ mm d}^{-1} \text{ w.e.}$ and $41 \text{ mm d}^{-1} \text{ w.e.}$ for 2007 and 2008, respectively, over the whole deployment period.

Selected results of the 2007 model run are shown in Figure 8. Figure 8a shows, for the area in Figure 7a, the temporal variation in total melt over the model region ("07Integrated") both in absolute daily volumes and relative to a mean of $1.5 \times 10^7 \text{ m}^3 \text{ d}^{-1} \text{ w.e.}$ Two distinct periods of increasing melt followed by an abrupt termination are evident, one from day 213 to 217 and one from 220 to 223. Near the end of the deployment period, two single days of large negative deviations from the mean occur on days 230 and 232.

Day-to-day variations in melt in 2008 (relative to the mean for the integrated melt over the model domain, $1.4 \times 10^7 \text{ m}^3 \text{ d}^{-1} \text{ w.e.}$) are as much as $+68\%$ and -64% (melt record

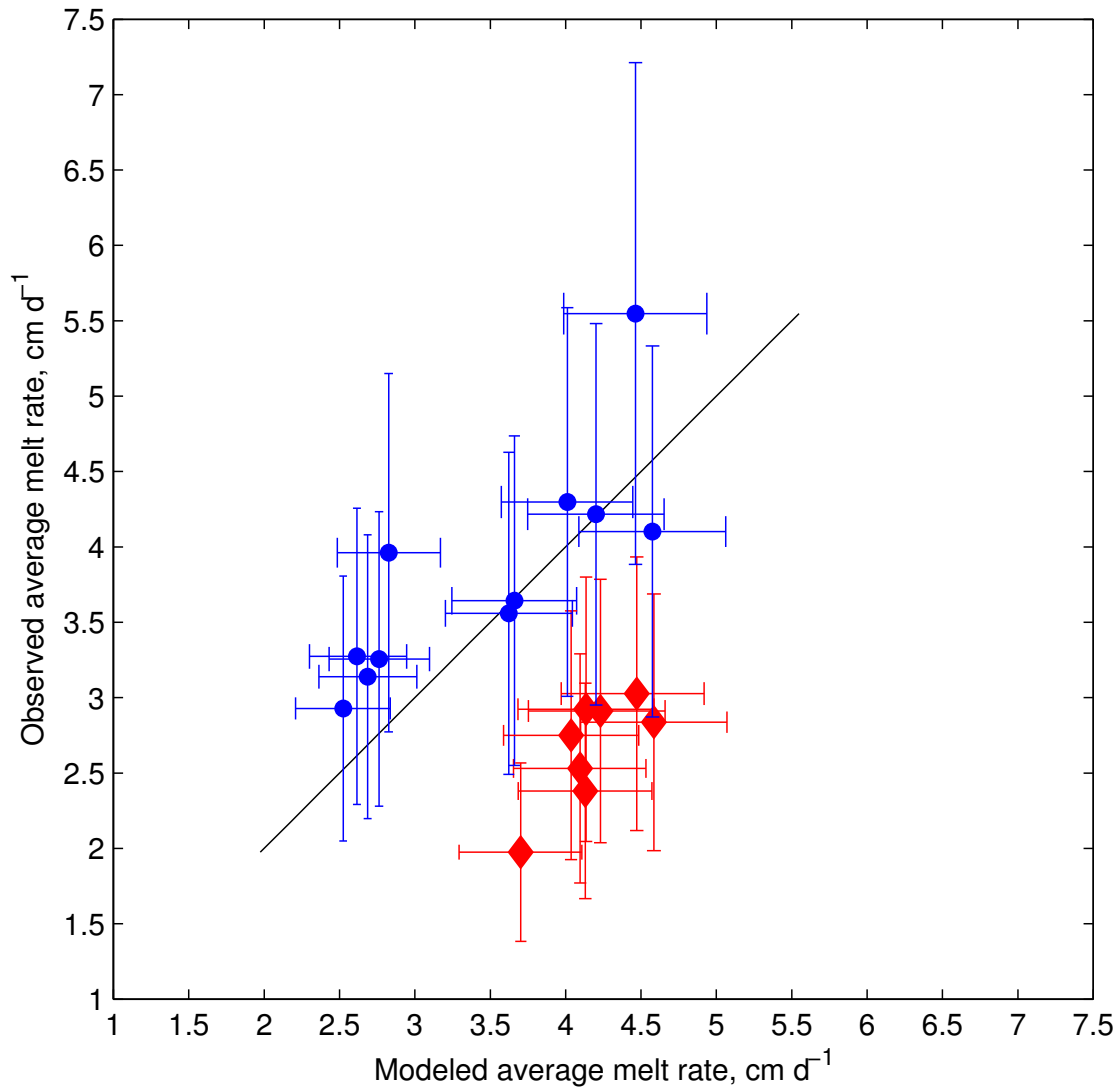


Figure 6: Comparison between measured and modeled melt rates in the model cells where stake measurements were made in 2008. Errors of 30% of the individual measurements are assigned to the stake measurements to account for local variability. Horizontal error bars are errors calculated from the perturbation analysis described in Section 2.1.2. Black line traces the values where modeled and observed melt rates are equal. Modeled melt rates that are not statistically consistent with the observed melt rates are plotted with red diamonds. All stations in this group are located in the front cluster, the area where we expect self-drilling to be most prevalent.

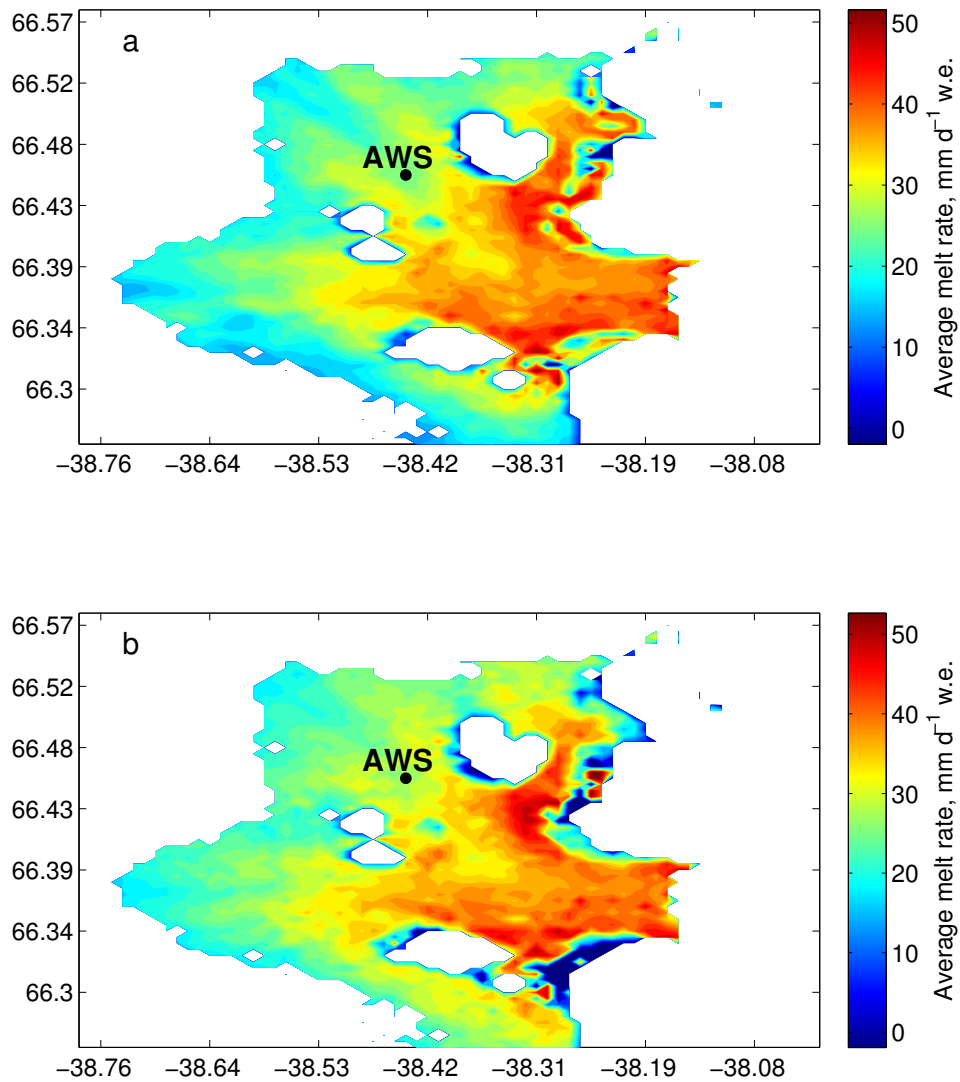


Figure 7: (a) Days of year 208-235, 2007. (b) Days of year 182-232, 2008. Black dot indicates position of AWS. Geographic coordinates designate model gridpoint intersections with ticks for every 10 model cells in each direction. Error in estimated values is typically $\pm 11-13\%$ (see Section 3.2.1).

“08Integrated” shown in Figure 9a). A period with small variations around the mean lasts from the beginning of the deployment until day 210. A clear build-up and peak in melting then occurs from day 210 to 219, peaking at day 212. The peak on day 212 (68% higher than the mean) is the highest daily melt in the deployment. This is followed by a period of below-average melt, lasting until the end of the time series.

The assigned error bars in Figures 8a and 9a are averages of the daily errors determined at the 16 specific sites for 2007 and 19 sites for 2008, calculated as a percentage of the average daily melt at these sites. The means of this percentage (i.e., the error) are $\pm 11\%$ and $\pm 13\%$, for 2007 and 2008 respectively.

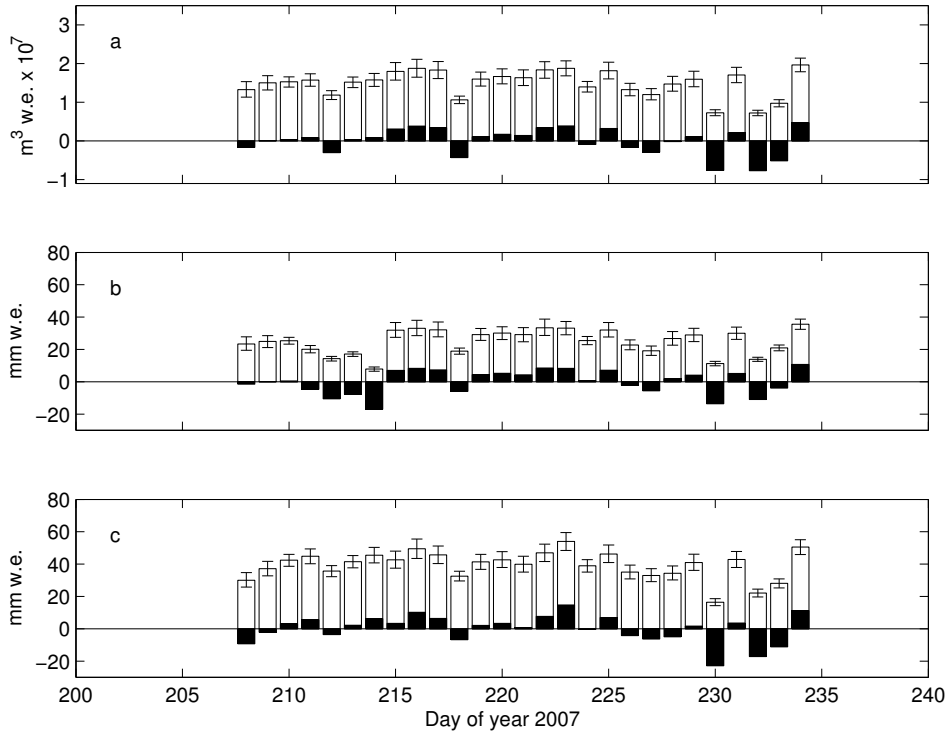


Figure 8: Melt in absolute quantities (white bars) with error bars calculated from the sensitivity analysis (see Section 2.1.2), and melt relative to mean (black bars), 2007. (a) Integrated melt over entire model domain (record 07Integrated), with mean value $1.5 \times 10^7 \text{ m}^3 \text{ d}^{-1} \text{ w.e.}$ (b) Melt calculated in upstream model cell containing average position of GPS station IS30 (record 07upstream), with mean value $24.8 \text{ mm d}^{-1} \text{ w.e.}$ (c) Melt calculated in downstream model cell containing average position of GPS station IS35 (record 07downstream), with mean value $39.3 \text{ mm d}^{-1} \text{ w.e.}$

3.2.2 Local melt records

For 2007 and 2008, we consider a number of local melt records corresponding to the grid cells containing the average position of a given GPS receiver throughout the deployment. We select locations both up- and downstream (2007: IS30 and IS35, respectively; 2008: IS53 and IS42, respectively) (Figure 1). The corresponding melt estimates are “07upstream”, “07downstream”, “08upstream”, and “08downstream”, respectively. For model calibration purposes, we also calculate a melt record for the model cell containing the AWS, termed “08AWS”.

Figures 8b and 8c show melt records 07upstream and 07downstream, which overall are quite similar. Melt fluctuations from the mean are slightly larger in the 07downstream record with a maximum deviation from the mean of 58%, while the upstream maximum is 55%. Other subtle differences are also evident in the records. For example, melt increases strongly from day 214 to 215 upglacier, while no change (within error bars) is observed at the front during the same time period.

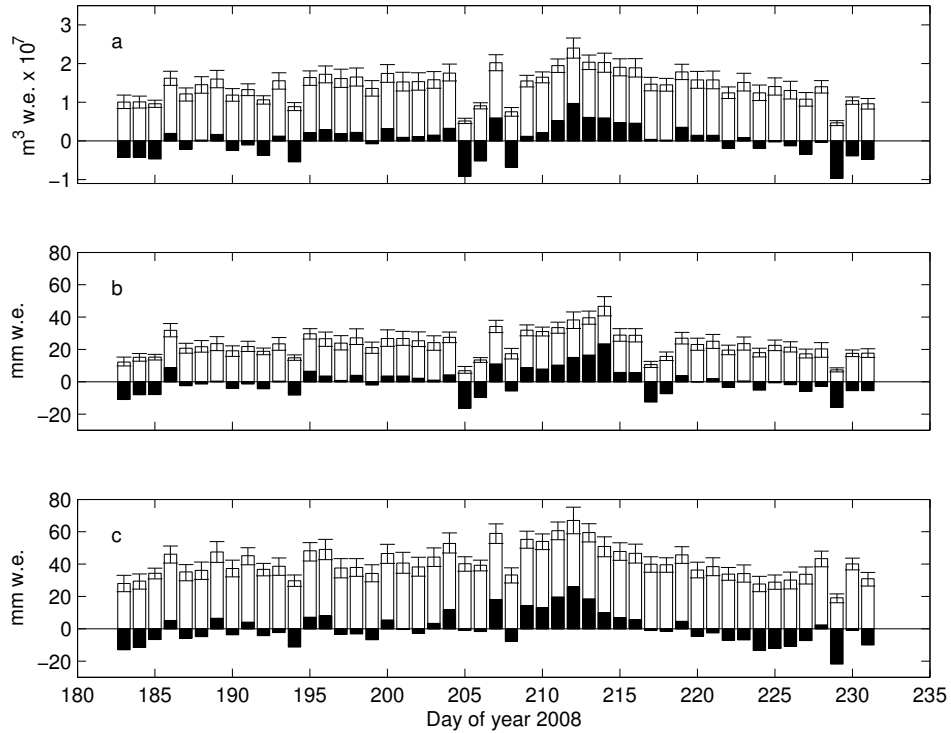


Figure 9: Melt in absolute quantities (white bars) with error bars calculated from the sensitivity analysis (see Section 2.1.2), and melt relative to mean (black bars), 2008. (a) Integrated melt over entire model domain (record 08Integrated), with mean value $1.4 \times 10^7 \text{ m}^3 \text{ d}^{-1} \text{ w.e.}$ (b) Melt calculated in upstream model cell containing average position of GPS station IS53 (record 08upstream), with mean value $23.1 \text{ mm d}^{-1} \text{ w.e.}$ (c) Melt calculated in downstream model cell containing average position of GPS station IS42 (record 08downstream), with mean value $41 \text{ mm d}^{-1} \text{ w.e.}$

Similar characteristics are also noted in the 2008 upstream and downstream melt records (Figures 9b and 9c). Here, smaller-scale differences are also apparent. For example, the peak melting occurs two days earlier (day 212) at the downstream site compared to the upstream site (day 214).

In general, for both years, the pattern of melt calculated at specific locations resembles the pattern seen in the total melt across the glacier.

Mean daily errors upstream are -3.1 and $+3.3 \text{ mm w.e.}$ for 2007 and -3.4 and $+3.5 \text{ mm w.e.}$ for 2008 (Figures 8b and 9b), corresponding to approximately $\pm 13\%$ and $\pm 15\%$ of mean melt in the upstream locations, respectively. Mean daily errors downstream are -4.3 and $+4.4 \text{ mm w.e.}$ for 2007 and -5.3 and $+5.0 \text{ mm w.e.}$ for 2008 (Figures 8c and 9c), corresponding to $\pm 11\%$ and $\pm 13\%$ of mean downstream melt, respectively.

3.3 Comparison of melt rates and ice speed variations

We investigate the potential effect of runoff on flow speed through statistical analyses of the modeled melt records and the observed surface velocities. For 2007 and 2008 we perform local cross-correlation analyses of upstream melt estimates (07upstream/08upstream) with upstream velocity records, and the downstream melt estimates (07downstream/08downstream) with downstream velocity records. We also correlate estimates of the total melt, integrated across the entire model domain (07Integrated/08Integrated) to the front area velocities. Finally, we perform a similar analysis using the estimated 2008 melt record from the AWS site (08AWS) since the AWS was co-located with a GPS receiver to within 20 m.

In a qualitative sense, we observe that when the melt is above the mean, the velocity also tends to be above the mean, as can be seen in the top two panels of Figures 10 and 11. This pattern is borne out quantitatively by the results of the cross-correlation analysis.

3.3.1 Summer of 2007

Figure 10a shows the temporal variation of the integrated surface melt record (07Integrated, in blue), the upstream record (07upstream, in red), and the downstream record (07downstream, in green) with respect to mean values of $1.5 \times 10^7 \text{ m}^3 \text{ d}^{-1}$ w.e., 24.8 mm d^{-1} w.e., and 39.3 mm d^{-1} w.e., respectively (see Figure 7). To facilitate comparison between signals, melt variations in the figure are normalized relative to the maximum amplitude in each zero-mean time series. Figure 10b shows the temporal variation of GPS-derived ice velocity for three representative glacier sites (blue for the downstream trunk, green for the front, and red for the upstream sites). Speeds are shown as deviations from the mean, which are 15.6 , 23.2 , and 12.9 m d^{-1} , respectively. Figure 10c shows correlation coefficients for several values centered around zero lag between matching pairs, that is, between the 07Integrated melt and the ice speed of the frontal station, the 07downstream melt and the speed of the downstream station, and 07upstream melt and the upstream station speed.

The largest correlation coefficients r that result from testing these records for the effect of surface melt on ice speed variations are $r=0.68$, 0.42 , and 0.42 , respectively. The correlation coefficients for all three cases peak when the velocity is delayed by one day relative to surface melt. (There is a secondary, local maximum at negative delays for the 07upstream/upstream correlation. However, correlation values at negative time delays, which are included for completeness, have no physical meaning.) To evaluate the statistical significance of these correlation values, we first calculate autocorrelation functions for surface melt variations and speed variations to assess the degree of independence,

or randomness, of those samples. These tests reveal a decorrelation time of two days; we define decorrelation time as the lag beyond which the autocorrelation function falls within the values of a normally-distributed function at the 95% confidence limit. Therefore, we reduce the degrees of freedom available to calculate significance from 27, the total number of samples, to 13. The p-values for the three correlation coefficients, using 13 degrees of freedom and a one-tailed test (warranted by the hypothesis that ice velocity does not affect surface melt), are $p=0.0068$, 0.0595 , and 0.0595 , respectively, indicating significant correlations for all three comparisons at $>90\%$ levels (IS25, IS30, and IS35), and $>99\%$ levels for the comparison involving the integrated melt and ice speed of the downstream trunk area (IS25).

3.3.2 Summer of 2008

Results for the summer of 2008 are consistent with those of 2007. Figure 11 shows surface melt variations (panel a), ice velocity variations (panel b), and the correlation values (panel c) for the comparison of melt records with their respective velocity records. There is a maximum positive correlation coefficient of $r=0.57$ in the 08Integrated/front area station comparison. As in 2007, the maximum correlation coefficient peak occurs when the velocity signal lags the melt signal by one day. The local comparisons yield correlation coefficients of $r=0.53$ for 08downstream/downstream station and $r=0.11$ for the 08AWS/AWS station, also with a one-day delay producing the highest r-value. While notably smaller than at the sites on the lower glacier, there is also a distinguishable peak around this coefficient where the surrounding correlation coefficients (± 1 day relative to the peak) are $r=-0.09$ and $r=-0.05$, respectively. In the 08upstream/upstream station correlation, an r-value of 0.46 occurs with a one-day delay, consistent with the results at the front of the glacier.

As in the 2007 records, the autocorrelations of surface melt and ice velocity signals yield a decorrelation time of two days, or a total of ~ 24 degrees of freedom for the $N=49$ data points (days) in the original records. Since the resulting p-values for the comparisons discussed above are $p = 0.0012$, $p = 0.0027$, $p = 0.2963$, and $p = 0.009$, respectively, they reveal correlation coefficients for a one-day delay that are all statistically significant on $>99\%$ levels for all but the 08AWS/AWS velocity record comparison.

4 Discussion

In general, melt/velocity correlation coefficients are comparable for the two years of observation. All comparisons in 2007 and 2008 yield the highest correlation coefficients

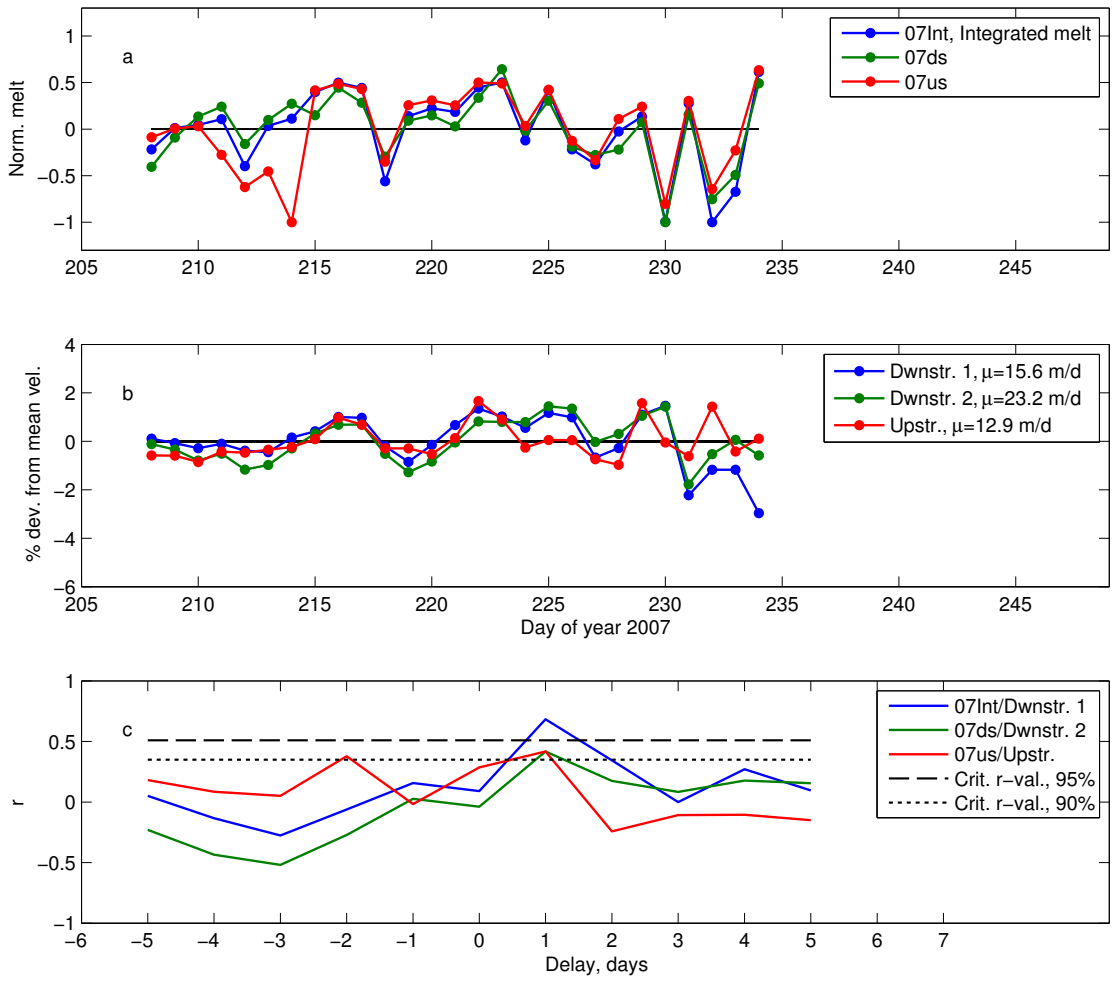


Figure 10: Comparisons of melt and velocity, 2007: (a) Melt signals 07Integrated, 07downstream, and 07upstream. All signals are plotted as deviation from mean and normalized relative to maximum amplitude for comparison. (b) Deviations from mean measured surface speed at downstream GPS site 1 (IS25), downstream GPS site 2 (IS35), and upstream GPS site (IS30) in %. (c) Correlation coefficients for comparisons 07Integrated/downstream 1, 07downstream/downstream 2, and 07upstream/upstream. Dashed line is critical r value ($r = 0.51$) for significance at the 95% level, dotted line is critical r value ($r = 0.35$) for significance at the 90% level. Both with 13 degrees of freedom, one-tailed distribution.

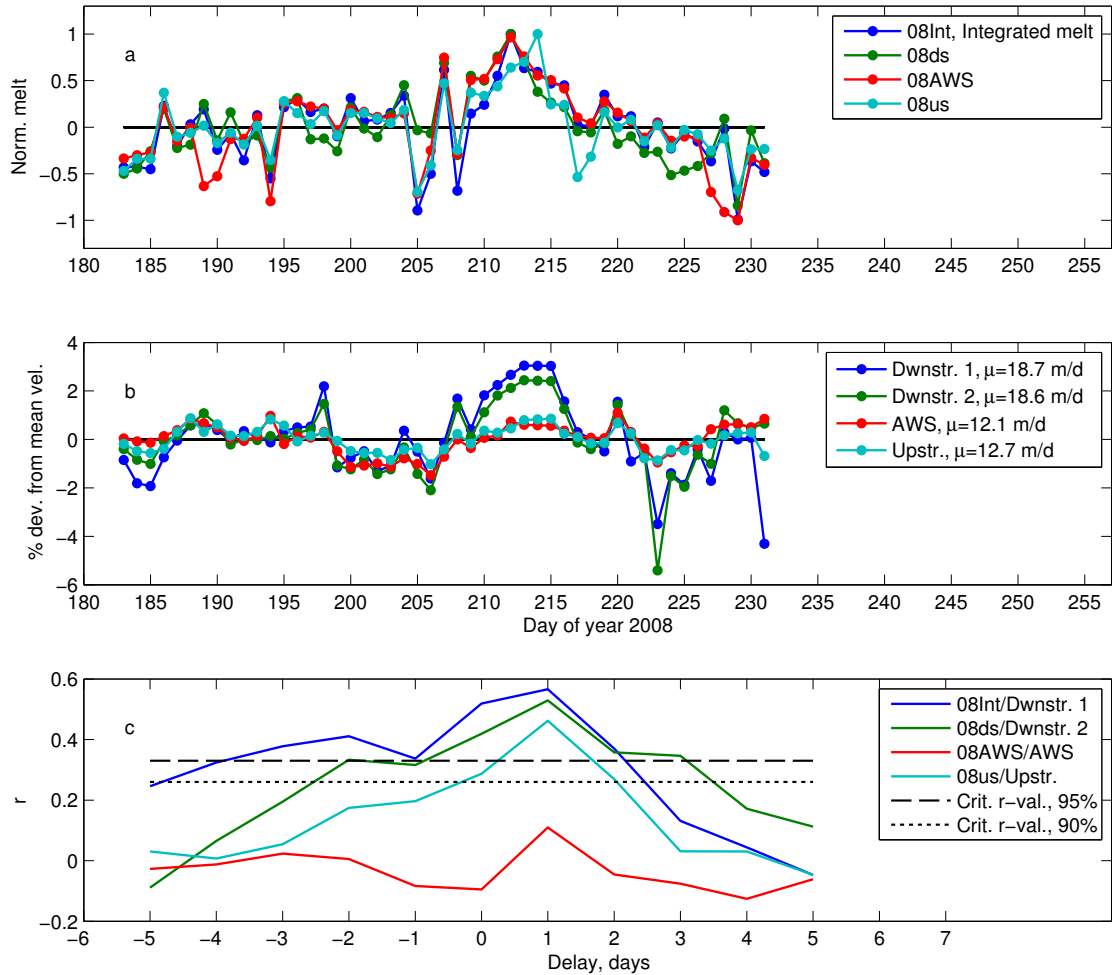


Figure 11: Comparisons of melt and velocity, 2008: (a) Melt signals 08Integrated, 08downstream, 08AWS, and 08upstream. All signals are plotted as deviation from mean and normalized relative to maximum amplitude for comparison. (b) Deviations from mean measured surface speed at downstream GPS site 1 (IS41), downstream GPS site 2 (IS42), AWS GPS site (IS51), and upstream GPS site (IS53) in %. (c) Correlation coefficients for comparisons 08Integrated/downstream 1, 08downstream/downstream 2, 08AWS/AWS, and 08upstream/upstream. Dashed line is critical r value ($r = 0.33$) for significance at the 95% level, dotted line is critical r value ($r = 0.26$) for significance at the 90% level. Both with 24 degrees of freedom, one-tailed distribution.

when the velocity is delayed one day relative to the melt signal. Adjacent correlation values are significantly smaller, indicative of a well-peaked correlation function. We note that the 2007 melt data are calculated using a synthetic temperature record which is only half the length of the 2008 record, potentially influencing the correlation values. That the one day optimal delay is seen everywhere may be related to the overall coherence of the ice body. However, the stronger correlations observed lower on the glacier suggest some spatial dependence in the glacier response to runoff. For all comparisons, except the 08AWS/AWS velocity record, we see a statistically significant correlation at the 90% level or above (for 2008, 99% levels). We therefore reject the null hypothesis that melt does not have any effect on ice velocity, keeping in mind that even significant correlation does not imply causation.

For both 2007 and 2008, the highest r -values result from correlating the integrated daily melt signal with the velocity records representative of the glacier front area. The strong correlation near the front, especially for 2008, suggests that melt affects velocity behavior in a direct way in this area. If the correlation coefficient can be interpreted as a measure of the strength of the effect of melt on velocity, our results indicate that this effect is stronger near the front of the glacier than farther upstream. There are several reasons this may be the case. The front of Helheim Glacier is heavily crevassed because of high strain rates ($\sim 0.5 \text{ yr}^{-1}$). We suggest that the strain rate field creates conditions favorable for the rapid transit of runoff from the surface to the bed. This region of the glacier is near flotation (*de Juan et al.*, 2010) and is probably sensitive to additional surface meltwater perturbing the already high basal water pressure. Conversely, we see lower correlation values in the areas where the surface velocities are slower, for example by stations IS51 and IS53, 2008 (Figure 1b). The station farthest upstream, IS53, has a higher average velocity than the station downstream of it, IS51, indicating the existence of a compression zone between the two sites. The correlation of the melt and the velocity signals is lower at IS51 (AWS site) than at any other site considered in 2008. We note, however, that the up-glacier sites are at higher altitudes where less melt is generated, possibly limiting the effect of basal lubrication.

With our daily time resolution of the velocity record, our results point to a transit time of 12-36 hours from generation of melt at the surface to an effect is observed in the displacement record. In this interval we expect the time lag to be closer to 12 hours than 36 hours, which is still longer than the response times found on the ice-sheet flank by, e.g., *Shepherd et al.* (2009).

The full range of velocity variations for the timeseries shown in Figures 10 and 11, after the effects of glacial earthquakes and advection have been removed, is about +3% to -5.5%, with typical variations of about $\pm 2\%$. For the 2% case, the corresponding absolute velocity variations range from about $0.2\text{--}0.5 \text{ m d}^{-1}$, or $\sim 70\text{--}180 \text{ m yr}^{-1}$. *Joughin et al.*

(2008b) find melt water-induced velocity variations on West Greenland outlet glaciers (Jakobshavn Isbræ and a number of smaller, marine terminating glaciers in this region), determined in 24-day averages, to be about half this large. For the purposes of comparison, we produce 29, 24-day running averages for our daily 2008 time series centered on days July 10 - August 7 (days of year 192-220). We use station IS41, close to the glacier front, for the comparison: this station has a mean daily velocity of 18.4 m d^{-1} after corrections for glacial earthquakes and advection have been applied. The 24-day averaging naturally smoothes day-to-day variations and yields a peak difference between the seasonal mean speed and the highest 24-day average speed of $\sim 1\%$, corresponding to a variability of $\sim 55 \text{ m yr}^{-1}$, i.e., within the $51\text{-}77 \text{ m yr}^{-1}$ reported by *Joughin et al.* (2008b) in West Greenland. We therefore believe our results to be generally in good agreement with those of *Joughin et al.* (2008b), and note that daily variations in speed due to runoff do not differ dramatically in amplitude from the seasonal.

Our knowledge of Helheim Glacier's water budget is incomplete because no record of discharge exists. We also lack information on basal water pressures and storage times, data usually acquired by drilling to the bed or through dye-tracing experiments (e.g., *Kamb et al.*, 1985). It is therefore not possible at this point to determine if Helheim's subglacial hydrology is dominated by a low-pressure tunnel system, a system of distributed linked cavities and small channels, or both (see, e.g., *Kamb et al.*, 1985; *Kamb*, 1987; *Bjornsson*, 1998; *Bartholomäus et al.*, 2008).

Above-normal runoff due to surface melt near the front of the glacier can have an effect in filling crevasses and accelerating calving processes, causing accelerations of the glacier trunk, as described by *Sohn et al.* (1998). Enhanced calving by hydro-fracturing has been modeled by *Benn et al.* (2007). As demonstrated by *Nettles et al.* (2008), the glacier dynamics observed in the GPS signals are modulated partly by calving at the front, coeval with glacial earthquakes. We observe that, of the seismic events occurring within the period of melt calculation in 2007, two occur on day 225, two days after the maximum melt observed. The same pattern is seen in 2008, when on day 214 two glacial earthquakes were detected, again two days after a period of strong melt water production. This suggests a relationship between melt output and calving. However, in 2008, a glacial earthquake also occurred on day 232 following several days of below mean melt. The relatively short time series used and the small sample size in this study is thus insufficient to test this intriguing hypothesis.

5 Conclusions

We have developed a distributed surface energy balance model for Helheim Glacier and validated it against field observations for 2008. The model was run over a period of 27 full days for 2007 and 49 full days for 2008 to estimate daily runoff from surface melt over the snow-free part of the glacier (i.e., below 1000 m a.s.l.). The calibrated model performed well and produced results in agreement with ablation observations made at an AWS on the glacier.

Estimated melt rates are similar for both years. Average modeled melt rates for the grid cell containing the AWS were 3.2 cm d^{-1} ($\sim 29.0 \text{ mm d}^{-1}$ w.e.) for 2007 and 2008. Average melt rates for the frontal area of the glacier are 4.44 cm d^{-1} (40.7 mm d^{-1} w.e.) and 4.36 cm d^{-1} (40.0 mm d^{-1} w.e.) for 2007 and 2008, respectively. Up-glacier of the AWS, modeled melt rates are 2.42 cm d^{-1} (22.2 mm d^{-1} w.e.) in 2007 and 2.24 cm d^{-1} (20.5 mm d^{-1} w.e.) in 2008 for the entire deployment periods. The slightly lower melt rates in 2008 are mainly due to the time series starting earlier in the melt season when melt rates were lower.

The melt signal at Helheim has a large altitudinal gradient, which can partly be ascribed to the elevation difference of $\sim 900 \text{ m}$ between the glacier front and the upglacier part of the catchment. Variations in albedo also contribute to the spatial differences in melt, with the lower, heavily crevassed reaches of the glacier having lower albedo.

Total melt output and model results from selected cells are correlated with observations of speed from GPS network deployments on Helheim Glacier in 2007 and 2008. The highest correlations occur for locations near the front of the glacier in both years. For all comparisons but one, we find that the correlations are significant at $>90\%$ levels. For both years, 12-36 hour delays between melt water generation at the surface and glacier speed increases are found. We suggest that the lower bound of this interval represents the transition time for runoff to travel from the surface to the bed of the glacier, while acknowledging that our 1-day temporal resolution may influence this interpretation.

Our results indicate a dependence of ice velocity on runoff variations at a fast flowing outlet glacier. The effect is larger near the front of the glacier where melt rates are higher. We argue that part of the spatial dependence of this effect is caused by the difference in the magnitude of the melt water flux. However, we also speculate that the enhanced response near the front results from this region having a better hydraulic connection to the bed, thereby supplying additional water at a faster rate. Moreover, a large fraction of the generated runoff from the entire catchment is expected to be routed under the frontal area of the glacier, possibly causing a cumulative dynamic effect.

While large accelerations, primarily at the front of the glacier, are governed by calving

dynamics (e.g., *Nettles et al.*, 2008), it is clear from this study that variations in runoff volume contribute to the velocity behavior of Helheim Glacier. Temporally coincident large melt fluxes and calving events suggest that basal water lubrication might bring the glacier into a calving-prone state, but further research is required to test this hypothesis.

Acknowledgments

The Helheim 2007 and 2008 project was supported by the Gary Comer Science and Education Foundation, the U.S. National Science Foundation, the Danish Commission for Scientific Research in Greenland (KVUG), the Spanish Ministry of Science and Innovation (MICINN), the Geological Survey of Denmark and Greenland (GEUS), Geocenter Copenhagen, the Danish National Space Center, NASA, the Lamont-Doherty Climate Center, and the Dan and Betty Churchill Exploration Fund. GPS equipment and technical support were provided by UNAVCO, Inc. The authors wish to thank Dr. Michele Citterio, GEUS, for GIS assistance. The authors thank Martin Truffer (Associate Editor), Timothy C. Bartholomaus, and three anonymous reviewers for constructive reviews that helped improve the manuscript.

Bibliography

- Amundson, J. M., M. Truffer, M. P. Luethi, M. Fahnestock, M. West, and R. J. Motyka (2008), Glacier, fjord, and seismic response to recent large calving events, Jakobshavn Isbrae, Greenland, *Geophysical Research Letters*, 35(22), L22501, doi:{10.1029/2008GL035281}.
- Bartholomaus, T. C., R. S. Anderson, and S. P. Anderson (2008), Response of glacier basal motion to transient water storage, *Nature Geoscience*, 1(1), 33–37, doi:{10.1038/ngeo.2007.52}.
- Benn, D. I., C. R. Warren, and R. H. Mottram (2007), Calving processes and the dynamics of calving glaciers, *Earth-Science Reviews*, 82(3-4), 143–179, doi:{10.1016/j.earscirev.2007.02.002}.
- Bjornsson, H. (1998), Hydrological characteristics of the drainage system beneath a surging glacier, *Nature*, 395(6704), 771–774.
- Braithwaite, R. (1995), Positive degree-day factors for ablation on the Greenland Ice-sheet studied by energy-balance modeling, *Journal of Glaciology*, 41(137), 153–160.

- Brock, B. W., I. C. Willis, and M. J. Shaw (2006), Measurement and parameterization of aerodynamic roughness length variations at Haut Glacier d'Arolla, Switzerland, *Journal of Glaciology*, 52(177), 281–297.
- de Juan, J., P. Elosegui, M. Nettles, T. B. Larsen, J. L. Davis, G. S. Hamilton, L. A. Stearns, M. L. Andersen, G. Ekström, A. P. Ahlstrom, L. Stenseng, S. A. Khan, and R. Forsberg (2010), Sudden increase in tidal response linked to calving and acceleration at a large Greenland outlet glacier, *Geophysical Research Letters*, 37, doi:{10.1029/2010GL043289}.
- Ettema, J., M. R. van den Broeke, E. van Meijgaard, W. J. van de Berg, J. L. Bamber, J. E. Box, and R. C. Bales (2009), Higher surface mass balance of the Greenland ice sheet revealed by high-resolution climate modeling, *Geophysical Research Letters*, 36, L12501, doi:{10.1029/2009GL038110}.
- Greuell, W., and T. Konzelmann (1994), Numerical Modeling of the energy balance and the englacial temperature of the Greenland Ice-sheet - calculations for the ETH-Camp location (West Greenland, 1155 m asl), *Global and Planetary Change*, 9(1-2), 91–114.
- Hall, D. K., G. A. Riggs, and V. V. Salomonson (2007), MODIS/Terra Snow Cover Daily L3 Global 500m Grid V005, Julian days 205, 209, 218, 222, 224, 225, 227, 228, 230, 234. Updated daily, <http://nsidc.org/data/index.html>.
- Hall, D. K., G. A. Riggs, and V. V. Salomonson (2008), MODIS/Terra Snow Cover Daily L3 Global 500m Grid V005, Julian days 179, 180, 182, 183, 195, 199, 200, 202, 203, 204, 205, 207, 209, 214, 216, 217, 218, 222, 223, 225, 235, 238. Updated daily, <http://nsidc.org/data/index.html>.
- Hanna, E., P. Huybrechts, I. Janssens, J. Cappelen, K. Steffen, and A. Stephens (2005), Runoff and mass balance of the Greenland ice sheet: 1958-2003, *Journal of Geophysical Research - Atmospheres*, 110(D13), D13108, doi:{10.1029/2004JD005641}.
- Hock, R. (2005), Glacier melt: a review of processes and their modelling, *Progress in Physical Geography*, 29(3), 362–391.
- Hock, R., and B. Holmgren (2005), A distributed surface energy-balance model for complex topography and its application to Storglaciären, Sweden, *Journal of Glaciology*, 51(172), 25–36.
- Holtslag, A. A. M., and H. A. R. De Bruin (1988), Applied modeling of the nighttime surface-energy balance over land, *Journal of Applied Meteorology*, 27(6), 689–704.
- Howat, I. M., I. Joughin, and T. A. Scambos (2007), Rapid changes in ice discharge from Greenland outlet glaciers, *Science*, 315(5818), 1559–1561, doi:{10.1126/science.1138478}.

- Howat, I. M., I. Joughin, M. Fahnestock, B. E. Smith, and T. A. Scambos (2008a), Synchronous retreat and acceleration of southeast Greenland outlet glaciers 2000-06: ice dynamics and coupling to climate, *Journal of Glaciology*, 54(187), 646–660.
- Howat, I. M., S. Tulaczyk, E. Waddington, and H. Björnsson (2008b), Dynamic controls on glacier basal motion inferred from surface ice motion, *Journal of Geophysical Research*, 113, doi:{10.1029/2007JF000925}.
- Huybrechts, P., A. Letreguilly, and N. Reeh (1991), The Greenland Ice-sheet and greenhouse warming, *Global and Planetary Change*, 89(4), 399–412.
- Iken A., and R. Bindschadler (1986), Combined measurements of subglacial water-pressure and surface velocity of Findelengletscher, Switzerland - conclusions about drainage system and sliding mechanism, *Journal of Glaciology*, 32(110), 101–119.
- Joughin, I., S. B. Das, M. A. King, B. E. Smith, I. M. Howat, and T. Moon (2008b), Seasonal speedup along the western flank of the Greenland Ice Sheet, *Science*, 320(5877), 781–783, doi:{10.1126/science.1153288}.
- Joughin, I., I. M. Howat, M. Fahnestock, B. Smith, W. Krabill, R. B. Alley, H. Stern, and M. Truffer (2008c), Continued evolution of Jakobshavn Isbrae following its rapid speedup, *Journal of Geophysical Research - Earth Surface*, 113(F4), doi:{10.1029/2008JF001023}.
- Kamb, B. (1987), Glacier surge mechanism based on linked cavity configuration of the basal water conduit system, *Journal of Geophysical Research - Solid Earth*, 92(B9), 9083–9100.
- Kamb, B., C. Raymond, W. Harrison, H. Engelhardt, K. Echelmeyer, N. Humphrey, M. Brugmann, and T. Pfeffer (1985), Glacier surge mechanism - 1982-1983 surge of Variegated Glacier, Alaska, *Science*, 227(4686), 469–479.
- Liston, G., and K. Elder (2006), A meteorological distribution system for high-resolution terrestrial modeling (MicroMet), *Journal of Hydrometeorology*, 7(2), 217–234.
- Luckman, A., and T. Murray (2005), Seasonal variation in velocity before retreat of Jakobshavn Isbrae, Greenland, *Geophysical Research Letters*, 32(8), doi:{10.1029/2005GL022519}.
- Luckman, A., T. Murray, R. de Lange, and E. Hanna (2006), Rapid and synchronous ice-dynamic changes in East Greenland, *Geophysical Research Letters*, 33(3), L03503, doi: {10.1059/2005GL025048}.
- MacWhorter, M., and R. Weller (1991), Error in measurements of incoming shortwave radiation made from ships and buoys, *Journal of Atmospheric and Oceanic Technology*, 8(1), 108–117.

- Meesters, A., N. Bink, H. Vugts, F. Cannemeijer, and E. Henneken (1997), Turbulence observations above a smooth melting surface on the Greenland ice sheet, *Boundary-layer Meteorology*, 85(1), 81–110.
- Mernild, S. H., G. E. Liston, C. A. Hiemstra, and K. Steffen (2008), Surface Melt Area and Water Balance Modeling on the Greenland Ice Sheet 1995-2005, *Journal of Hydrometeorology*, 9(6), 1191–1211, doi:{10.1175/2008JHM957.1}.
- Munro, D. (1989), Surface-roughness and bulk heat-transfer on a glacier - comparison with eddy-correlation, *Journal of Glaciology*, 35(121), 343–348.
- Nettles, M., T. B. Larsen, P. Elósegui, G. S. Hamilton, L. A. Stearns, A. P. Ahlstrøm, J. L. Davis, M. L. Andersen, J. de Juan, S. A. Khan, L. Stenseng, G. Ekström, and R. Forsberg (2008), Step-wise changes in glacier flow speed coincide with calving and glacial earthquakes at Helheim Glacier, Greenland, *Geophysical Research Letters*, 35, L24503, doi:{10.1029/2008GL036127}.
- Nick, F. M., A. Vieli, I. Howat, and I. Joughin (2009), Large-scale changes in Greenland outlet glacier dynamics triggered at the terminus, *Nature Geoscience*, 2, 110–114, doi:{10.1038/ngeo394}.
- Paulson, C. A. (1970), The Mathematical Representation of Wind Speed and Temperature Profiles in the Unstable Atmospheric Surface Layer, *Journal of Applied Meteorology*, 9(6), 851–856.
- Reeh, N. (1991), Parameterization of melt rate and surface temperature, *Polarforschung*, 59(3), 113–128.
- Rignot, E., and P. Kanagaratnam (2006), Changes in the velocity structure of the Greenland ice sheet, *Science*, 311(5763), 986–990, doi:{10.1126/science.1121381}.
- Shepherd, A., A. Hubbard, P. Nienow, M. King, M. McMillan, and I. Joughin (2009), Greenland ice sheet motion coupled with daily melting in late summer, *Geophysical Research Letters*, 36, L01501, doi:{10.1029/2008GL035758}.
- Sohn, H., K. Jezek, and C. van der Veen (1998), Jakobshavn Glacier, West Greenland: 30 years of spaceborne observations, *Geophysical Research Letters*, 25(14), 2699–2702.
- Stearns, L. A. (2007), Outlet glacier dynamics in East Greenland and East Antarctica, Ph.D. thesis, University of Maine.
- Stearns, L. A., and G. S. Hamilton (2007), Rapid volume loss from two East Greenland outlet glaciers quantified using repeat stereo satellite imagery, *Geophysical Research Letters*, 34(5), L05503, doi:{10.1029/2006GL028982}.

- Stearns, L. A., G. S. Hamilton, and N. Reeh (2005), Multi-decadal record of ice dynamics on Daugaard Jensen Gletscher, East Greenland, from satellite imagery and terrestrial measurements, *Annals of Glaciology*, vol. 42, edited by Dowdeswell, J and Willis, IC, pp. 53–58, International Glaciological Society.
- Stroeve, J. C., J. E. Box, and T. Haran (2006), Evaluation of the MODIS (MOD10A1) daily snow albedo product over the Greenland ice sheet, *Remote Sensing of Environment*, 105(2), 155–171, doi:{10.1016/j.rse.2006.06.009}.
- van As, D., M. van den Broeke, C. Reijmer, R. van De Wal (2005), The summer surface energy balance of the high Antarctic plateau, *Boundary-layer Meteorology*, 115(2), 289–317, doi:{10.1007/s10546-004-4631-1}.
- van De Wal, R., and J. Oerlemans (1994), An energy-balance model for the Greenland Ice-sheet, *Global and Planetary Change*, 9(1-2), 115–131.
- van de Wal, R. S. W., W. Boot, M. R. van den Broeke, C. J. P. P. Smeets, C. H. Reijmer, J. J. A. Donker, and J. Oerlemans (2008), Large and rapid melt-induced velocity changes in the ablation zone of the Greenland Ice Sheet, *Science*, 321(5885), 111–113, doi:{10.1126/science.1158540}.
- van den Broeke, M., D. van As, C. Reijmer, and R. van de Wal (2004), Assessing and improving the quality of unattended radiation observations in Antarctica, *Journal of Atmospheric and Oceanic Technology*, 21(9), 1417–1431.
- van den Broeke, M., P. Smeets, J. Ettema, C. van der Veen, R. van der Wal, and J. Oerlemans (2008), Partitioning of melt energy and melt water fluxes in the ablation zone of the west Greenland ice sheet, *The Cryosphere*, 2, 179–189.
- Zwally, H., W. Abdalati, T. Herring, K. Larson, J. Saba, and K. Steffen (2002), Surface melt-induced acceleration of Greenland ice-sheet flow, *Science*, 297(5579), 218–222.

Quantitative estimates of velocity sensitivity to surface melt variations at a large Greenland outlet glacier

M. L. Andersen^{1,2}, M. Nettles³, T. B. Larsen¹, P. Elosegui⁴,
G. S. Hamilton⁵, L. A. Stearns⁶

submitted to Journal of Glaciology sept. 2010, ms no. 10J168

¹Geological Survey of Denmark and Greenland (GEUS), Copenhagen DK-1350, Denmark

²Centre for Ice and Climate, Niels Bohr Institute, Univ. of Copenhagen, Copenhagen DK-2100, Denmark

³Lamont-Doherty Earth Observatory, Columbia University, Palisades, NY 10964, USA

⁴Institute for Space Sciences (ICE) and Marine Technology Unit (UTM), CSIC, Barcelona, Spain

⁵Climate Change Institute, University of Maine, Orono, ME 04469, USA

⁶Department of Geology, University of Kansas, Lawrence, KS 66045, USA

Abstract

The flow speed of Greenland outlet glaciers is governed by several factors, the relative importance of which is poorly understood. The delivery of surface-generated melt water to the bed of alpine glaciers has been shown to influence glacier flow speed when the volume of water is sufficient to increase basal fluid pressure and hence basal lubrication. While this effect has also been demonstrated on the Greenland ice-sheet margin, little is known about the influence of surface melting on the large, marine-terminating outlet glaciers that drain the ice sheet. Previously, we demonstrated a correlation between variations in glacier flow speed and melt-water input at Helheim Glacier, East Greenland. Here, we use a validated model of melt-water input and GPS-derived surface velocities to quantify the sensitivity of glacier flow speed to changes in surface melt at Helheim Glacier during two summer seasons (2007 and 2008). We find relative changes in glacier speed due to melt-water input to be small, with variations of $\sim 45\%$ in melt producing changes in velocity of $\sim 2\text{--}4\%$. These velocity variations are, however, of similar absolute magnitude to those observed at smaller glaciers and on the ice-sheet margin. We find that the glacier's sensitivity to variations in melt-water input decreases approximately exponentially with distance from the calving front. Sensitivity to melt varies with time, but generally increases as the melt season progresses. By analogy with better-studied glacial systems, we interpret the time-varying sensitivity of glacier flow to

melt-water input to result from changes in subglacial hydraulic routing caused by the changing volume of melt-water input.

Introduction

Multiple observational and modeling studies show that the Greenland Ice Sheet is losing mass (e.g., *Van den Broeke et al.*, 2008; *Rignot et al.*, 2008; *Velicogna and Wahr*, 2006; *Chen et al.*, 2006; *Luthcke et al.*, 2006). In current estimates of the mass budget of the ice sheet, drainage in the form of iceberg calving from the termini of outlet glaciers accounts for approximately 50% of the total mass loss (*Van den Broeke et al.*, 2008; *Rignot et al.*, 2008; *Krabill et al.*, 2004). Modeling and prediction of this calving flux is complex and has not yet been fully accomplished, though understanding controls on dynamic ice loss is critical for improved predictions of sea-level rise and ice-sheet drawdown.

The ice volume drained through Greenland's outlet glaciers is related to their flow speed. Controls on rapid changes in glacier flow speed are only beginning to be understood. It is now clear that the flow velocity of Greenland's large, marine-terminating outlet glaciers responds to ice loss at the glacier terminus on interannual (e.g., *Howat et al.*, 2005), seasonal (e.g., *Joughin et al.*, 2008a), and shorter (*Amundson et al.*, 2008; *Nettles et al.*, 2008) timescales.

A number of studies conducted on the margin of the West Greenland ice sheet suggest that variations in surface melting also play an important role in modulating sliding speed and controlling observed surface velocities. Near Swiss Camp, north of Jakobshavn Isbræ, *Zwally et al.* (2002) observed acceleration of ice flow associated with summer melting, and *Van de Wal et al.* (2008) observed speed variations of up to 30% along the K-transect near Kangerlussuaq during 2005–2006. Similarly, *Shepherd et al.* (2009) found flow-speed increases on the ice sheet of up to 35% per positive degree day in the same area. On the land-terminating Russell Glacier, *Bartholomew et al.* (2010) observed summer surface velocities as much as 220% faster than the $\sim 100 \text{ m yr}^{-1}$ winter background speed in association with peaks in local temperature. Similarly large effects have been observed on alpine glaciers (e.g., *Iken and Bindenschadler*, 1986; *Anderson et al.*, 2004) and tidewater glaciers outside Greenland (e.g., *Meier et al.*, 1994; *Kamb et al.*, 1994). A suggested mechanism for such increases in flow speed is the drainage of surface melt water to the ice-rock interface via fracture propagation (*Van der Veen*, 2007), leading to enhanced basal sliding (*Zwally et al.*, 2002; *Fountain et al.*, 2005; *Das et al.*, 2008).

Less is known about the response of Greenland's large, fast-flowing outlet glaciers to changes in melt-water input. Using both remote sensing and field-based techniques for analysis of the ice-sheet margin and several outlet glaciers, *Joughin et al.* (2008b) found

seasonal accelerations of 50–100% on the ice sheet, with fractionally smaller variations of 9–14% on the outlet glaciers. However, *Joughin et al.* (2008b) treated the outlet glaciers *en masse*, and did not separate calving-related and melt-related accelerations. Few data have been available from individual large glaciers, and little is therefore known about spatial or temporal variability in the influence of melt on flow speed at these glaciers. Understanding this response, and its relative and absolute contributions to increased ice-discharge rates, is important for developing a more complete picture of the ice sheet's likely response to changes in environmental conditions.

Andersen et al. (2010) used a large, interdisciplinary data set to demonstrate a correlation between variations in melt-water production and the flow speed of Helheim Glacier, a large, marine-terminating outlet glacier in East Greenland. Here, we expand on that analysis to investigate the magnitude and temporal and spatial variability of Helheim Glacier's sensitivity to changes in melt-water input.

Data

During the summers of 2007 and 2008 we collected several geophysical data sets at and around Helheim Glacier, including GPS measurements of glacier surface position and meteorological observations at an automatic weather station (AWS) on the glacier. We also recorded time-lapse photographs of the glacier front and water-level variations in the glacial fjord. This combination of data sets allows us to assess the spatially and temporally varying influence of melt on flow speed.

Glacier surface velocity

We deployed a network of 12–22 continuously recording GPS receivers on Helheim Glacier during the summers of 2007 and 2008, for 54 days and 55 days, respectively (Figure 1). The networks extended from within a few km of the calving front to ~25 km upstream along the flow line. Daily velocities were calculated by fitting a linear model to position estimates determined kinematically at 15 s intervals, as described in *Nettles et al.* (2008). The velocity estimates have uncertainties of approximately 0.1 m d^{-1} .

The loss of ice from the glacier terminus during large-scale calving events has been shown to change the flow speed by as much as 20% at Helheim Glacier (*Nettles et al.*, 2008) and elsewhere (*Amundson et al.*, 2008). The effect of calving events on glacier speed must therefore be quantified and removed from the velocity signals in order to study the effect of melt on speed variations. The largest changes in daily glacier velocity are asso-

ciated with calving events for which glacial earthquakes are detected (see *Nettles et al.*, 2008) and these changes appear in the velocity record as step-like offsets. To identify the times at which calving-related velocity offsets may occur, we use the list of glacial earthquakes from *Nettles et al.* (2008) for events in 2007, and a list of events for 2008 identified in a similar manner, using the algorithm of *Ekström* (2006). In 2008, we identify two $M \sim 4.8$ seismic events at Helheim Glacier on day 214 and one event of $M \sim 4.7$ on day 232, as well as several smaller events (Figure 2).

Some calving-related velocity increases observed by *Amundson et al.* (2008) were not associated with glacial-earthquake detections (*Nettles and Ekström*, 2010). In 2008, we made observations of calving events using a time-lapse camera mounted on the northern wall of the Helheim fjord. The camera was configured to record images automatically every four minutes. Major calving events were identified by visual inspection (*Hamilton et al.*, 2008), and we assume an uncertainty of ± 30 minutes on the timing of these events due to their finite duration.

We also deployed a tide gauge to monitor variations in water level, sampling at one-minute intervals. The instrument was installed at an island in the fjord, approximately 25 km from the calving front. Calving events at the glacier front produce tsunami signals in the tide-gauge record, which we use to verify our visual and seismic detections of major calving events.

The combined calving data set for 2008 that we use to correct the velocity signal for calving-related velocity changes is shown in Figure 2, with the detected glacial earthquakes marked with red lines, the calving events observed from the photographs marked with black lines, and the tide gauge data bandpass filtered from 200-4000 s in blue. Smaller arrivals in the tide-gauge record not associated with detected calving events are assumed to be caused by icebergs rolling or breaking into several pieces, thereby causing disturbances in the water level. For the year 2007 we do not have time-lapse photography available, and we therefore use only the seismic detections from *Nettles et al.* (2008). Considering the simultaneous occurrence of events in all three 2008 data sets, we do not expect the lack of photographic data to have a significant effect on the 2007 results.

In order to assess the influence of melt, independent of the calving-related velocity changes, we subtract the offsets caused by the calving events from the GPS velocity record for all days subsequent to each event. For events occurring later than 18:00 UTC on a given day, the coincident velocity increase is primarily reflected in the estimated velocity on the following day. In this case, subsequent days were therefore corrected with the difference between the current and the next day's velocities. For events occurring earlier than 18:00 UTC, the correction of all subsequent days is made with the speed difference between the day of the event and the previous day.

Following correction for calving-related velocity jumps, we remove the mean and a single, best-fitting trend from the time series for each GPS station; the latter accounts approximately for the effects of advection of the station through the glacier flow field. In addition, for the dates on which maintenance visits were made to the stations, causing artificial displacements of the antennas, the average of the previous day's and the next day's speeds is assigned. For data gaps, values are linearly interpolated between the end points of the gap.

In the following analysis we assume that other external controls on the glacier flow velocity are negligible. For example, the ocean tides have been shown to affect the flow speed of the glacier on sub-daily time scales (*de Juan et al., 2010*), but their effect on estimates of daily average velocities is small.

Figure 3 shows the resulting corrections for station IS25 (2007), as an example. In the remainder of this work, we refer to the velocity time series corrected in this manner as 'calving-corrected' velocity records. No large changes in flow azimuth are associated with the changes in speed we observe, and we therefore use the terms 'speed' and 'velocity' interchangeably throughout this study.

Melt records

We estimated the melt history at each station location using a distributed surface-energy-balance model (SEB) of Helheim Glacier (*Andersen et al., 2010*). The SEB model was driven by observations from an automatic weather station (AWS) operated on the glacier trunk for 27 and 49 days in 2007 and 2008, respectively (Figure 1). The AWS recorded standard meteorological parameters, with which melt-water production at the surface was estimated. To distribute the model from one point to the entire glacier, we used a 2006 digital elevation model derived from an Advanced Spaceborne Thermal Emission and Reflection Radiometer (ASTER) image (*Stearns, 2007*) and the MOD10A1 Daily Snow Albedo product derived from Moderate Resolution Imaging Spectroradiometer (MODIS) observations (*Hall et al., 2007; Hall et al., 2008*). The model area was ~ 515 km² and comprised model cells on ice with elevations < 1000 m above sea level. Further details are given in *Andersen et al. (2010)*.

We calculate melt records for days of year 208-234, 2007, and days of year 183-232, 2008. We express the daily values of melt as residuals, i.e., as deviations from mean melt in millimeters water equivalent (mm w.e.). We produce local melt records for all GPS sites, as well as an integrated record of the total melt within the model region, expressed as the average melt per unit surface area as a function of time.

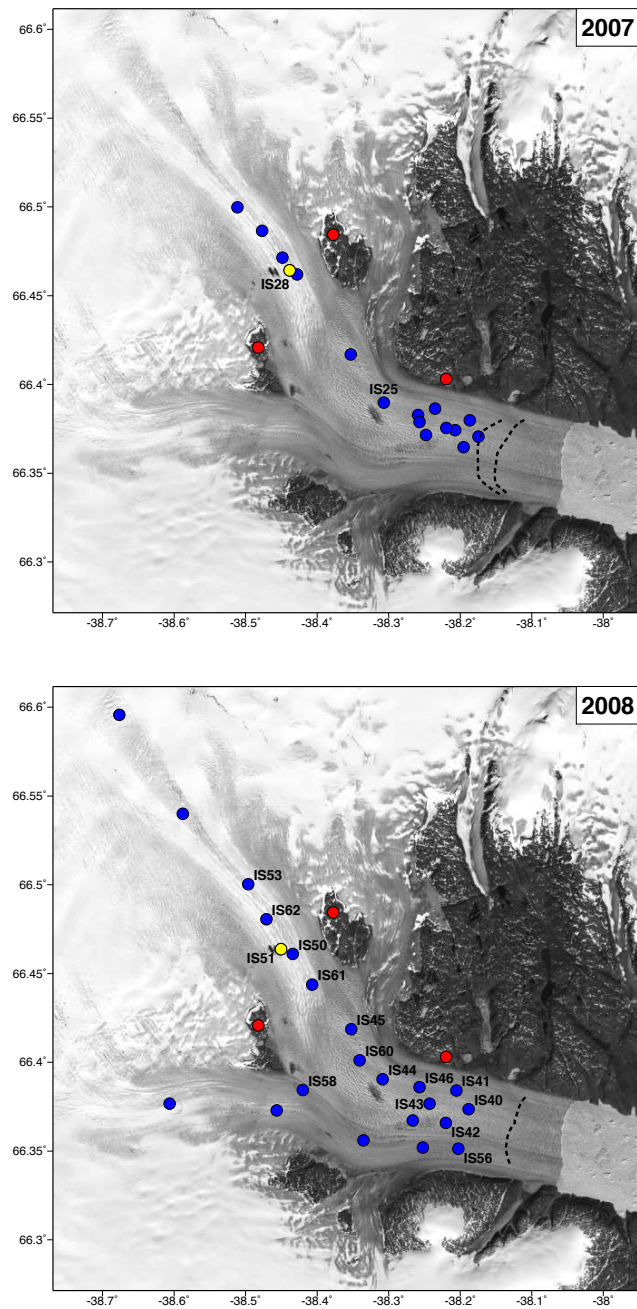


Figure 1: 2007 (top) and 2008 (bottom) GPS receiver network geometry and AWS location on Helheim Glacier, overlain on a 2001 LANDSAT image. Dots mark the position of (blue) GPS ice sites, (yellow) co-located AWS and GPS sites, and (red) GPS reference sites. Dotted lines are calving front positions on (top) 4 July 2007 (easternmost) and 24 August 2007, both from MODIS images, and (bottom) 31 July 2008, from field observations. Dark area immediately west of IS28 (2007) and IS51 (2008) is a yearly recurring melt water lake.

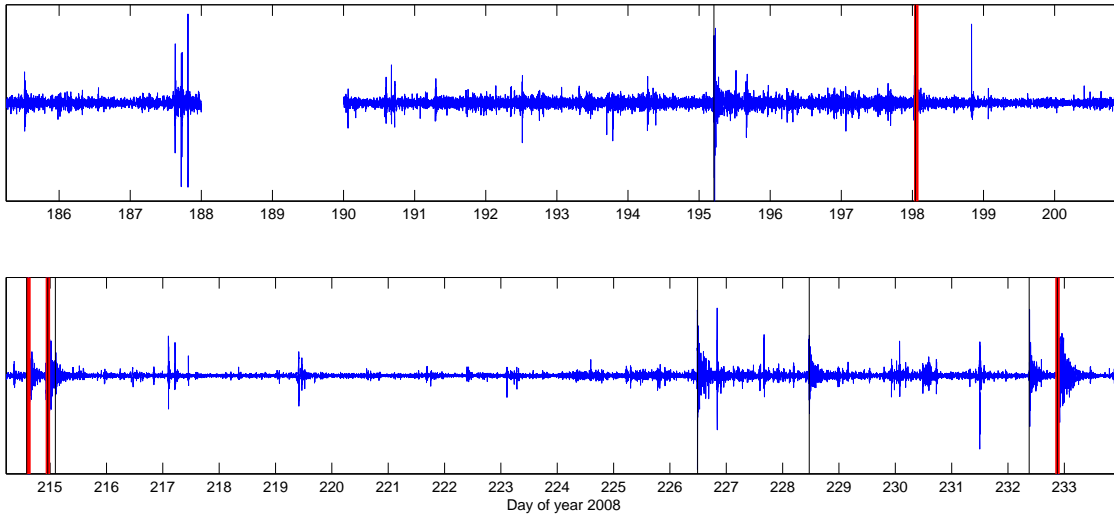


Figure 2: (blue) 2008 tide-gauge record, bandpass filtered from 200–4000 s, (red, bold) times of globally detected glacial earthquakes, and (black) calving observations from time lapse camera on the fjord wall. The tide gauge record was missing in days 188–189 and 201–213 due to a sensor malfunction.

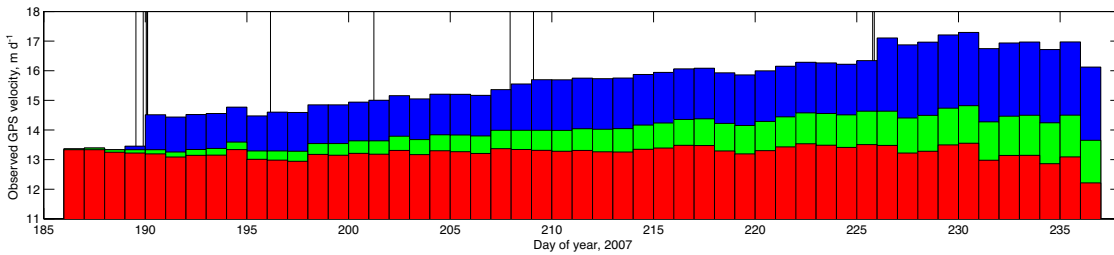


Figure 3: Glacier velocity at GPS station IS25, 2007, corrected for step-wise changes in velocity caused by glacial earthquakes. Blue bars show the raw time series, green bars the time series corrected for glacial earthquakes, red bars the time series with advective term subtracted. Black lines show times of detected glacial earthquakes.

Methods

In order to quantify the response of glacier flow speed to variations in melt-water generation at the surface, we develop a simple, linear model relating our melt-production time series to the observed flow-speed record. We evaluate the model results by comparing predicted velocities to observed values, using a measure of residual variance to assess goodness of fit. To allow for a time delay between melt and velocity response, we perform a temporal grid search.

Model

Given our limited knowledge of the relationship between changes in melt-water supply and changes in flow velocity, we choose to assume a linear relationship between melt input and variations in flow speed. We use a least-squares approach to obtain the model sensitivity value, or admittance, that best explains the observed velocity data, given an input melt signal. We solve the linear matrix equation:

$$\mathbf{y} = \mathbf{Ax} + \mathbf{ffl} \quad (1)$$

for x , minimizing the size of the error vector \mathbf{ffl} . \mathbf{A} contains the melt records and \mathbf{y} the observed velocity signals. All of the data are weighted equally. The model vector x simply contains the scalar sensitivity parameter(s) we seek, with the unit $\text{m d}^{-1} / \text{mm d}^{-1}$ w.e. (both quantities in the unit are expressed as variations from mean values).

We evaluate the goodness of fit by calculating the variance of the difference between the predicted and the observed velocities, normalized by the variance of the observed velocity signal:

$$Res.var. = \frac{\sum_{i=1}^N (y_i - \hat{y}_i)^2}{\sum_{i=1}^N (y_i - \bar{y})^2} \quad (2)$$

in which N is the number of days in the time series, y_i is the observed velocity value on day i ; \hat{y}_i is the predicted velocity value on day i and \bar{y} is the mean value of the observed velocity time series, which in this context is equal to zero, since the observed signal has already had the mean removed. The residual variance is then a measure of how much of the surface velocity signal remains unexplained by the melt-input model, such that a value of 1 indicates total lack of prediction, and a value of 0, perfect prediction.

Temporal grid search

To allow for a possible time lag between the melt and velocity signals, we perform a temporal grid search in which we shift the velocity signal in one-day steps over the interval $[-5;5]$ days relative to the melt signal. We perform the linear inversion for a sensitivity value at each step, which yields 11 sensitivity values with which we compute 11 model velocity records. The lowest residual variance for this suite of models is found at a lag of one day, consistent with the optimal cross-correlation lag found by *Andersen et al.* (2010) using a nearly identical data set. An example of the results from this analysis, for a station near the calving front (IS41, 2008), is shown in Figure 4. Figure 5 shows the melt signal for the location of 2008 GPS station IS41 together with the daily IS41 mean

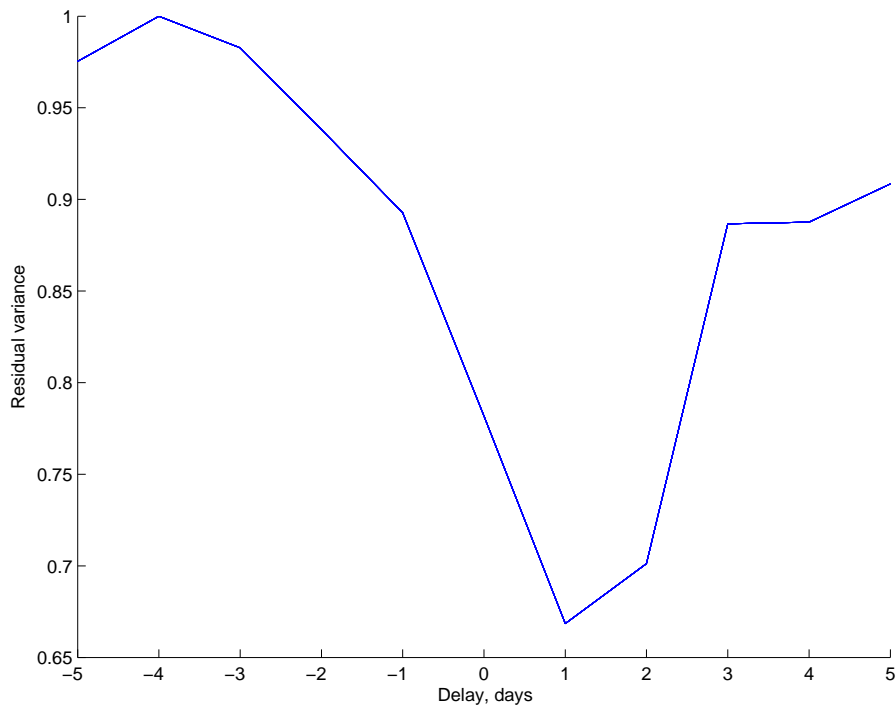


Figure 4: Residual variance for models of glacier response to integrated melt at 2008 GPS station IS41, fitted for each lag/lead in a [-5;5] day interval. The best fit is obtained with velocity lagging melt input by one day.

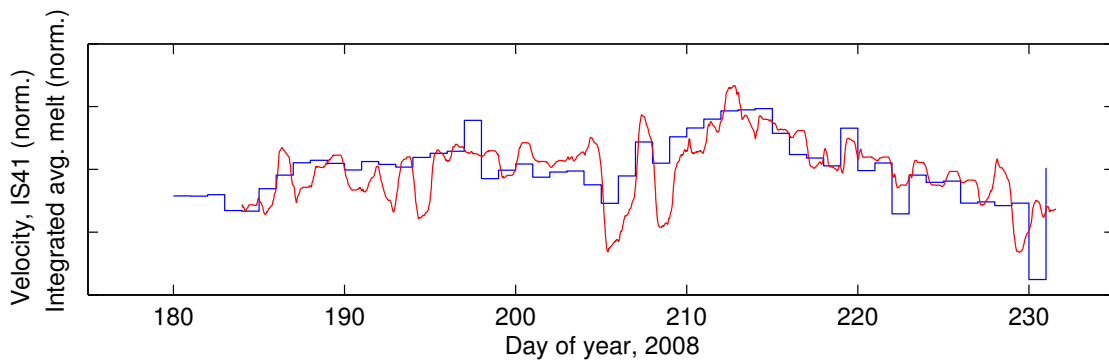


Figure 5: Comparison of (blue) calving-corrected velocity signal for 2008 location IS41 and (red) integrated average melt. Records are normalized for comparison. Melt signal is calculated hourly, but smoothed with a 24-hour running average.

velocity values, after the shift is applied. In the following analysis, we delay the velocity signal by one day relative to the melt signal to correspond to the best fit found in the grid search above. We do not allow for any further time delays.

Analysis and Results

We first test a simple model in which the glacier response to melt-water input is required to be uniform in space and time; we then assess the need for further complexity.

Spatial variability

Spatially uniform melt sensitivity

We first assume that the velocity of all areas of the glacier is equally sensitive to variations in melt and thus solve for one sensitivity value for the entire glacier. We perform the fit separately for 2007 and 2008. Using the integrated glacier-melt record as the input signal leads to sensitivity values of $0.02 \text{ m d}^{-1}/\text{mm d}^{-1}$ w.e. for both 2007 and 2008 with fairly large residual-variance values of 0.87 for 2007 and 0.89 for 2008. Using the local melt records we see sensitivity values of 0.006 and $0.007 \text{ m d}^{-1}/\text{mm d}^{-1}$ w.e. for 2007 and 2008, respectively. The fit using the local records produces slightly larger misfit values of 0.92 for 2007 and 0.89 for 2008. The resulting model fits from a single glacier-wide sensitivity value are illustrated in Figure 6. This result is consistent with the analysis of *Andersen et al.* (2010), who found spatial variability in the correlation of melt and velocity variations, suggesting the possibility of a spatially varying pattern of glacier sensitivity to melt input.

Spatially varying melt sensitivity

To test for possible spatial variability in velocity sensitivity to melt input, we determine the model parameters (sensitivities) locally by solving for x in Equation 1 at each GPS station location, thereby acquiring one sensitivity value per site. We experiment with using both the integrated and local melt records as input to the model.

Using the integrated melt signal as the input, we find residual-variance values of 0.66–1.0 for 2007, and values of 0.64–1.0 for 2008. Using the local melt records as input produces slightly poorer fits with residual-variance values in the range 0.75–1.0 in 2007 and 0.65–1.0 in 2008. Thus, it appears that some stations do not respond to melt variations at all (residual variances of 1.0) while melt variations explain one third to one half of the calving-corrected velocity signal at other stations. Given the slightly better fits using the integrated melt, and its greater simplicity, we use the integrated melt record in the discussion that follows.

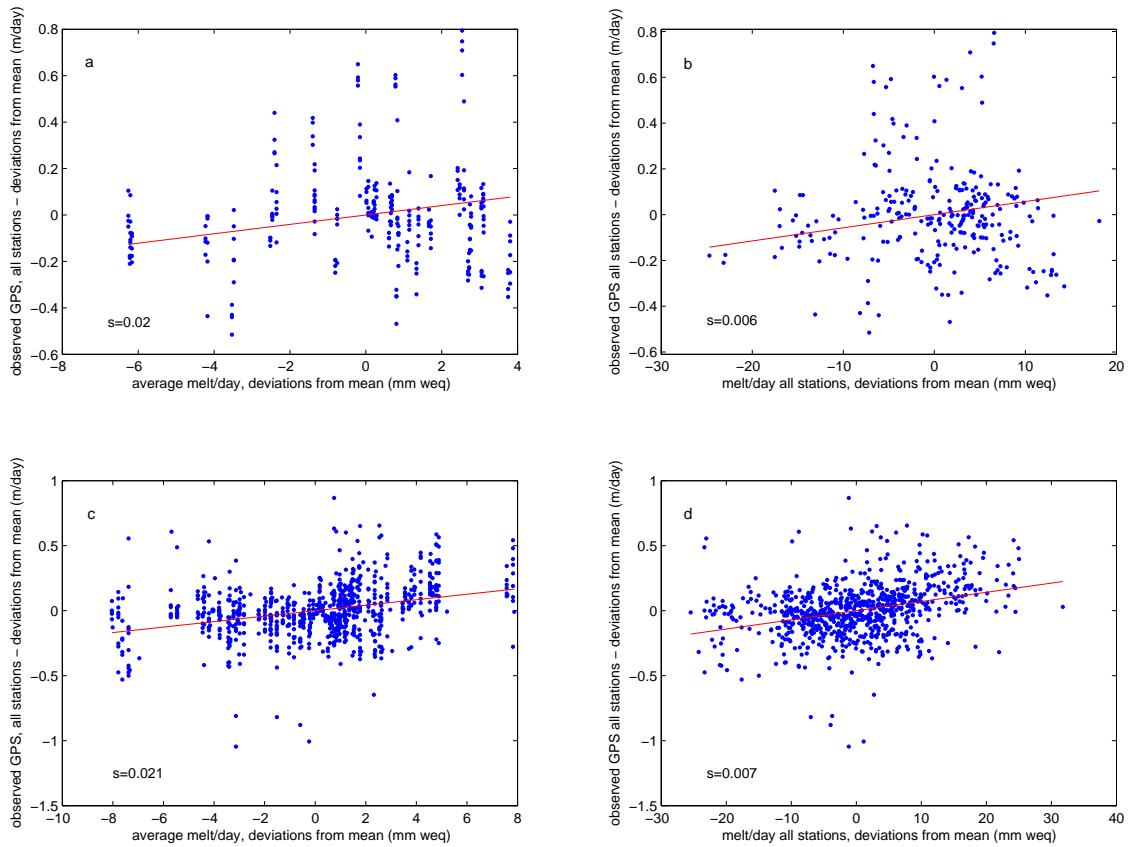


Figure 6: Results of melt-sensitivity model using a single, spatially invariant sensitivity parameter, s . (a) Integrated melt and GPS-station velocities, 2007. (b) Local melt and GPS-station velocities, 2007. (c) Integrated melt and GPS-station velocities, 2008. (d) Local melt and GPS-station velocities, 2008.

In general, stations located closer to the calving front appear more sensitive to melt input than those further away. Stations IS41 (2008) and IS25 (2007), located 4 and 6 km behind the calving front, are representative of near-terminus behavior; fits to the data are shown in Figure 7. The majority of the melt-producing catchment is located upstream of these stations, and it is perhaps not surprising that the average, integrated melt signal fits the velocity data from these stations well. Residual variances for stations IS25 and IS41 are 0.66 for 2007 and 0.64 for 2008, implying that $\sim 33\text{--}36\%$ of the calving-corrected velocity behavior can be explained by melt variations (Figure 7). The sensitivity values determined in this inversion are 0.04 and $0.06 \text{ m d}^{-1}/\text{mm d}^{-1} \text{ w.e.}$ for 2007 and 2008, respectively. As an example, the sensitivity calculated for 2008 indicates that an increase in integrated melt of $5 \text{ mm d}^{-1} \text{ w.e.}$, above the $11.5 \text{ mm d}^{-1} \text{ w.e.}$ mean, prompts a 0.3 m d^{-1} velocity increase above the mean of 18.4 m d^{-1} (Figure 7).

The variation in sensitivity to melt input with distance from the calving front is shown in Figure 8. A clear decrease in sensitivity with increasing distance along the flow line is apparent. A regression analysis shows that the correlation of sensitivities to distance

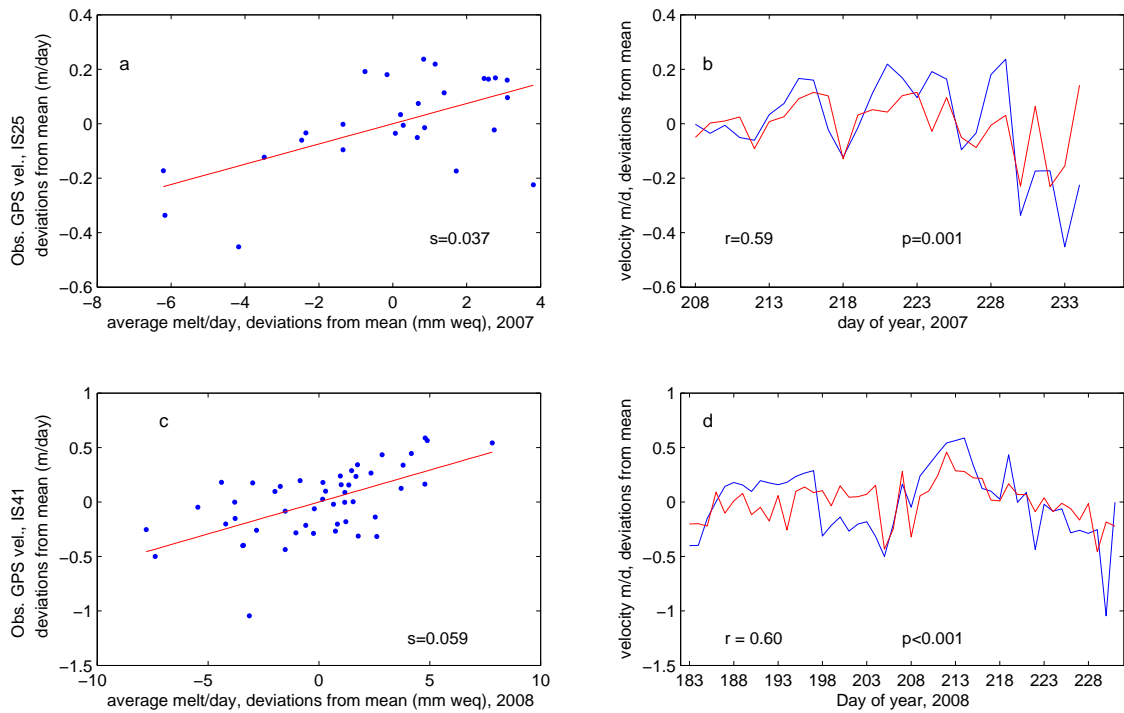


Figure 7: Model fit at stations IS25 and IS41, 2007 and 2008. (a) Scatter plot of deviations from mean melt, 12 mm d^{-1} w.e., and deviations from mean velocity, 15.6 m d^{-1} , for GPS station IS25, 2007. Red line shows best fit in a linear least-squares sense with slope $s=0.037$, i.e., $\sim 4 \text{ cm d}^{-1}$ increased velocity per mm w.e. melt above mean. (b) Predicted (red) and (blue) observed velocities. Correlation coefficient $r=0.59$ between modeled and observed velocities is significant at $>99\%$ levels. (c) Scatter plot of deviations from mean melt, 11.5 mm d^{-1} w.e., and deviations from mean velocity, 18.4 m d^{-1} , for GPS station IS41, 2008. Red line shows best fit in a linear least-squares sense with slope $s=0.059$, i.e., $\sim 6 \text{ cm d}^{-1}$ increased velocity per mm w.e. melt above mean. (d) Predicted (red) and (blue) observed velocities. Correlation coefficient $r=0.66$ between modeled and observed velocities is significant at $>99\%$ levels.

from the calving front is significant at $>99\%$ levels (Figure 8, top panel). When three stations with high residual-variance values and short time series are identified as outliers (IS40, IS46, and IS56, marked with red diamonds in the figure), an exponential fit to the data is preferable. The RMS residual of the linear fit is $0.015 \text{ m d}^{-1}/\text{mm d}^{-1}$ w.e. while the RMS residual of the exponential fit is $0.006 \text{ m d}^{-1}/\text{mm d}^{-1}$ w.e.

To test the impact of our calving-correction scheme on the retrieved sensitivity values and the observed spatial pattern, we repeat the same analysis for 2008 after correcting for only the three largest earthquake events (two on day 214 and one on day 232). Doing so leads to slightly lower sensitivity values (within 1σ) and slightly higher misfits overall. The spatial dependence of the sensitivities changes very little, however, indicating the robustness of this result to the details of the time-series correction.

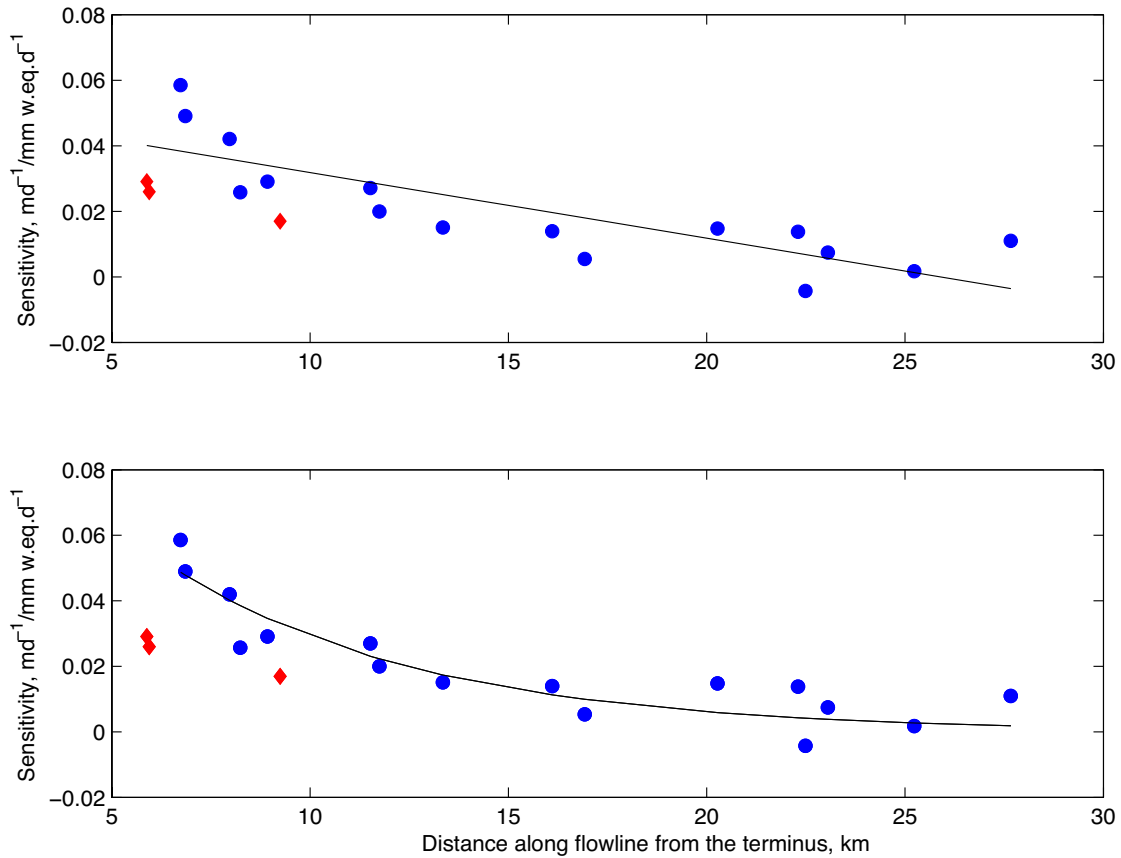


Figure 8: Top: Distance from terminus, plotted with spatially varying sensitivity values for 2008. RMS residual of the linear fit is $0.015 \text{ m d}^{-1}/\text{mm d}^{-1}$ w.e. r -value of the correlation is -0.8 with $p=0.00006$. Points with short time series (<35 days) are marked with red diamonds and are omitted in the fit. Bottom: Same as top, but with an exponential relationship fitted to the points. RMS residual is $0.006 \text{ m d}^{-1}/\text{mm d}^{-1}$ w.e.

Temporal variability

We also wish to investigate potential temporal variation in the sensitivity of glacier velocity to melt-water input. The available melt record from 2007 is relatively short (27 days) and we therefore focus this analysis on data from 2008, when the melt record is longer (49 days). We calculate sensitivities and residual variances for five moving windows of lengths 5, 11, 15, 19, and 21 days, for eight stations selected from across the glacier trunk in 2008 (IS41, IS42, IS43, IS44, IS51, IS53, IS58, and IS61, Figure 1), beginning at the first day of overlap between the melt record and the velocity time series. We repeat the fitting procedure with shifts of one day until the end of the moving window reaches the last day of overlap between the two time series. Thus, for each station, we generate five time series of sensitivity and residual variance. Figure 9 shows the 11, 15, and 19 day windows for station IS41.

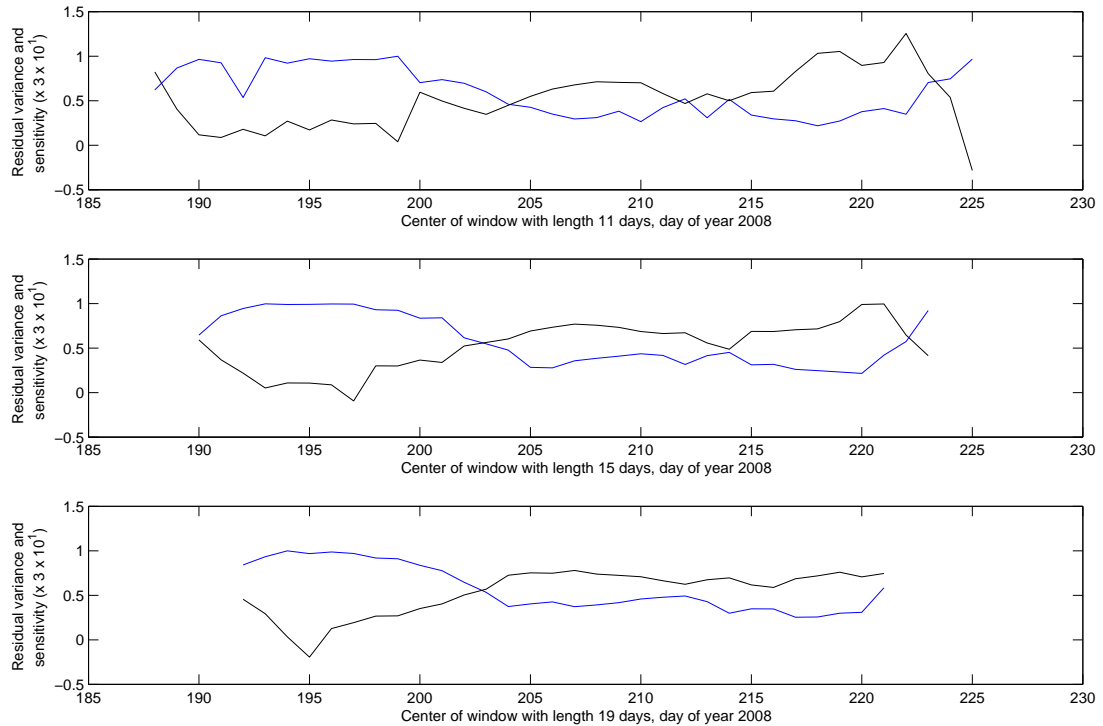


Figure 9: Result of sliding-window inversion using integrated melt signal and 2008 GPS station IS41. Black line shows sensitivity, blue line shows residual variance. Top panel: 11-day window; middle panel: 15-day window; bottom panel: 19-day window.

The curves produced by the five window lengths resemble each other, increasing in smoothness with window length, as a natural consequence of the longer averaging. A gradual decrease in residual variance over the considered period is evident, with the lowest residual variances occurring when the window is centered around days 219 ± 1 . This is the case for all five tested window lengths. Residual variances of the windows centered around these days are as low as 0.22 (11-day window), 0.21 (15-day window), and 0.26 (19-day window), suggesting that melt input explains most of the calving-corrected velocity variability during these periods.

We also observe a change in the modeled sensitivity values. Until the window centered on day ~ 214 , the sensitivity increases slowly. Immediately after this, the sensitivity values rise steeply; in Figure 9 this is especially clear in the 11-day window. The low values of residual variance and high values of sensitivity are sustained for a period of ~ 5 one-day shifts of the window, after which we see an increase in residual variance accompanied by a drop in sensitivity. The same behavior is observed across the glacier, at all eight stations analyzed; the sensitivities calculated for the 15-day window are shown in Figure 10.

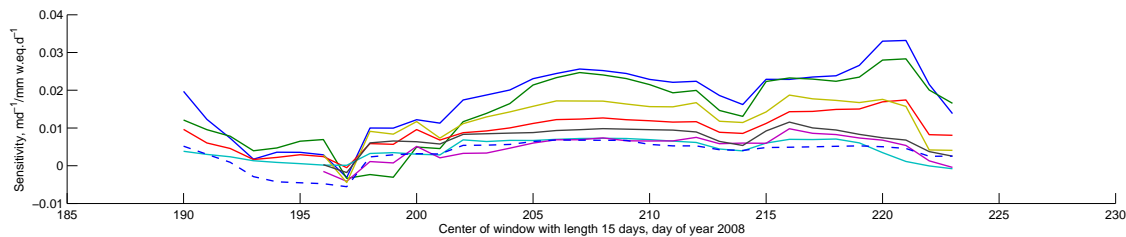


Figure 10: Development of sensitivity values over the season for eight representative stations using a 15-day window. IS41 (blue), IS42 (green), IS43 (yellow), IS44 (red), IS51 (cyan), IS53 (blue, dashed), IS58 (purple), IS61 (black).

Discussion

Overall, we find that the total amount of velocity variability explained by melt at Helheim Glacier is small, but significant. The observed additional speedup of $\sim 3.5\%$ (~ 240 m yr^{-1} , using average 2008 summer speed measured close to the front) above the mean corresponds to an additional yearly solid-mass discharge of ~ 0.9 Gt from the trunk of Helheim Glacier. Using a common melt-sensitivity value across the entire glacier predicts the observed velocities poorly, whether using integrated or local melt records as input (Figure 6). Allowing for separate sensitivity values at each station location produces better fits, with a coherent pattern of spatial variability. The sensitivity of velocity to melt input decays approximately exponentially with increasing distance from the calving front (Figure 8). We also observe intra-seasonal variability in the fraction of the velocity signal explained by varying melt-water input, with the fraction of variance explained by the model increasing later in the melt season. At the same time, we observe an increase in sensitivity (Figure 9). The temporal pattern of this increase is similar among the stations, but the amplitude drops with distance up glacier (Figure 10).

Joughin et al. (2008b) showed that the West Greenland ice-sheet margin speeds up significantly ($50\text{--}100\%$, or $31\text{--}76$ m yr^{-1}) during the summer melt season. The effect on outlet glaciers in the same region was found to be smaller in a relative sense, but of similar absolute magnitude ($9\text{--}14\%$, or $51\text{--}77$ m yr^{-1}). The $\sim 3.5\%$ of Helheim Glacier's summer speed variability we attribute to variations in melt input is somewhat lower than the relative speedup values observed by *Joughin et al.* (2008b). However, the set of outlet glaciers studied by *Joughin et al.* (2008b) have slower mean flow speeds than Helheim Glacier. We note also that those authors did not remove calving-related accelerations from their time series, possibly resulting in an overestimate of the fraction of acceleration attributed to melt. In addition, *Joughin et al.* (2008b) used 24-day speed averages and a longer time series than is available to us, thereby perhaps capturing a seasonal signal we are unable to observe. Fractionally, the melt-related speed variability we observe is also substantially smaller than that observed on the ice sheet by *Shepherd et al.*

(2009), on Russell Glacier (*Bartholomew et al.*, 2010), and on alpine glaciers (e.g., *Iken and Bindshadler*, 1986; *Anderson et al.*, 2004).

In an absolute sense, the melt-related speedup we observe is comparable to, or larger than, that seen on the ice-sheet margin and at some alpine glaciers. In the summers of 2007 and 2008, average flow speeds near the terminus of Helheim Glacier were $\sim 19\text{--}25$ m d⁻¹, or 7–9 km yr⁻¹. The 2–4% speedups we observe in 2008 correspond to $\sim 140\text{--}365$ m yr⁻¹, about twice the magnitude of the absolute speedup reported by *Joughin et al.* (2008b) for the West Greenland outlet glaciers and slightly higher than the peak speedup reported for Russell Glacier by *Bartholomew et al.* (2010).

At Columbia Glacier, Alaska, which is similar in size and also marine terminating, *Kamb et al.* (1994) and *Meier et al.* (1994) studied the association between water storage, basal pressure and surface displacement and observed speed-up and slow-down events believed to be associated with subglacial pressure variations. At the downstream “km 59” site at Columbia Glacier, they observed speed variations of $\sim 0.5\text{--}2$ m d⁻¹, or $\sim 180\text{--}730$ m yr⁻¹, which is consistent with our results from Helheim. It should be noted that these authors, like *Joughin et al.* (2008b), did not remove calving-related accelerations in their analysis.

It therefore appears that the overall flow speed of Helheim Glacier is less sensitive to melt input than the land-terminating ice-sheet margin, a land-terminating outlet glacier (Russell Glacier), and alpine glaciers, in a relative sense, though the absolute amplitude of the melt response is similar to or larger than that of other glacial systems. We are unable to observe the subglacial hydrological system at Helheim Glacier directly, and literature on the subglacial hydrology of the large Greenland outlet glaciers is limited. However, at those glaciers where observations are available, strong correlations between variations in basal water pressure and variations in sliding velocity have been documented (e.g., *Iken and Bindshadler*, 1986; *Kamb et al.*, 1994; *Kamb et al.*, 1985). Observations of surface displacement in combination with other hydrological and meteorological measurements used as a proxy for basal water pressure suggest a similar correlation (e.g., *Anderson et al.*, 2004; *Bartholomew et al.*, 2008; *Björnsson*, 1998). A common interpretation of these studies is that an increase in basal water pressure causes or sustains cavitation, which leads to increased bed separation and consequently increased sliding speed. Similarly, we interpret the dependence of glacier speed on melt-water input that we observe at Helheim Glacier to result from increases in subglacial water pressure as surface melt water drains to the bed.

We expect, then, that melt input will affect Helheim Glacier’s sliding speed only where, and when, the melt input is sufficient to decrease the effective pressure (overburden pressure minus basal water pressure) at the bed. The high background flow speeds at Helheim ($\sim 6\text{--}25$ m d⁻¹ in the study region) are expected to generate large amounts of

basal water due to frictional and strain heating, even in the absence of surface-melt-water input. The additional water provided to the bed by surface melting might, as a result, be fractionally small, and the glacier probably maintains an efficient drainage system that easily discharges additional melt input. Both effects might reduce the sensitivity of the glacier to melt water-input.

We observe the highest sensitivity to melt-water input in the region of the glacier just behind the calving front. We hypothesize that this increased sensitivity results from a combination of conditions, including easier access of melt water to the bed due to extensive crevassing, high basal water pressure, and a less efficient drainage system than elsewhere under the glacier. It is likely that the glacier is close to flotation near the front (*de Juan et al.*, 2010) leading to high basal water pressure; we have also observed turbid water upwelling into an open relict-moulin structure just behind the calving front, an additional indication of high basal water pressure. In this area behind the front, the glacier's inferred high sliding speed leads to faster closing of open water channels, resisting the formation or maintenance of efficient, channelized drainage. In addition, the reported shape of the bed (<https://www.cresis.ku.edu/~jmeisel/helheim/version4/>) is overdeepened behind the calving front, such that subglacial water would need to flow upslope to exit the glacier, making it difficult to sustain a low-pressure, well-channelized drainage system. All of these factors possibly contribute to higher basal pressure under the region of the glacier nearest the calving front, making the glacier more sensitive to additional melt input in this area.

Another factor that might contribute to the spatial variability in sensitivity to melt input and the importance of melt in explaining velocity variability is the strain field across the glacier. Compressional strain could limit the flow of melt water to the bed by resisting the establishment — or accelerating the closing — of deep crevasses, moulins, and other englacial conduits. The area of the glacier immediately above the bend (Figure 1) is predominantly compressive, as illustrated by multi-year field observations of a melt-water lake located in close proximity to IS51 in 2008 and IS28 in 2007. Mean strain rates, calculated from daily along-flow strain rates between stations on the flow line, are shown in Figure 11. The strain rates are calculated as $\dot{\epsilon} = \Delta v / D$, where Δv is the difference in velocity between two stations, and D is the distance between them. Both values are acquired from the GPS position data. Areas exposed to compressional strain yield negative strain rates and areas of extension produce positive rates. The colors of the markers in Figure 11 indicate the residual-variance values from our model of velocity response to melt input at the station immediately downstream of the mid-point plotted. A weak relationship appears to exist between the sign of the strain rate and the residual variance: Poorer fits are typically obtained in areas of compressional strain. An exception is IS50, which exhibits high residual variance in spite of being situated downstream of an extensional strain area. We suggest that less velocity variability is

explained by melt in areas where it is more difficult for surface melt water to penetrate to the bed.

The temporal variations in sensitivity and variance reduction we observe suggest additional complexity in the relationship between melt and velocity variations. Melt-water input explains a larger fraction of the calving-corrected speed variations later in the season (~80%) than in the earlier part. In addition, the glacier responds more strongly to a given melt-water input later in the season, when mean melt-water input is also higher.

The time windows yielding the lowest residual-variance values and highest sensitivities in 2008 are centered around days 210–213 (Figure 9), immediately following the peak of melt water production (Figure 5). The melt-water-driven velocity increase of 3–4% at the sites closest to the terminus at this time represents the largest calving-corrected speed anomaly observed in 2008. The greater late-season responsiveness provides an additional explanation for the low sensitivities of sites IS40, IS46, and IS56, the outliers in the exponential fit shown in Figure 8: the time series are shorter for those three stations, and were recorded during the earliest part of the season. We hypothesize that the intense melt-water production occurring around days 210–213 causes basal pressure across Helheim Glacier to increase, resulting in a closer association between melt and velocity. Sensitivity decreases again late in the season, possibly because a new equilibrium has been attained by the drainage system, or because of a drop in melt-water production.

The higher sensitivity we observe at times of greater melt indicates some nonlinearity in the responsiveness of Helheim Glacier to melt-water input, and suggests that an increase in background melt rates might lead to an increase in outlet-glacier sensitivity to that melt, in a weak positive feedback cycle. This nonlinear behavior is observed at least 20 km behind the calving front, suggesting that the area of increased sensitivity may extend with increasing temperatures to comprise a larger part of the glacier trunk. This interpretation has implications for glacier response to warming air temperatures, and merits further exploration.

Conclusions

We have investigated the impact of variations in melt-water input on surface velocity at Helheim Glacier using model-based melt records and GPS-derived surface velocities. We find that, although melt-driven velocity variations represent only a few percent of the total glacier speed, the additional ice flux due to melt-water input is similar to that observed by other workers on the land-terminating portions of the ice-sheet margin. The sensitivity of glacier-speed variations to changes in melt-water input is spatially

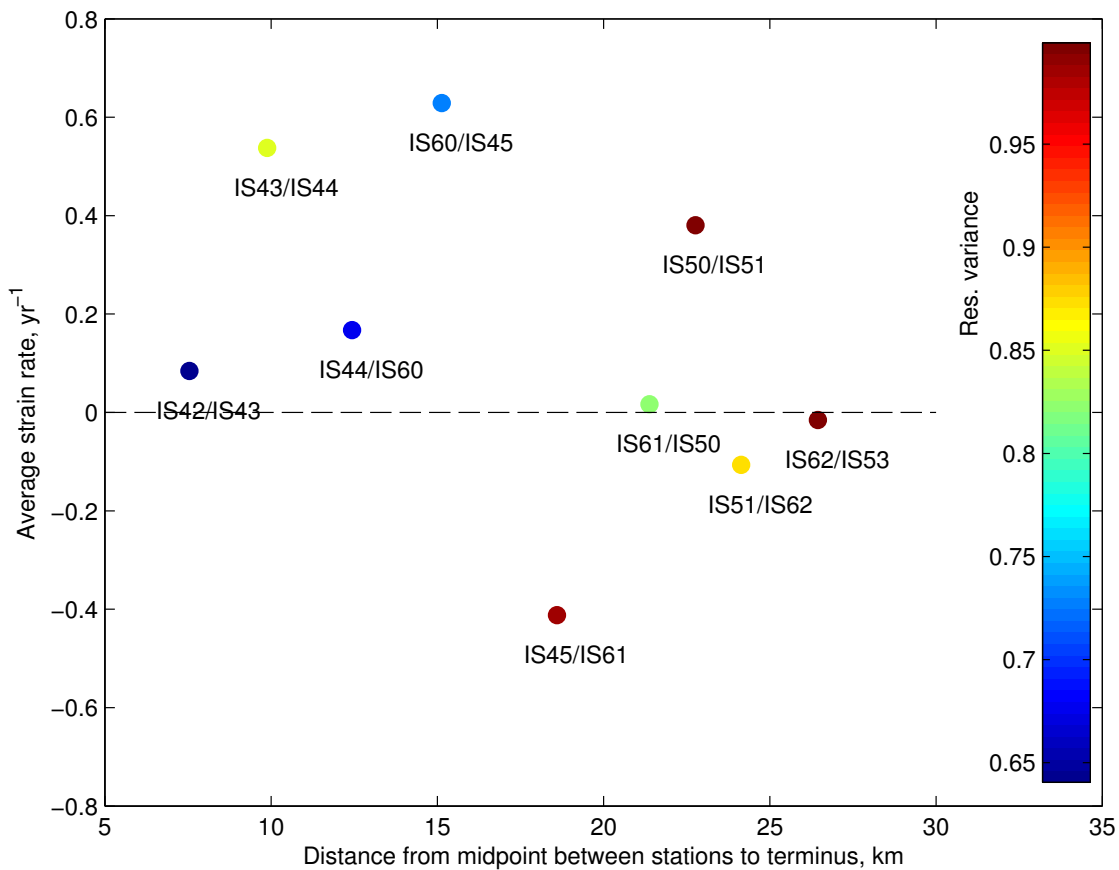


Figure 11: Mean strain rates between the selected stations. Negative strain rates signify compressional strain, positive are extensional. Colors indicate the residual-variance value for the station downstream of the mid point. See map in Figure 1 for station locations.

variable, and decays approximately exponentially with distance along the flow line from the calving front. We interpret this variation in melt sensitivity to result from varying subglacial hydrological conditions. We find some evidence for modulation of the melt-water response by strain conditions in the ice, with the velocity data less well explained by the melt signal in areas of compressional strain. Our observations suggest a region of high basal water pressure near the calving front of Helheim Glacier, perhaps associated with near-flotation conditions and a distributed subglacial drainage system.

We also find a temporal dependence in the fraction of velocity variance explained by melt water input. In early July 2008, Helheim Glacier shows little to no dependence on melt input. In late July to mid-August, as much as 80% of the calving-corrected velocity variability can be explained by melt-water variations. Sensitivity to melt also increases, coincident with a week-long speed anomaly of 3–4% above the mean near the calving front. This temporal evolution in sensitivity to melt input indicates a nonlinear velocity response to surface melt, and points to the need for a better understanding of

the response to melting, particularly as atmospheric temperatures warm.

We believe our results to be generally applicable to Greenland's fast flowing, marine-terminating outlet glaciers. Though the additional ice flux due to increased surface melting may represent only a few percent of the total flux through these high-discharge glaciers, the absolute magnitude of the additional flux may be substantial.

Acknowledgments

The Helheim 2007 and 2008 project was supported by the Gary Comer Science and Education Foundation, the U.S. National Science Foundation, the Danish Commission for Scientific Research in Greenland (KVUG), the Spanish Ministry of Science and Innovation (MICINN), the Geological Survey of Denmark and Greenland (GEUS), Geocenter Copenhagen, the Danish National Space Center, NASA, the Lamont-Doherty Climate Center, and the Dan and Betty Churchill Exploration Fund. GPS equipment and technical support were provided by UNAVCO, Inc. The authors wish to thank Kristin Schild, University of Maine, for assistance in the field, and Julia de Juan, CSIC for assistance with data processing.

Bibliography

- Amundson, J. M., M. Truffer, M. P. Luethi, M. Fahnestock, M. West, and R. J. Motyka (2008), Glacier, fjord, and seismic response to recent large calving events, Jakobshavn Isbrae, Greenland, *Geophysical Research Letters*, 35(22), L22501, doi:{10.1029/2008GL035281}.
- Andersen, M. L., T. Larsen, M. Nettles, P. Elosegui, D. van As, G. S. Hamilton, L. A. Stearns, J. L. Davis, A. P. Ahlström, J. de Juan, G. Ekström, L. Stenseng, S. A. Khan, R. Forsberg, and D. Dahl-Jensen (2010), Spatial and temporal melt variability at Helheim Glacier, East Greenland, and its effect on ice dynamics, *Journal of Geophysical Research, Earth Surface* (in press).
- Anderson, R. S., S. P. Anderson, K. R. MacGregor, E. D. Waddington, S. O'Neel, C. A. Riihimaki, and M. G. Loso (2004), Strong feedbacks between hydrology and sliding of a small alpine glacier, *Journal of Geophysical Research*, 109, doi:{10.1029/2004JF000120}.
- Bartholomaeus, T. C., R. S. Anderson, and S. P. Anderson (2008), Response of glacier basal motion to transient water storage, *Nature Geoscience*, 1(1), 33–37, doi:{10.1038/ngeo.2007.52}.

- Bartholomew, I., P. Nienow, D. Mair, A. Hubbard, M. A. King, and A. Sole (2010), Seasonal evolution of subglacial drainage and acceleration in a Greenland outlet glacier, *Nature Geoscience*, 3(6), 408–411, doi:{10.1038/NGEO863}.
- Björnsson, H. (1998), Hydrological characteristics of the drainage system beneath a surging glacier, *Nature*, 395(6704), 771–774.
- Chen, J. L., C. R. Wilson, and B. D. Tapley (2006), Satellite gravity measurements confirm accelerated melting of Greenland ice sheet, *Science*, 313(5795), 1958–1960, doi:{10.1126/science.1129007}.
- Das, S. B., I. Joughin, M. D. Behn, I. M. Howat, M. A. King, D. Lizarralde, and M. P. Bhatia (2008), Fracture propagation to the base of the Greenland Ice Sheet during supraglacial lake drainage, *Science*, 320(5877), 778–781, doi:{10.1126/science.1153360}.
- de Juan, J., P. Elósegui, M. Nettles, T. B. Larsen, J. L. Davis, G. S. Hamilton, L. A. Stearns, M. L. Andersen, G. Ekström, A. P. Ahlstrøm, L. Stenseng, S. A. Khan, and R. Forsberg (2010), Sudden increase in tidal response linked to calving and acceleration at a large Greenland outlet glacier, *Geophysical Research Letters*, 37, doi:{10.1029/2010GL043289}.
- Ekström, G. (2006), Global detection and location of seismic sources by using surface waves, *Bull. Seismol. Soc. Am*, 96, 1201–1212, doi:{10.1785/0120050175}.
- Fountain, A. G., R. W. Jacobel, R. Schlichting, and P. Jansson (2005), Fractures as the main pathways of water flow in temperate glaciers, *Nature*, 433, 618–621.
- Hall, D. K., G. A. Riggs, and V. V. Salomonson (2007), MODIS/Terra Snow Cover Daily L3 Global 500m Grid V005, Julian days 205, 209, 218, 222, 224, 225, 227, 228, 230, 234. Updated daily, <http://nsidc.org/data/index.html>.
- Hall, D. K., G. A. Riggs, and V. V. Salomonson (2008), MODIS/Terra Snow Cover Daily L3 Global 500m Grid V005, Julian days 179, 180, 182, 183, 195, 199, 200, 202, 203, 204, 205, 207, 209, 214, 216, 217, 218, 222, 223, 225, 235, 238. Updated daily, <http://nsidc.org/data/index.html>.
- Hamilton, G. S., S. A. Khan, K. M. Schild, L. A. Stearns, M. Nettles, A. P. Ahlstrøm, M. L. Andersen, J. L. Davis, G. Ekström, P. Elósegui, R. Forsberg, J. de Juan, T. B. Larsen, and L. Stenseng (2008), Iceberg Calving and Flow Dynamics at Helheim Glacier, East Greenland, from Time-Lapse Photography, *Eos Trans. AGU* 89(53), *Fall Meet. Suppl.*, Abstract C13A-0565.
- Howat, I., I. Joughin, S. Tulaczyk, and S. Gogineni (2005), Rapid retreat and acceleration of Helheim Glacier, east Greenland, *Geophysical Research Letters*, 32(22), doi:{10.1029/2005GL024737}.

- Iken, A., and R. A. Bindschadler (1986), Combined measurement of subglacial water-pressure and surface velocity of Findelengletscher, Switzerland - conclusions about drainage system and sliding mechanism, *Journal of Glaciology*, 32(110), 101–119.
- Joughin, I., I. M. Howat, M. Fahnestock, B. Smith, W. Krabill, R. B. Alley, H. Stern, and M. Truffer (2008a), Continued evolution of Jakobshavn Isbræ following its rapid speedup, *Journal of Geophysical Research - Earth Surface*, 113(F4), doi:10.1029/2008JF001023.
- Joughin, I., S. B. Das, M. A. King, B. E. Smith, I. M. Howat, and T. Moon (2008b), Seasonal speedup along the western flank of the Greenland Ice Sheet, *Science*, 320(5877), 781–783, doi:10.1126/science.1153288.
- Kamb, B., C. Raymond, W. Harrison, H. Engelhardt, K. Echelmeyer, N. Humphrey, M. Brugmann, and T. Pfeffer (1985), Glacier surge mechanism - 1982-1983 surge of Variegated Glacier, Alaska, *Science*, 227(4686), 469–479.
- Kamb, B., H. Engelhardt, M. A. Fahnestock, N. Humphrey, M. Meier, and D. Stone (1994), Mechanical and hydrologic basis for the rapid motion of a large tidewater glacier. 2. Interpretation, *Journal of Geophysical Research - Solid Earth*, 99(B8), 15,231–15,244.
- Krabill, W., E. Hanna, P. Huybrechts, W. Abdalati, J. Cappelen, B. Csatho, E. Frederick, S. Manizade, C. Martin, J. Sonntag, R. Swift, R. Thomas, and J. Yungel (2004), Greenland Ice Sheet: Increased coastal thinning, *Geophysical Research Letters*, 31(24), doi:{10.1029/2004GL021533}.
- Luthcke, S. B., H. J. Zwally, W. Abdalati, D. D. Rowlands, R. D. Ray, R. S. Nerem, F. G. Lemoine, J. J. McCarthy, and D. S. Chinn (2006), Recent Greenland ice mass loss by drainage system from satellite gravity observations, *Science*, 314(5803), 1286–1289, doi:{10.1126/science.1130776}.
- Meier, M., S. Lundstrom, D. Stone, B. Kamb, H. Engelhardt, W. W. Dunlap, M. Fahnestock, R. M. Krimmel, and R. Walters (1994), Mechanical and hydrologic basis for the rapid motion of a large tidewater glacier. 1. Observations, *Journal of Geophysical Research, Solid Earth*, 99(B8), 15,219–15,229.
- Nettles, M., and G. Ekström (2010), Glacial Earthquakes in Greenland and Antarctica, *Annual Reviews of Earth and Planetary Science*, 38, 467–491, doi:{10.1146/annurev-earth-040809-152414}.
- Nettles, M., T. B. Larsen, P. Elósegui, G. S. Hamilton, L. A. Stearns, A. P. Ahlstrøm, J. L. Davis, M. L. Andersen, J. de Juan, S. A. Khan, L. Stenseng, G. Ekström, and R. Forsberg (2008), Step-wise changes in glacier flow speed coincide with calving and glacial

- earthquakes at Helheim Glacier, Greenland, *Geophysical Research Letters*, 35, L24503, doi:{10.1029/2008GL036127}.
- Rignot, E., J. E. Box, E. Burgess, and E. Hanna (2008), Mass balance of the Greenland ice sheet from 1958 to 2007, *Geophysical Research Letters*, 35(20), doi:{10.1029/2008GL035417}.
- Shepherd, A., A. Hubbard, P. Nienow, M. King, M. McMillan, and I. Joughin (2009), Greenland ice sheet motion coupled with daily melting in late summer, *Geophysical Research Letters*, 36, L01501, doi:{10.1029/2008GL035758}.
- Stearns, L. A. (2007), Outlet glacier dynamics in East Greenland and East Antarctica, Ph.D. thesis, University of Maine.
- Van de Wal, R. S. W., W. Boot, M. R. Van den Broeke, C. J. P. P. Smeets, C. H. Reijmer, J. J. A. Donker, and J. Oerlemans (2008), Large and rapid melt-induced velocity changes in the ablation zone of the Greenland Ice Sheet, *Science*, 321(5885), 111–113, doi:{10.1126/science.1158540}.
- Van den Broeke, M., P. Smeets, J. Ettema, C. van der Veen, R. van der Wal, and J. Oerlemans (2008), Partitioning of melt energy and melt water fluxes in the ablation zone of the west Greenland ice sheet, *The Cryosphere*, 2, 179–189.
- Van der Veen, C. J. (2007), Fracture propagation as means of rapidly transferring surface meltwater to the base of glaciers, *Geophysical Research Letters*, 34(1), doi:{10.1029/2006GL028385}.
- Velicogna, I., and J. Wahr (2006), Acceleration of Greenland ice mass loss in spring 2004, *Nature*, 443(7109), 329–331, doi:{10.1038/nature05168}.
- Zwally, H., W. Abdalati, T. Herring, K. Larson, J. Saba, and K. Steffen (2002), Surface melt-induced acceleration of Greenland ice-sheet flow, *Science*, 297(5579), 218–222.

Detection and spectral characterization of calving related seismic signals, Helheim Glacier, South East Greenland

M. L. Andersen^{1,2}, T. B. Larsen¹, M. Nettles³

Manuscript in preparation

¹Geological Survey of Denmark and Greenland (GEUS), Copenhagen DK-1350, Denmark

²Centre for Ice and Climate, Niels Bohr Institute, Univ. of Copenhagen, Copenhagen DK-2100, Denmark

³Lamont-Doherty Earth Observatory, Columbia University, Palisades, NY 10964, USA

Abstract

Seismogenic signals associated with calving and ice rupture in the large Greenland outlet glaciers can provide new and valuable information about the cryospheric processes involved. Teleseismically detected glacial earthquakes are found at Helheim Glacier to be preceded by long duration rumblings with a characteristic frequency content distinctively different from both tectonic earthquakes and the background noise. These rumblings have an average duration of 28-29 minutes and have high-frequency as well as low-frequency content. We have developed a frequency-domain detection algorithm for the rumblings recorded at a broad-band station ISO, located ~ 100 km from the glacier. The seismic detector has been calibrated with observations of calving from a time-lapse camera near the glacier front. Our analysis shows a seasonal variation in the occurrence of rumblings with a peak in mid-September coinciding with the end of the melt season.

1 Introduction

Large outlet glaciers drain the Greenland ice sheet. In recent years these have accelerated with increased ice loss to the ocean as a consequence (*Rignot and Kanagaratnam, 2006*;

Stearns and Hamilton, 2007; Thomas et al., 2009). About half of the solid mass loss from the ice sheet happens through calving processes at the termini of the outlet glaciers along the coast (*Van den Broeke et al., 2009*). Calving events are found to be seismogenic (e.g., *Nettles et al., 2008; O'Neel et al., 2007*) allowing for investigations of the cryospheric processes using both teleseismic data as well as regional and local recordings. Monitoring of the occurrence of glacial earthquakes (*Ekström et al., 2003; Ekström, 2006; Ekström et al., 2006*) can provide clues to understanding the development of ice loss from the Greenland Ice Sheet. Detailed investigations of the pre-calving and calving behavior of large outlet glaciers give insight into the actual processes that is the cause of mass loss from the terminus.

Teleseismic data have formed the basis for detailed investigations of seismic events originating from tidewater glaciers all across Greenland (*Tsai et al., 2008; Tsai and Ekstrom, 2007*) while campaign-based studies have previously been conducted in West Greenland (*Amundson et al., 2008; Rial et al., 2009*), Alaska (*O'Neel et al., 2007; O'Neel and Pfeffer, 2007*), and East Greenland (*Nettles et al., 2008*). *Rial et al. (2009)* discussed glacial rumblings at Jakobshavn Isbræ, terminating in 'culminating events'. They find that these culminating events do not directly arise from calving processes at the front, rather it is speculated that they are the result of ruptures propagating in the ice, initiated by calving. However, it is clear from *Nettles et al. (2008)* that teleseismically detected seismic events at Helheim are in fact associated with (large) calving events. While the source mechanism of the Helheim events is still unclear, the timing of the events suggests a direct physical connection between the actual loss of ice at the front and the behavior of the iceberg immediately after calving.

We wish to investigate whether rumbling events similar to the ones found by *Rial et al. (2009)* also occur at Helheim Glacier, East Greenland, what their characteristics are, how they relate to glaciological data, and if they exhibit a seasonal dependence similar to the one observed for other glacial earthquakes (*Ekström et al., 2006; Jonsdottir et al., 2009*).

To achieve this goal we develop a frequency-domain detection algorithm. We analyze time domain seismic records together with a list of confirmed occurrences of calving to find a characteristic seismic spectrum associated with the calving events for the detector. The detector is then able to pick seismic activity "events" related to Helheim Glacier from a local seismic record. A list of events is thus constructed, allowing us to analyze the temporal pattern of seismic activity over almost two years. We discuss and compare our findings with seismological observations made at other tidewater glaciers (*O'Neel et al., 2007; Rial et al., 2009*), with teleseismically detected glacial earthquakes and with glaciological data.

Understanding these events, their pattern and further development of the method might provide a tool for automatic monitoring of the conditions of the outlet glaciers of Green-

land, complementing the methods already in use (remote sensing, time-lapse imagery, etc.). A large, international monitoring-effort (GLISN) has been launched with the purpose of collecting data from multiple locations around the coast and interior of Greenland, one goal of which it is to understand the seismicity emitted from the outlet glaciers in relation to climate change (<http://www.glisn.info>).

2 Data and methods

2.1 Data

2.1.1 Recorded seismic data/data preparation

The station used in this study, designated ISO, was installed in the settlement of Iser-toq, approximately 100 km ($\Delta = 0.87$ degrees) from Helheim Glacier (see Figure 1). The location was selected due to the year-round accessibility using public helicopter route flying, and access to mains power for the station at the installation site. These considerations are crucial in a remote area as East Greenland, where logistics are costly. Data was recorded using a Streckeisen STS-2 broadband seismometer and a RefTek 130 data logger with a sample rate of 20 samples/second. Using the software package *gsac* the instrument response was deconvolved. To avoid end-effects polluting the signals, the seismograms were cut into 28-hour pieces centered at 12:00 UTC and overlapping two hours with the previous and next days. We use the vertical component, *Z*, in the velocity seismograms for surface wave detection.

In the following we describe the spectral characteristics and occurrence of seismicity arising from Helheim Glacier as recorded at the ISO station. As such, it is important to ensure that the events we include in our analysis can be shown to have their source location at Helheim Glacier. This can be done to a satisfying degree by cross-referencing a qualitative record of calving observations with the seismic record (see Section 2.1.3). Additionally, for a few events, teleseismic detections of glacial earthquakes are available (*Nettles et al.*, 2008; *Nettles and Ekström*, 2010), fixing the source location to Helheim Glacier. Finally, in one case we also use data from the GSN station located in Kangerlussuaq, West Greenland (station code SFJD) for inclusion of one event for analysis (see Section 2.1.2).

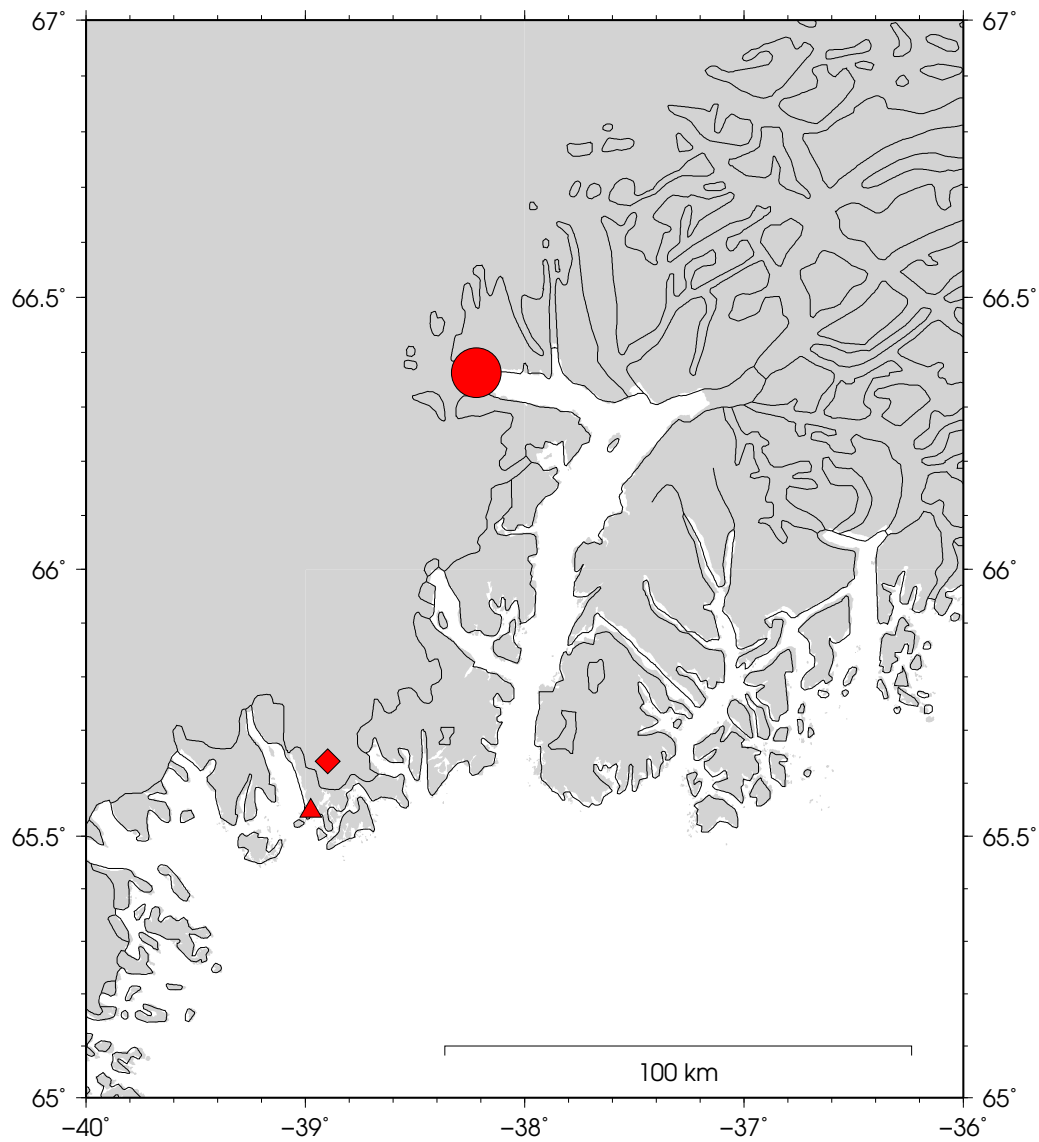


Figure 1: Map of the Helheim Glacier region, East Greenland. Red circle marks the glacier, red triangle marks the site of ISO seismic station in the settlement of Isortoq. Red diamond marks the location of the PROMICE automatic weather station. The black line traces the coast/ice-margin digitized by the Geological Survey of Denmark and Greenland.

2.1.2 Teleseismic detections of glacial earthquakes

Analysis of seismograms from the Global Seismographic Network (GSN) by *Nettles et al.* (2008) and *Nettles and Ekström* (2010), using the method of *Ekström* (2006), yielded a list of 14 teleseismically detected glacial earthquakes for 2007 and 2008 with source location at Helheim Glacier. The set of events detected in 2007 included automatic detections (5 events) and detections from interactive inspection of the GSN stack (6 events); in total 11 events (*Nettles et al.*, 2008). The 2008 set only included three automatic detections. We removed events not covered by the ISO seismic record (occurring outside the period of operation or during data gaps), leaving four events for 2007 and 2008 (see Table 1). One event, number 2, is not detected globally, but picked by manual inspection of the ISO and SFJD records. Figure 2 shows the ISO and SFJD records of the evening of day 225, 2007. A consistent offset is observed between the three events marked with boxes, two of which are teleseismically detected.

Year	Day	Time (UTC)	Magnitude	Event no.
2007	225	18:42.20	N/A	1
2007	225	20:06.26	N/A	2
2007	225	20:37.52	4.8	3
2008	232	21:05.28	4.7	4

Table 1: Teleseismically detected glacial earthquakes at Helheim Glacier. Only events occurring within the operational period of the Isertoq seismic station (ISO) are listed. Event 2 is not detected from the GSN stack, but appear in the SFJD record with the appropriate offset and is thus included. The time of this event is the time of maximum amplitude at ISO with an estimated travel time of 29 seconds subtracted.

2.1.3 Time-lapse camera

During the summer of 2008 a camera was mounted on the fjord wall, directed at the glacier front, providing visual observations of calving events. The camera was a digital SLR-type model mounted in a weather-proof enclosure and images were recorded every five minutes. The images were inspected manually and a calving record was thereby developed. The uncertainty in the observation of the time of calving is considerable; not all events are captured in the record as the image can be obscured by e.g. weather or, late in the season, darkness, and the time resolution is low. Additionally, logging of the actual time of calving depends on the judgment of the observer. In this study all photos were inspected by the same experienced person.

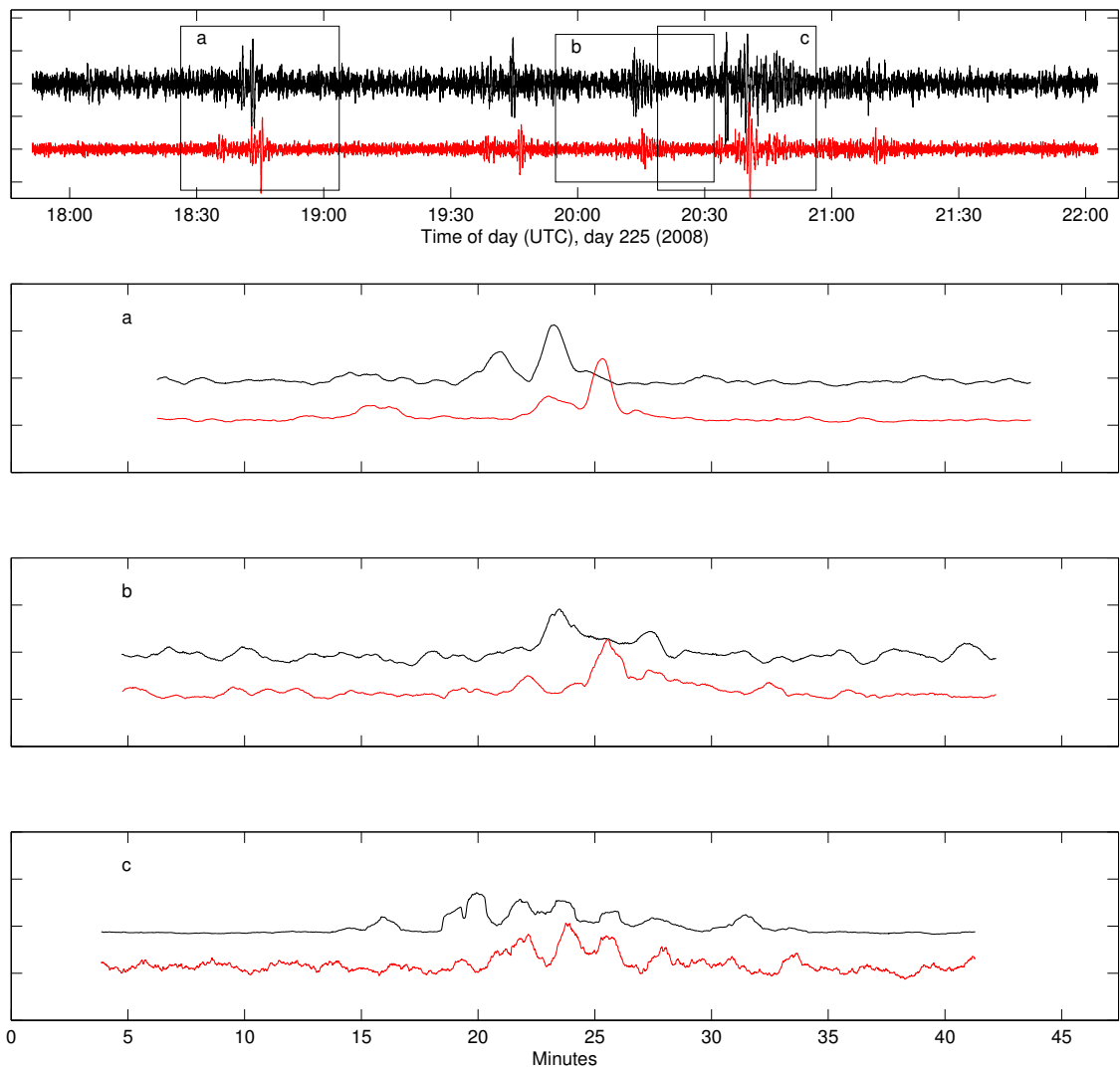


Figure 2: Top: ISO (black) and SFJD (red) seismograms filtered from 33-66 s with boxes indicating the segments examined in panels a, b, and c below. Panels a, b, and c show the envelopes of the indicated events with same color coding as in the top panel. A consistent offset between peaks of ~ 125 seconds is observed. (While the event occurring at $\sim 19:45$ min. is also evident in the SFJD record, the offset is not consistent with that of events a, b, and c. We assume it has a different source location.) (a) The envelope of the first event, filtered at 33-66 s periods. The event was teleseismically detected with source time at day 225 (Aug 13), 18:42:20 UTC. (b) The envelope of the second event filtered at 33-66 s periods. The event has not been automatically teleseismically detected. (c) The envelope of the third event filtered at 1-1.5 s periods. The event was teleseismically detected with source time at day 225 (Aug 13), 20:37:52 UTC.

In total, nine major calving events were extracted from the photographic record. Events not falling within the operation of the seismic station ISO, teleseismically detected (present in Table 1), or not obviously recognized, were removed leaving four for further analysis (see Table 2).

Year	Day	Approx. time (UTC)	Event no.
2008	195	04:54	5
2008	215	02:14	6
2008	226	11:35	7
2008	232	09:07	8

Table 2: Observed calving events, coincident with seismic activity validated by manual inspection of the seismic record. Times are from the camera clock. The listed times are approximate as per the observer’s judgment.

The two lists of events (Tables 1 and 2) can now be combined, yielding a list of eight events in total for analysis.

2.1.4 Tectonic earthquakes

Ordinary, tectonic earthquakes appear in the ISO record. These need to be removed in order to isolate seismicity likely to be arising from glacial activity.

To identify tectonic signals in the ISO record, we first create a list of events from a catalog search in the United States Geological Survey database (USGS, <http://earthquake.usgs.gov/earthquake>). The list is combined of two subsets: A search listing all earthquakes occurring within a radius of 3000 km from Helheim Glacier, and a global search of large earthquakes which are expected to be present in the ISO data. The circular area search includes earthquakes of all magnitudes, while the global search is limited to events with magnitudes larger than 6.0. The combined list comprises 748 unique events in the time span of July 1 2007 to December 31 2008. We then calculate the travel times for each event from the source location to Helheim Glacier using the iasp91 Earth model (*Kennett and Engdahl, 1991*). Signal values are then set to zero in a time window beginning at the theoretical P-arrival time and 150 minutes forward in time.

Furthermore, we remove a number of local earthquakes found in the catalog maintained by the Geological Survey of Denmark and Greenland. This list contains 135 events occurring in the area of latitude 64N to 68N and longitude 33.0W to 44.0W from July 1 2007 to December 31 2008.

2.2 Analysis

Figure 3 shows two examples of glacial events as they typically appear in the seismograms recorded at the ISO station. In the top panel the two teleseismically detected events from day 225, 2007 (Table 1) are plotted. The duration of these events is ~ 20 minutes. Also seen is activity during the ~ 2 hours between the events. This intermittent activity is similar in the time domain to the ‘glacial rumblings’ described by *Rial et al.* (2009) in the sense that it exhibits a gradual onset of energy and contains high amplitudes of high-frequency arrivals. As seen in Figure 3, these high-amplitude arrivals are evident in both the rumblings and the detected events and appear to be similar to what is termed ‘culminating events’ by *Rial et al.* (2009). The lower panel in Figure 3 shows glacial activity during a calving event observed in the time lapse camera record on day 195, 2008. Again, a gradual onset is noticed as well as a clear high-amplitude arrival, followed by a small ‘aftershock’ as also observed by *Rial et al.* (2009) at Jakobshavn Isbræ. These authors also notice that the calving starts the event. In Figure 3 (lower panel), the red line marks the precise time of calving (04.54), as noted by the observer, which coincides with the beginning of the event in the seismic record (~ 29 seconds have been added to account for the surface wave travel time from Helheim Glacier to the ISO station). A visual comparison between the activity recorded at ISO and the seismograms recorded at Columbia Glacier by *O’Neel et al.* (2007) confirms similar time-domain pattern.

To determine the similarity of the events, we analyze power spectra of sections of seismic activity arising from Helheim Glacier during 2007 and 2008, within the time of operation of the seismic station (Figure 4) and known to be associated with calving events. The lists derived from GSN analysis and time lapse photography (sections 2.1.2 and 2.1.3) are combined into a list of eight events for analysis (traces 1-8 in Figure 4). We also examine a period of no detectable seismicity in order to discern seismic signals generated by the glacier from ambient noise (trace 9 in Figure 4). Finally, for comparison, we calculate the power spectrum density of a local tectonic earthquake (trace 10 in Figure 4).

Spectral analysis

The calculated power spectral densities of the list of events are shown in Figure 5 for the frequency band .05 Hz to 10 Hz (Nyquist frequency). All glacial traces have a peak at ~ 0.18 - 0.33 Hz, as does the section of ambient noise (0.32 Hz). Therefore, we believe the peaks during the glacial events seen at these frequencies to be the background noise. This is consistent with the predominant frequencies of the microseism band in the summer in East Greenland (0.1-0.3 Hz) as described by *Harben and Hjortenberg* (1993). All glacial events are relatively broad-band and all but one (number 6) exhibit power am-

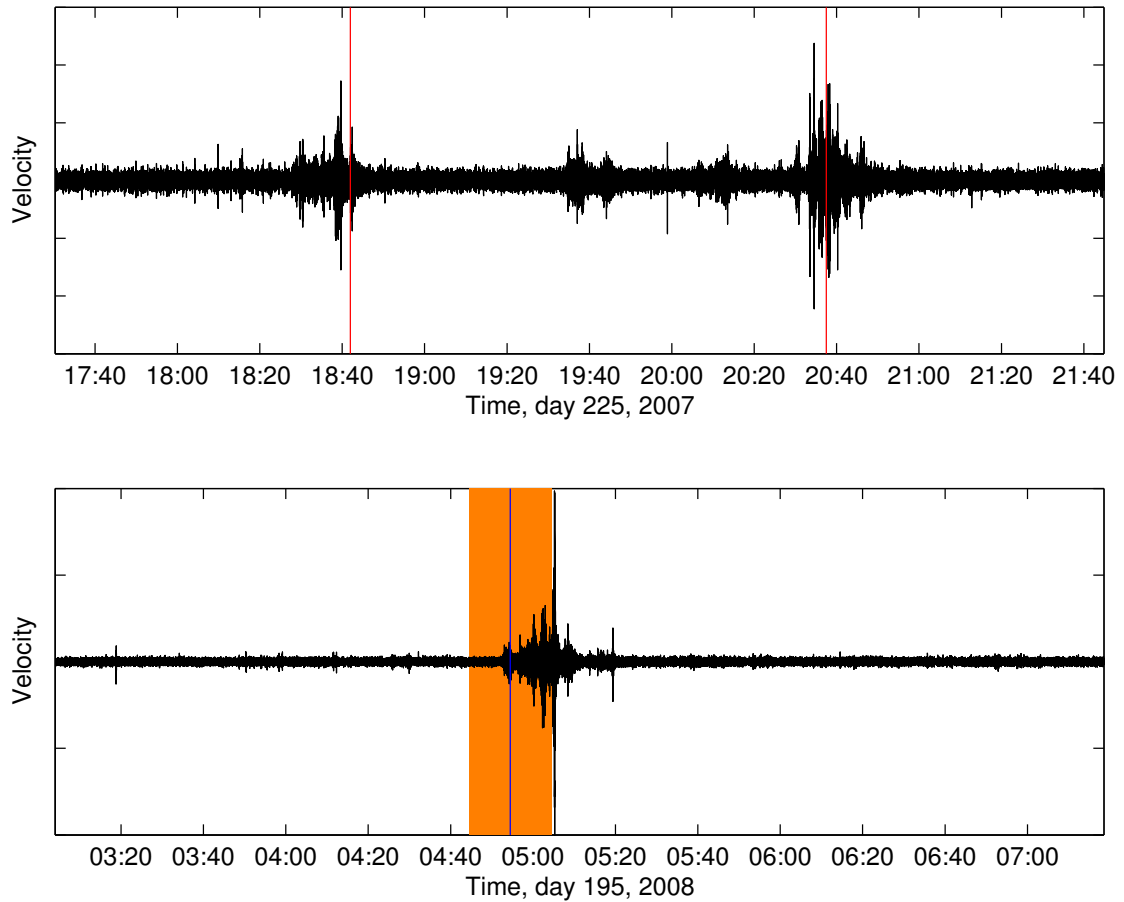


Figure 3: Two seismograms from the ISO station filtered in the high-frequency band 1.1-2 Hz. The length of the time window plotted is the same for both top and bottom. Top: Activity on day 225 of 2007. Red lines mark the teleseismic detection times. Bottom: Activity on day 195, 2008. The blue line marks the time of a calving event from the camera observations. The orange area indicates ± 10 minutes uncertainty on the camera observation time.

plitudes within the same order of magnitude in the 1-10 Hz band. They are clearly distinguishable from the background noise trace and the tectonic event. This indicates common spectral characteristics of the glacial events and suggests that detection is possible in the frequency domain. We can not clearly distinguish rumbling events that are associated with observable calving events (through teleseismic or visual methods) from those that are not. This is illustrated by the similarity of spectra from event 2 and 3 (Table 1, Figure 5). This leads us to conclude that the majority of the detected events are associated with ice loss occurrences.

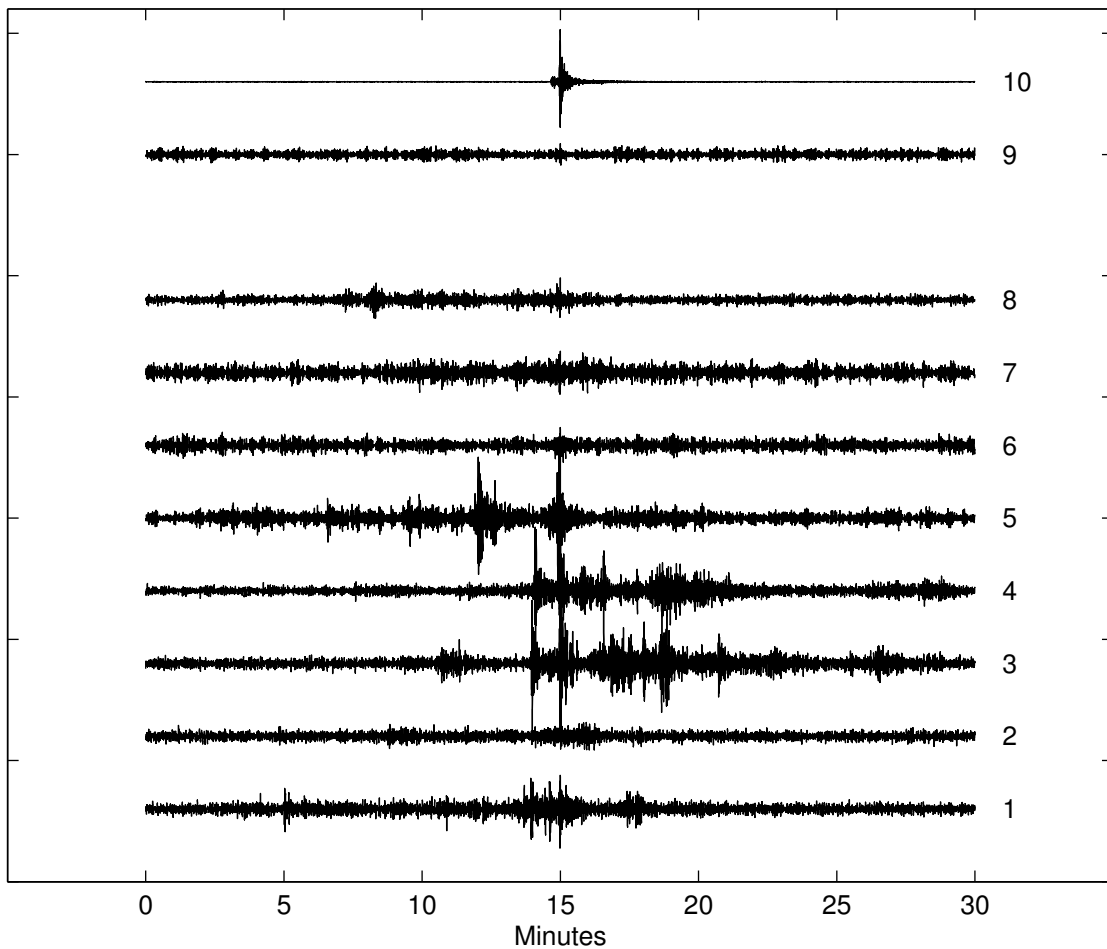


Figure 4: 30 minute segments of the ISO seismic record (filtered at periods 0.5-3 s) centered at maximum amplitude for events derived from teleseismic detections and the time lapse photographic record (numbers corresponding to their appearance in Tables 1 and 2). Trace number 9 and 10 are ambient noise and a local, tectonic event ($M_{4.0}$, $\Delta=0.95$ degrees), respectively. Traces 1-9 are not scaled, i.e., they exhibit true relative amplitude. The tectonic event (trace 10) is scaled down for clarity.

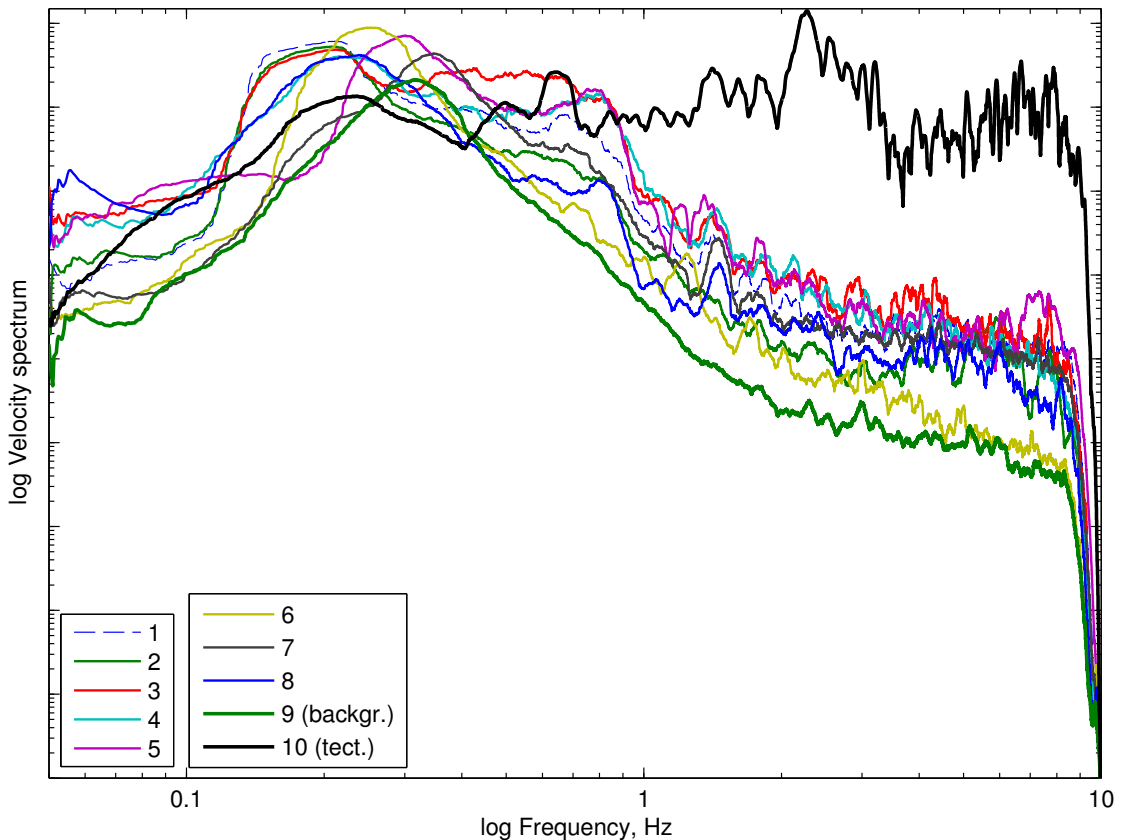


Figure 5: Power spectral densities for the segments shown in Figure 4 with numbers corresponding to numbers in Figure 4. Spectra are smoothed with a running average of length 0.09 Hz for clarity and are not normalized, i.e., they exhibit true relative amplitude. Bold traces are background noise (9, green) and local tectonic event (10, black). The glacial events (1-8) show similar spectral characteristics. The steep roll-off at 10 Hz is caused by the filter used, which has a low-pass cutoff of 10 Hz (the Nyquist frequency).

2.2.1 Frequency domain detection

With this, we develop a frequency-domain based detection algorithm: A 20 min. wide time window is moved over the seismograms in steps of one minute. For each step the power density spectrum is calculated and the power in specific bands is monitored. The width of the window allows it to be fully immersed in a glacial event of the typical length. The sliding-window design of the detector algorithm promotes detection of long-duration events like glacial earthquakes and rumblings, while teleseismic arrivals are not likely to yield a strong, *persistent* detection signal in this frequency band.

2.2.2 Design of the detector

The glacial events as recorded at the ISO station are shown to contain both low and high frequency energy. In order to robustly detect the glacial seismic activity it is therefore necessary to consider the power present in at least two frequency bands for each time step.

We therefore monitor the calculated spectra as the window passes over several select glacial events in the time domain, which enables us to pick the appropriate pass band for detection of glacial seismicity. The left panel in Figure 6 shows the low frequency band with plots of the power spectrum before and after the event (black), and centered on the event (red). It is clear that the glacial event excites different frequencies in the low frequency band than the quiet periods before and after. Especially the band 22-33 seconds (~ 0.03 - 0.05 Hz) is seen to have significant power during the event. Other bands show even clearer rises in amplitude over the event, e.g. 0.54-0.8 Hz (not shown). However, experiments show that the frequencies excited by wind/waves overlap completely with this band, causing the detector to produce many false detections during strong weather events. This is demonstrated in Figure 7 which shows a vertical component velocity seismogram from the ISO station from days 299-303, 2007, filtered from 0.54-0.8 Hz. An automatic weather station (AWS) from the PROMICE monitoring project (www.promice.dk) was in operation on the ice sheet flank close to the ISO seismic station (approximately 11 km from the site, see Figure 1) during this time. The red curve plotted with the seismogram is hourly average wind speeds measured at this AWS. A period of strong winds (hourly averages >20 m/s) is seen to coincide with increased seismicity. Picking a slightly higher frequency pass band minimizes this effect, yet still produces detections when the window passes over events (Figure 6, right panel). Therefore the band 2-2.5 Hz is selected for detection in the high frequency range and periods of 22-66 seconds (0.015 - 0.045 Hz) are chosen for low frequency detection.

For periods of time when the power in both bands is above a pre-calibrated threshold, we log a detection. Figure 8 shows one such case for events 1, 2, and 3 on day 225, 2007 (Table 1, seismogram shown in Figure 3, top panel).

Simultaneous peaks of energy in these two bands is a robust criterion for flagging glacial activity. Other phenomena can cause amplitude in especially the high frequency band, which necessitates monitoring of coincident energy in the lower frequency band. Importantly, this method also discards events carrying power in both bands, but not arising from the glacier, since dispersion will cause a time-shift between the phase arrivals which will therefore not trigger the detector.

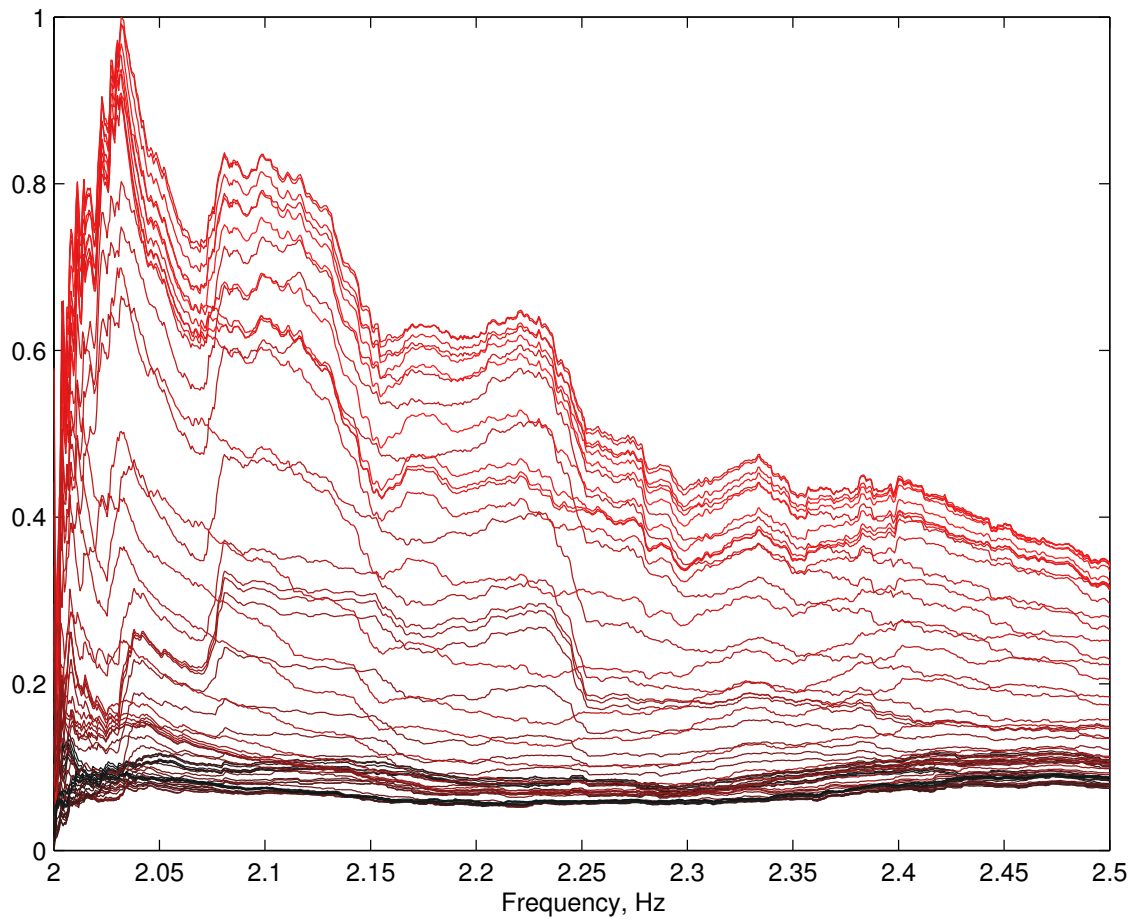


Figure 6: Normalized power spectra of the 20 min. sliding window passing over the teleseismically detected glacial earthquake of day 225 18:42, 2007. The plot shows all spectra in the 2–2.5 Hz band calculated during 62 time steps beginning before and ending after the event. The color ranges from black to red and is a linear function of the distance from the center of the window to the event. Thus, the most red lines indicate the spectra where the 20 min. window is centered on the event. As the window passes over the event increasing power is observed in this band.

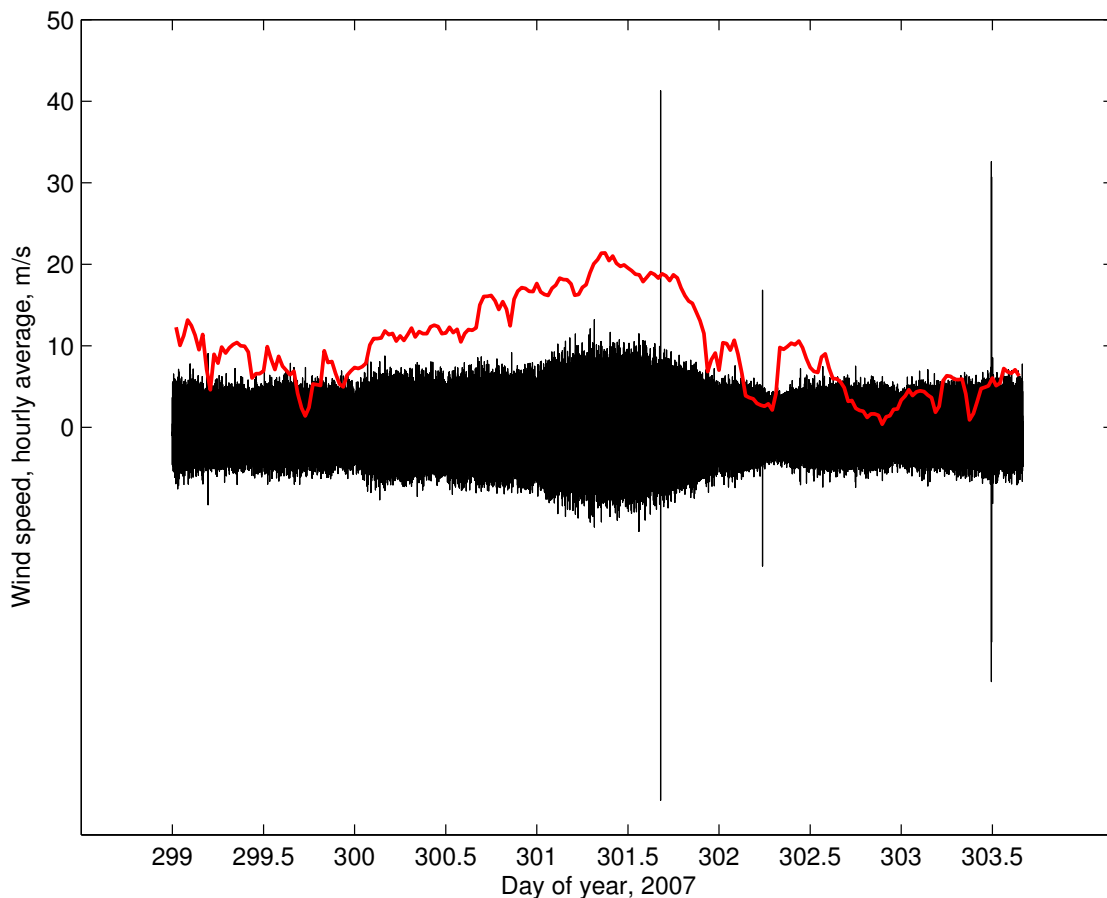


Figure 7: Vertical component velocity seismogram from ISO station for days of year 299-303.5, 2007 (0.54-0.8 Hz) (black), plotted along with wind speed measurements from an automatic weather station (AWS) placed on the ice sheet flank, ~ 11 km from the seismic station (red). AWS data is provided by the PROMICE monitoring project (www.promice.dk).

3 Results

The detector is run for the periods of 2007 and 2008 for which data exists (August 2007 to January 2008 and May 2008 to December 2008). Seven of the eight calving events from the combined list can be found in our detection record, validating the method. The last is categorized as “small calving event” in the observation log and is clear in the detection trace when manually inspected. However, the threshold value for the high frequency energy is not exceeded, causing the detector not to trigger.

In total we detect 626 events for 2007 and 803 events for 2008. This is an average of 4 per day and 3 per day for the two years, respectively. The bar-plot in Figure 9 shows the distribution of events detected per day over the two years. The number of detections per day ranges from zero to 12. We see a decrease in occurrences over the fall months

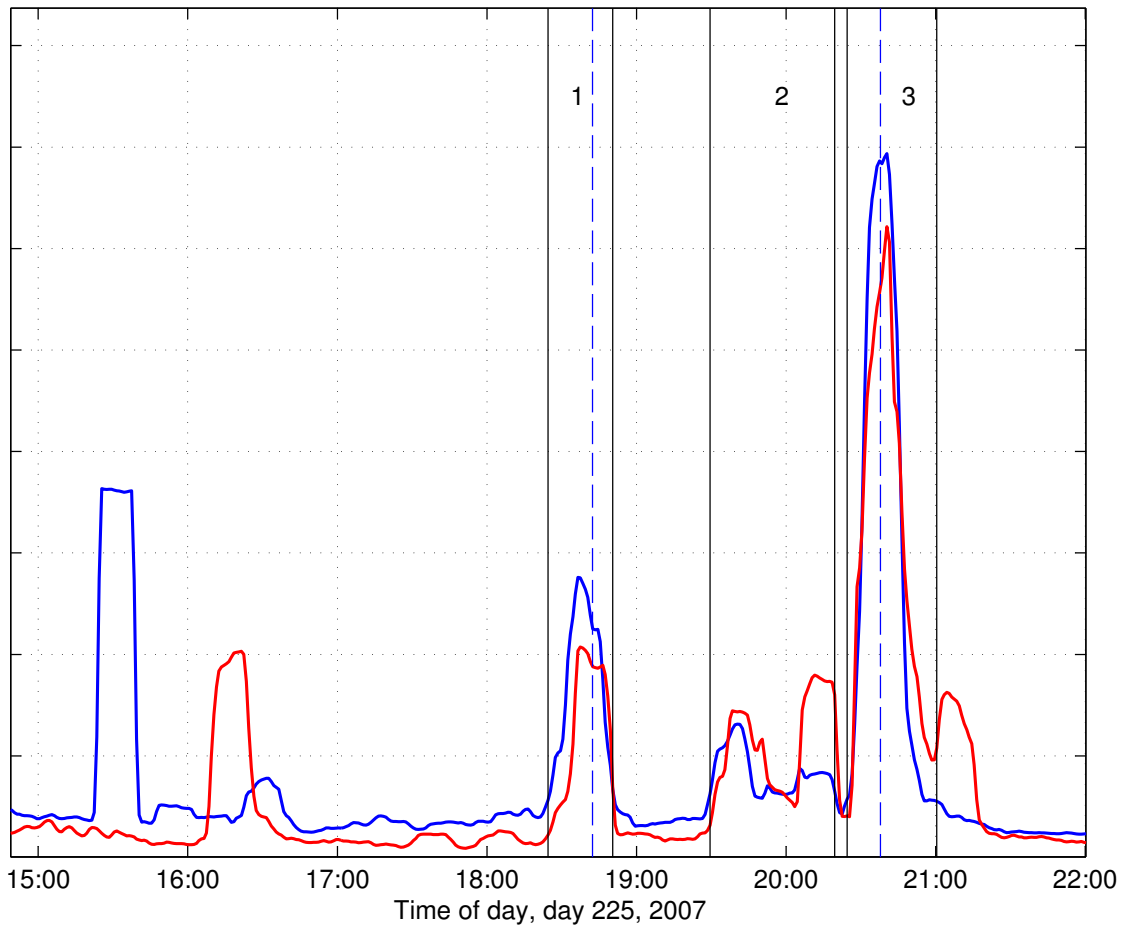


Figure 8: Detector output, day 225, 2007. Red line is low and blue line is high frequency energy, scaled for clarity. Black vertical lines indicate three detections beginnings and endings. Blue dashed lines are teleseismically detected glacial earthquakes. See seismogram in Figure 3.

of 2007. An increase is then evident in the early summer of 2008 and peak activity is reached around mid-September, after which a decrease is again observed, similar to the pattern seen in 2007. The timing of the peaks of activity is similar in both years and coincide with the end of the melt season (mid-September).

We also determine the duration of each detected event. A small number of events each year (<5) last for up to 28 hours, i.e. the full length of the data file. In addition to this, there is a group of 34 events in 2007 and 12 events in 2008, lasting from 8.33 to 19.5 hours. There is no obvious explanation for this and we suspect that the ISO station data during these times is influenced by an unknown cultural source of noise. Focusing on the shorter-duration events, Figure 10 shows the distribution of duration of the detections from zero to 10,000 seconds. Most events have a duration of 12-17 minutes for both years. The distribution rolls off steeply after this peak and at 20-21 minutes duration,

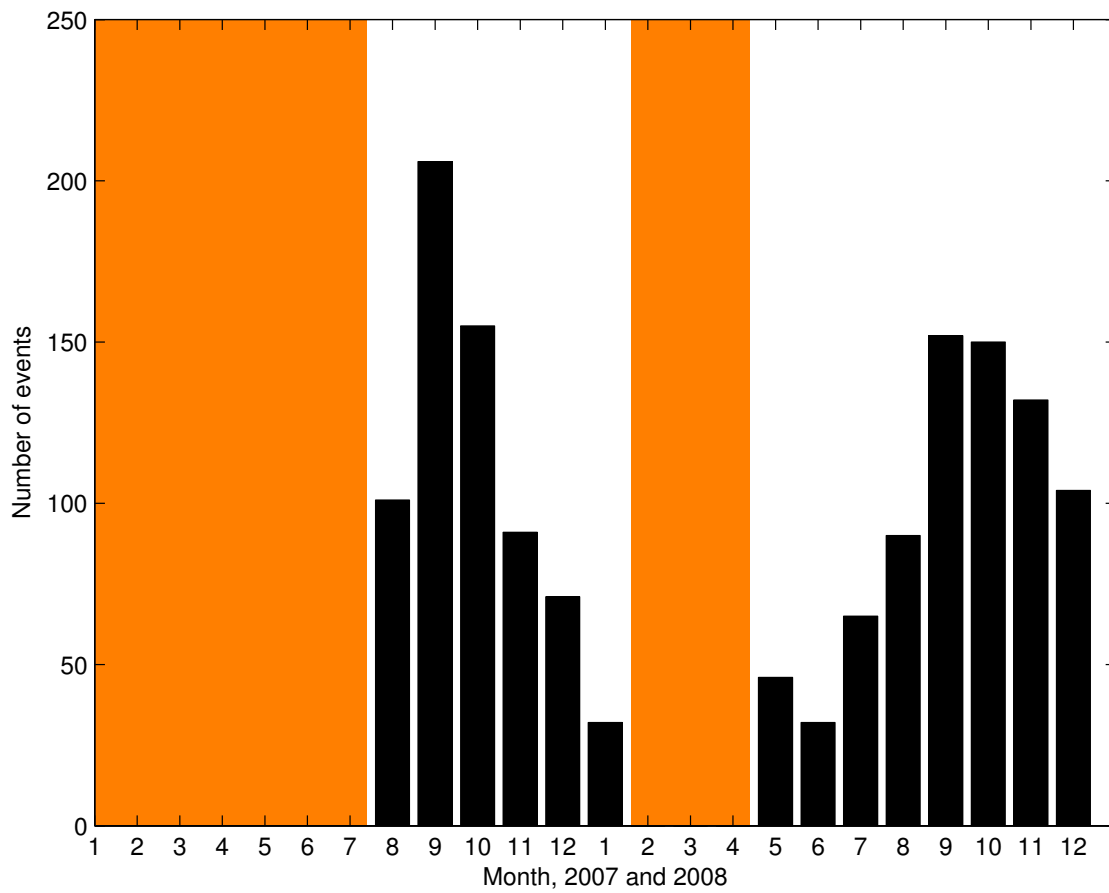


Figure 9: Number of detections per month for the period of detection runs, August 1 2007-January 24 2008 and May 1 to December 31 2008. Orange areas indicate no data.

the number of events is less than one fifth of what is found in the 12-17 minute interval. The average duration of the events up to 10.000 s (shown in Figure 10) is ~ 29 and ~ 28 minutes for 2007 and 2008, respectively.

4 Discussion

Joughin *et al.* (2008) showed a correlation between glacial earthquakes and large-scale ice-loss events from the terminus of Helheim Glacier for the years 2001–2006. The calving activity has not been documented in the same way for 2007 and 2008, but in 2007 5 glacial earthquakes were automatically detected using the method of Ekström (2006) (Nettles *et al.*, 2008). In 2008 the number of detections was three. Therefore, we interpret the drop in seismicity to be associated with a drop in calving activity from 2007 to 2008. Our findings are consistent with this, in that we see 33% more detections per day for 2007 than for 2008 with an average of four and three events per day for 2007 and 2008,

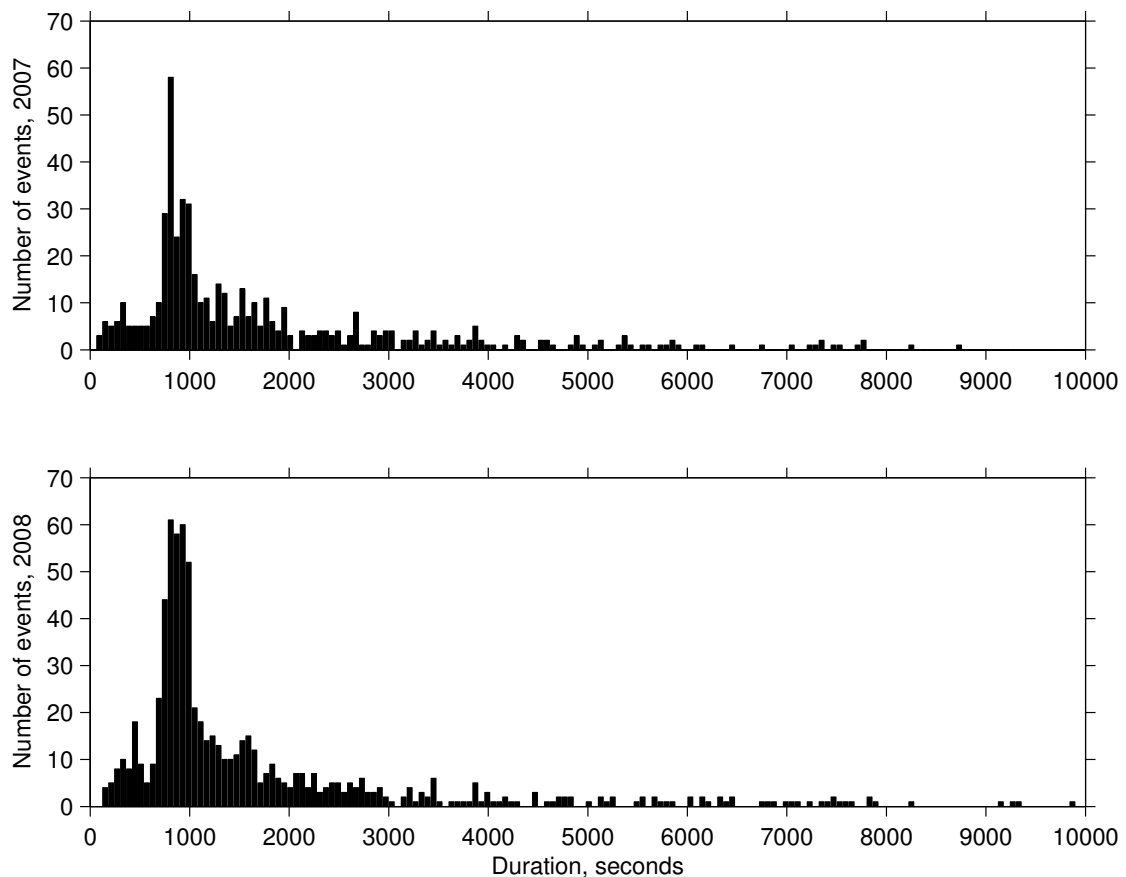


Figure 10: Histogram showing distribution of detected event duration for 2007 (top) and 2008 (bottom)

respectively.

On Jakobshavn Isbræ (West Greenland), *Rial et al.* (2009) detected a lower number of events per day (0.5 events/day) during the summer of 2006. A direct comparison is difficult since that work is based on short period data only, and different detection criteria. *O'Neel et al.* (2007) recorded more than 35 events/hr at Columbia Glacier, Alaska, during certain periods of 2004/2005. These data were recorded with a relatively dense array of instruments located on the walls bordering the glacier which allows for detection of much smaller events than is the case with this work.

Our detected seismic activity exhibits a clear seasonal signal which indicates that there is an influence from the surrounding climate, including potentially the influence from melt water. In this broad sense our findings are consistent with those of *Ekström et al.* (2006), in which monthly average number of events detected all over Greenland are shown to peak in July, August, and September. However, there are more subtle differences: for both years discussed here, the seismic activity we detect peaks near the end of the melt season (mid-September, Figure 9) and not at the peak of the melt season which is in

early August, as described in *Andersen et al.* (2010). This ~ 6 weeks offset is somewhat surprising and indicates that the relationship between climate and co-seismic ice-loss events is not trivial. At Myrdalsjökull Glacier, Iceland, *Jonsdottir et al.* (2009) reported on seismicity in the 1–4 Hz band arising from calving. A strong seasonal signal was observed there, peaking in October and correlating well with records of rain-fall. *Jonsdottir et al.* (2009) suggested the seasonal variability was caused by increased calving flux due to added runoff from rain, enhancing the sliding. In the work of *Rial et al.* (2009), the deployment of instruments covers the summer months only, and a potential variation over the season is thus not investigated.

We see the majority of the events lasting ~ 15 minutes (Figure 10). This is within the same order of magnitude as events detected at Columbia Glacier (*O'Neel et al.*, 2007) and falls within the durations found by *Rial et al.* (2009) at Jakobshavn (10–40 min.). We also notice a number of days in both years with detected, uninterrupted seismic activity for up to ~ 30 hours, which naturally precludes other events from being detected on those days. It is unclear whether this activity is glacially related, but it does exhibit the features that trigger detection of other, confirmed events.

5 Conclusions

We have developed a frequency-domain based detection algorithm for the purpose of detecting seismic signals caused by calving from data recorded ~ 100 km from Helheim Glacier. The detector has been calibrated against a number of calving events observed either through teleseismic detections (2007) or by way of time lapse photography (2008).

The detector was run for the months August 2007 through January 2008 and May through December 2008. We found a clear seasonal signal in the number of detections made with a peak occurring in mid-September (coincident with the end of the melt season) for both years considered. Detection numbers during the winter were low.

The majority of the events had a duration of ~ 15 min., consistent with the lower range of durations found by other workers on Jakobshavn Isbræ, West Greenland.

We notice a drop in seismicity from 2007 to 2008 with 33% more detections per day in 2007 than in 2008. This is consistent with the drop in teleseismically detected events between the two years, which have been shown to coincide with large scale calving events. This is therefore interpreted as indicative of a decrease in ice loss.

Automatic seismic detections of glacial activity might provide a useful and relatively low-cost way of monitoring the ice-loss occurring from the ice sheet through solid mass loss at the marine terminating outlet glaciers.

Bibliography

- Amundson, J. M., M. Truffer, M. P. Luethi, M. Fahnestock, M. West, and R. J. Motyka (2008), Glacier, fjord, and seismic response to recent large calving events, Jakobshavn Isbrae, Greenland, *Geophysical Research Letters*, 35(22), L22501, doi:{10.1029/2008GL035281}.
- Andersen, M. L., T. Larsen, M. Nettles, P. Elosegui, D. van As, G. S. Hamilton, L. A. Stearns, J. L. Davis, A. P. Ahlstrøm, J. de Juan, G. Ekström, L. Stenseng, S. A. Khan, R. Forsberg, and D. Dahl-Jensen (2010), Spatial and temporal melt variability at Helheim Glacier, East Greenland, and its effect on ice dynamics, *Journal of Geophysical Research, Earth Surface* (in press).
- Ekström, G. (2006), Global detection and location of seismic sources by using surface waves, *Bull. Seismol. Soc. Am*, 96, 1201–1212, doi:{10.1785/0120050175}.
- Ekström, G., M. Nettles, and G. Abers (2003), Glacial earthquakes, *Science*, 302, 622–624.
- Ekström, G., M. Nettles, and V. Tsai (2006), Seasonality and Increasing Frequency of Greenland Glacial Earthquakes, *Science*, 311, 1756–1758, doi:{DOI:10.1126/science.1122112}.
- Harben, P. E., and E. Hjortenberget (1993), Variation in microseism power and direction of approach in northeast Greenland, *Bulletin of the Seismological Society of America*, 83(6), 1939–1958, doi:{}.
- Jonsdottir, K., R. Roberts, V. Pohjola, B. Lund, Z. H. Shomali, A. Tryggvason, and R. Boovarsson (2009), Glacial long period seismic events at Katla volcano, Iceland, *Geophysical Research Letters*, 36, doi:{10.1029/2009GL038234}.
- Joughin, I., I. Howat, R. B. Alley, G. Ekstrom, M. Fahnestock, T. Moon, M. Nettles, M. Truffer, and V. C. Tsai (2008), Ice-front variation and tidewater behavior on Helheim and Kangerdlugssuaq Glaciers, Greenland, *Journal of Geophysical Research - Earth Surface*, 113(F1), F01004, doi:10.1029/2007JF000837.
- Kennett, B. L. N., and E. R. Engdahl (1991), Traveltimes for global earthquake location and phase identification, *Geophysical Journal International*, 105(2), 429–465.
- Nettles, M., and G. Ekström (2010), Glacial Earthquakes in Greenland and Antarctica, *Annual Reviews of Earth and Planetary Science*, 38, 467–491, doi:{10.1146/annurev-earth-040809-152414}.
- Nettles, M., T. B. Larsen, P. Elósegui, G. S. Hamilton, L. A. Stearns, A. P. Ahlstrøm, J. L. Davis, M. L. Andersen, J. de Juan, S. A. Khan, L. Stenseng, G. Ekström, and R. Forsberg (2008), Step-wise changes in glacier flow speed coincide with calving and glacial

- earthquakes at Helheim Glacier, Greenland, *Geophysical Research Letters*, 35, L24503, doi:{10.1029/2008GL036127}.
- O'Neel, S., and W. T. Pfeffer (2007), Source mechanisms for monochromatic icequakes produced during iceberg calving at Columbia Glacier, AK, *Geophysical Research Letters*, 34, doi:{doi:10.1029/2007GL031370}.
- O'Neel, S., H. P. Marshall, D. E. McNamara, and W. T. Pfeffer (2007), Seismic detection and analysis of icequakes at Columbia Glacier, Alaska, *Journal of Geophysical Research*, 112, doi:{10.1029/2006JF000595}.
- Rial, J. A., T. C., and S. K (2009), Glacial rumblings from Jakobshavn ice stream, Greenland, *Journal of Glaciology*, 55(191), 389–399, doi:{}.
- Rignot, E., and P. Kanagaratnam (2006), Changes in the velocity structure of the Greenland ice sheet, *Science*, 311(5763), 986–990, doi:{10.1126/science.1121381}.
- Stearns, L. A., and G. S. Hamilton (2007), Rapid volume loss from two East Greenland outlet glaciers quantified using repeat stereo satellite imagery, *Geophysical Research Letters*, 34(5), L05503, doi:{10.1029/2006GL028982}.
- Thomas, R., E. Frederick, W. Krabill, S. Manizade, and C. Martin (2009), Recent changes on Greenland outlet glaciers, *Journal of Glaciology*, 55(189), 147–162.
- Tsai, V. C., and G. Ekstrom (2007), Analysis of glacial earthquakes, *Journal of Geophysical Research - Earth Surface*, 112(F3), doi:{10.1029/2006JF000596}.
- Tsai, V. C., J. R. Rice, and M. Fahnestock (2008), Possible mechanisms for glacial earthquakes, *Journal of Geophysical Research - Earth Surface*, 113(F3), doi:{10.1029/2007JF000944}.
- Van den Broeke, M., J. Bamber, J. Ettema, E. Rignot, E. Schrama, and W. J. van den Berg (2009), Partitioning Recent Greenland Mass Loss, *Science*, 326, 984–986, doi:{}.

Appendices

Appendix A

Co-author statements, Paper I

Co-author statement

**Spatial and temporal melt variability at Helheim
Glacier, East Greenland, and its effect on ice dynamics**

Accepted by Journal of Geophysical Research – Earth Surface, September 2010

M. L. Andersen, T. B. Larsen, M. Nettles, P. Elósegui, D. van As, G. S. Hamilton, L. A. Stearns, J. L. Davis, A. P. Ahlstrøm, J. de Juan, G. Ekström, L. Stenseng, S. A. Khan, R. Forsberg, D. Dahl-Jensen

Co-author names are alphabetically listed in the separate sections below.

Experiment design: **M.L. Andersen**, A. P. Ahlstrøm, J. L. Davis, G. Ekström, P. Elósegui, R. Forsberg, G. S. Hamilton, S. A. Khan, T. B. Larsen, M. Nettles, L. A. Stearns

Collection/analysis of field and observatory data: **M. L. Andersen**, A. P. Ahlstrøm, J. L. Davis, G. Ekström, P. Elósegui, R. Forsberg, G. S. Hamilton, J. de Juan, S. A. Khan, M. Nettles, L. A. Stearns, L. Stenseng

Development of energy balance model and analysis: **M.L. Andersen**, D. van As

Manuscript/revision of manuscript: **M. L. Andersen**, D. Dahl-Jensen, J. L. Davis, G. Ekström, P. Elósegui, G. S. Hamilton, J. de Juan, S. A. Khan, T. B. Larsen, M. Nettles, L. A. Stearns, L. Stenseng, D. van As

M. L. Andersen planned and led the deployment of the automatic weather station, implemented the surface-energy-balance model, conducted the computer analysis of melt/velocity correlations, and wrote and revised the manuscript with input from and discussions with the co-authors.

Name (block letters):

TINE B. LARSEN

Signature:



Co-author statement

**Spatial and temporal melt variability at Helheim
Glacier, East Greenland, and its effect on ice dynamics**

Accepted by Journal of Geophysical Research – Earth Surface, September 2010

M. L. Andersen, T. B. Larsen, M. Nettles, P. Elósegui, D. van As, G. S. Hamilton, L. A. Stearns, J. L. Davis, A. P. Ahlstrøm, J. de Juan, G. Ekström, L. Stenseng, S. A. Khan, R. Forsberg, D. Dahl-Jensen

Co-author names are alphabetically listed in the separate sections below.

Experiment design: **M.L. Andersen**, A. P. Ahlstrøm, J. L. Davis, G. Ekström, P. Elósegui, R. Forsberg, G. S. Hamilton, S. A. Khan, T. B. Larsen, M. Nettles, L. A. Stearns

Collection/analysis of field and observatory data: **M. L. Andersen**, A. P. Ahlstrøm, J. L. Davis, G. Ekström, P. Elósegui, R. Forsberg, G. S. Hamilton, J. de Juan, S. A. Khan, M. Nettles, L. A. Stearns, L. Stenseng

Development of energy balance model and analysis: **M.L. Andersen**, D. van As

Manuscript/revision of manuscript: **M. L. Andersen**, D. Dahl-Jensen, J. L. Davis, G. Ekström, P. Elósegui, G. S. Hamilton, J. de Juan, S. A. Khan, T. B. Larsen, M. Nettles, L. A. Stearns, L. Stenseng, D. van As

M. L. Andersen planned and led the deployment of the automatic weather station, implemented the surface-energy-balance model, conducted the computer analysis of melt/velocity correlations, and wrote and revised the manuscript with input from and discussions with the co-authors.

Name (block letters): MEREDITH NETTLES

Signature: 

Co-author statement

**Spatial and temporal melt variability at Helheim
Glacier, East Greenland, and its effect on ice dynamics**

Accepted by Journal of Geophysical Research – Earth Surface, September 2010

M. L. Andersen, T. B. Larsen, M. Nettles, P. Elósegui, D. van As, G. S. Hamilton, L. A. Stearns, J. L. Davis, A. P. Ahlstrøm, J. de Juan, G. Ekström, L. Stenseng, S. A. Khan, R. Forsberg, D. Dahl-Jensen

Co-author names are alphabetically listed in the separate sections below.

Experiment design: **M.L. Andersen**, A. P. Ahlstrøm, J. L. Davis, G. Ekström, P. Elósegui, R. Forsberg, G. S. Hamilton, S. A. Khan, T. B. Larsen, M. Nettles, L. A. Stearns

Collection/analysis of field and observatory data: **M. L. Andersen**, A. P. Ahlstrøm, J. L. Davis, G. Ekström, P. Elósegui, R. Forsberg, G. S. Hamilton, J. de Juan, S. A. Khan, M. Nettles, L. A. Stearns, L. Stenseng

Development of energy balance model and analysis: **M.L. Andersen**, D. van As

Manuscript/revision of manuscript: **M. L. Andersen**, D. Dahl-Jensen, J. L. Davis, G. Ekström, P. Elósegui, G. S. Hamilton, J. de Juan, S. A. Khan, T. B. Larsen, M. Nettles, L. A. Stearns, L. Stenseng, D. van As

M. L. Andersen planned and led the deployment of the automatic weather station, implemented the surface-energy-balance model, conducted the computer analysis of melt/velocity correlations, and wrote and revised the manuscript with input from and discussions with the co-authors.

Name (block letters): PEDRO ELOSEGUI

Signature:



Co-author statement

**Spatial and temporal melt variability at Helheim
Glacier, East Greenland, and its effect on ice dynamics**

Accepted by Journal of Geophysical Research – Earth Surface, September 2010

M. L. Andersen, T. B. Larsen, M. Nettles, P. Elósegui, D. van As, G. S. Hamilton, L. A. Stearns, J. L. Davis, A. P. Ahlstrøm, J. de Juan, G. Ekström, L. Stenseng, S. A. Khan, R. Forsberg, D. Dahl-Jensen

Co-author names are alphabetically listed in the separate sections below.

Experiment design: **M.L. Andersen**, A. P. Ahlstrøm, J. L. Davis, G. Ekström, P. Elósegui, R. Forsberg, G. S. Hamilton, S. A. Khan, T. B. Larsen, M. Nettles, L. A. Stearns

Collection/analysis of field and observatory data: **M. L. Andersen**, A. P. Ahlstrøm, J. L. Davis, G. Ekström, P. Elósegui, R. Forsberg, G. S. Hamilton, J. de Juan, S. A. Khan, M. Nettles, L. A. Stearns, L. Stenseng

Development of energy balance model and analysis: **M.L. Andersen**, D. van As

Manuscript/revision of manuscript: **M. L. Andersen**, D. Dahl-Jensen, J. L. Davis, G. Ekström, P. Elósegui, G. S. Hamilton, J. de Juan, S. A. Khan, T. B. Larsen, M. Nettles, L. A. Stearns, L. Stenseng, D. van As

M. L. Andersen planned and led the deployment of the automatic weather station, implemented the surface-energy-balance model, conducted the computer analysis of melt/velocity correlations, and wrote and revised the manuscript with input from and discussions with the co-authors.

Name (block letters):

Signature:

A handwritten signature in blue ink, appearing to read 'M. L. Andersen', is written over the signature line.

Co-author statement

**Spatial and temporal melt variability at Helheim
Glacier, East Greenland, and its effect on ice dynamics**

Accepted by Journal of Geophysical Research – Earth Surface, September 2010

M. L. Andersen, T. B. Larsen, M. Nettles, P. Elósegui, D. van As, G. S. Hamilton, L. A. Stearns, J. L. Davis, A. P. Ahlstrøm, J. de Juan, G. Ekström, L. Stenseng, S. A. Khan, R. Forsberg, D. Dahl-Jensen

Co-author names are alphabetically listed in the separate sections below.

Experiment design: **M.L. Andersen**, A. P. Ahlstrøm, J. L. Davis, G. Ekström, P. Elósegui, R. Forsberg, G. S. Hamilton, S. A. Khan, T. B. Larsen, M. Nettles, L. A. Stearns

Collection/analysis of field and observatory data: **M. L. Andersen**, A. P. Ahlstrøm, J. L. Davis, G. Ekström, P. Elósegui, R. Forsberg, G. S. Hamilton, J. de Juan, S. A. Khan, M. Nettles, L. A. Stearns, L. Stenseng

Development of energy balance model and analysis: **M.L. Andersen**, D. van As

Manuscript/revision of manuscript: **M. L. Andersen**, D. Dahl-Jensen, J. L. Davis, G. Ekström, P. Elósegui, G. S. Hamilton, J. de Juan, S. A. Khan, T. B. Larsen, M. Nettles, L. A. Stearns, L. Stenseng, D. van As

M. L. Andersen planned and led the deployment of the automatic weather station, implemented the surface-energy-balance model, conducted the computer analysis of melt/velocity correlations, and wrote and revised the manuscript with input from and discussions with the co-authors.

Name (block letters): **LEIGH A. STEARNS**

Signature: 

Co-author statement

**Spatial and temporal melt variability at Helheim
Glacier, East Greenland, and its effect on ice dynamics**

Accepted by Journal of Geophysical Research – Earth Surface, September 2010

M. L. Andersen, T. B. Larsen, M. Nettles, P. Elósegui, D. van As, G. S. Hamilton, L. A. Stearns, J. L. Davis, A. P. Ahlstrøm, J. de Juan, G. Ekström, L. Stenseng, S. A. Khan, R. Forsberg, D. Dahl-Jensen

Co-author names are alphabetically listed in the separate sections below.

Experiment design: **M.L. Andersen**, A. P. Ahlstrøm, J. L. Davis, G. Ekström, P. Elósegui, R. Forsberg, G. S. Hamilton, S. A. Khan, T. B. Larsen, M. Nettles, L. A. Stearns

Collection/analysis of field and observatory data: **M. L. Andersen**, A. P. Ahlstrøm, J. L. Davis, G. Ekström, P. Elósegui, R. Forsberg, G. S. Hamilton, J. de Juan, S. A. Khan, M. Nettles, L. A. Stearns, L. Stenseng

Development of energy balance model and analysis: **M.L. Andersen**, D. van As

Manuscript/revision of manuscript: **M. L. Andersen**, D. Dahl-Jensen, J. L. Davis, G. Ekström, P. Elósegui, G. S. Hamilton, J. de Juan, S. A. Khan, T. B. Larsen, M. Nettles, L. A. Stearns, L. Stenseng, D. van As

M. L. Andersen planned and led the deployment of the automatic weather station, implemented the surface-energy-balance model, conducted the computer analysis of melt/velocity correlations, and wrote and revised the manuscript with input from and discussions with the co-authors.

Name (block letters): JAMES L. DAVIS

Signature: James L. Davis

Co-author statement

**Spatial and temporal melt variability at Helheim
Glacier, East Greenland, and its effect on ice dynamics**

Accepted by Journal of Geophysical Research – Earth Surface, September 2010

M. L. Andersen, T. B. Larsen, M. Nettles, P. Elósegui, D. van As, G. S. Hamilton, L. A. Stearns, J. L. Davis, A. P. Ahlstrøm, J. de Juan, G. Ekström, L. Stenseng, S. A. Khan, R. Forsberg, D. Dahl-Jensen

Co-author names are alphabetically listed in the separate sections below.

Experiment design: **M.L. Andersen**, A. P. Ahlstrøm, J. L. Davis, G. Ekström, P. Elósegui, R. Forsberg, G. S. Hamilton, S. A. Khan, T. B. Larsen, M. Nettles, L. A. Stearns

Collection/analysis of field and observatory data: **M. L. Andersen**, A. P. Ahlstrøm, J. L. Davis, G. Ekström, P. Elósegui, R. Forsberg, G. S. Hamilton, J. de Juan, S. A. Khan, M. Nettles, L. A. Stearns, L. Stenseng

Development of energy balance model and analysis: **M.L. Andersen**, D. van As

Manuscript/revision of manuscript: **M. L. Andersen**, D. Dahl-Jensen, J. L. Davis, G. Ekström, P. Elósegui, G. S. Hamilton, J. de Juan, S. A. Khan, T. B. Larsen, M. Nettles, L. A. Stearns, L. Stenseng, D. van As

M. L. Andersen planned and led the deployment of the automatic weather station, implemented the surface-energy-balance model, conducted the computer analysis of melt/velocity correlations, and wrote and revised the manuscript with input from and discussions with the co-authors.

Name (block letters): **ANDREAS PETER AHLSTRØM**

Signature:

 30/9-2010

Co-author statement

**Spatial and temporal melt variability at Helheim
Glacier, East Greenland, and its effect on ice dynamics**

Accepted by Journal of Geophysical Research – Earth Surface, September 2010

M. L. Andersen, T. B. Larsen, M. Nettles, P. Elósegui, D. van As, G. S. Hamilton, L. A. Stearns, J. L. Davis, A. P. Ahlstrøm, J. de Juan, G. Ekström, L. Stenseng, S. A. Khan, R. Forsberg, D. Dahl-Jensen

Co-author names are alphabetically listed in the separate sections below.

Experiment design: **M.L. Andersen**, A. P. Ahlstrøm, J. L. Davis, G. Ekström, P. Elósegui, R. Forsberg, G. S. Hamilton, S. A. Khan, T. B. Larsen, M. Nettles, L. A. Stearns

Collection/analysis of field and observatory data: **M. L. Andersen**, A. P. Ahlstrøm, J. L. Davis, G. Ekström, P. Elósegui, R. Forsberg, G. S. Hamilton, J. de Juan, S. A. Khan, M. Nettles, L. A. Stearns, L. Stenseng

Development of energy balance model and analysis: **M.L. Andersen**, D. van As

Manuscript/revision of manuscript: **M. L. Andersen**, D. Dahl-Jensen, J. L. Davis, G. Ekström, P. Elósegui, G. S. Hamilton, J. de Juan, S. A. Khan, T. B. Larsen, M. Nettles, L. A. Stearns, L. Stenseng, D. van As

M. L. Andersen planned and led the deployment of the automatic weather station, implemented the surface-energy-balance model, conducted the computer analysis of melt/velocity correlations, and wrote and revised the manuscript with input from and discussions with the co-authors.

Name (block letters): JULIA DE JUAN

Signature:



Co-author statement

**Spatial and temporal melt variability at Helheim
Glacier, East Greenland, and its effect on ice dynamics**

Accepted by Journal of Geophysical Research – Earth Surface, September 2010

M. L. Andersen, T. B. Larsen, M. Nettles, P. Elósegui, D. van As, G. S. Hamilton, L. A. Stearns, J. L. Davis, A. P. Ahlstrøm, J. de Juan, G. Ekström, L. Stenseng, S. A. Khan, R. Forsberg, D. Dahl-Jensen

Co-author names are alphabetically listed in the separate sections below.

Experiment design: **M.L. Andersen**, A. P. Ahlstrøm, J. L. Davis, G. Ekström, P. Elósegui, R. Forsberg, G. S. Hamilton, S. A. Khan, T. B. Larsen, M. Nettles, L. A. Stearns

Collection/analysis of field and observatory data: **M. L. Andersen**, A. P. Ahlstrøm, J. L. Davis, G. Ekström, P. Elósegui, R. Forsberg, G. S. Hamilton, J. de Juan, S. A. Khan, M. Nettles, L. A. Stearns, L. Stenseng

Development of energy balance model and analysis: **M.L. Andersen**, D. van As

Manuscript/revision of manuscript: **M. L. Andersen**, D. Dahl-Jensen, J. L. Davis, G. Ekström, P. Elósegui, G. S. Hamilton, J. de Juan, S. A. Khan, T. B. Larsen, M. Nettles, L. A. Stearns, L. Stenseng, D. van As

M. L. Andersen planned and led the deployment of the automatic weather station, implemented the surface-energy-balance model, conducted the computer analysis of melt/velocity correlations, and wrote and revised the manuscript with input from and discussions with the co-authors.

Name (block letters): **GÖRAN EKSTRÖM**

Signature: 

Co-author statement

**Spatial and temporal melt variability at Helheim
Glacier, East Greenland, and its effect on ice dynamics**

Accepted by Journal of Geophysical Research – Earth Surface, September 2010

M. L. Andersen, T. B. Larsen, M. Nettles, P. Elósegui, D. van As, G. S. Hamilton, L. A. Stearns, J. L. Davis, A. P. Ahlstrøm, J. de Juan, G. Ekström, L. Stenseng, S. A. Khan, R. Forsberg, D. Dahl-Jensen

Co-author names are alphabetically listed in the separate sections below.

Experiment design: **M.L. Andersen**, A. P. Ahlstrøm, J. L. Davis, G. Ekström, P. Elósegui, R. Forsberg, G. S. Hamilton, S. A. Khan, T. B. Larsen, M. Nettles, L. A. Stearns

Collection/analysis of field and observatory data: **M. L. Andersen**, A. P. Ahlstrøm, J. L. Davis, G. Ekström, P. Elósegui, R. Forsberg, G. S. Hamilton, J. de Juan, S. A. Khan, M. Nettles, L. A. Stearns, L. Stenseng

Development of energy balance model and analysis: **M.L. Andersen**, D. van As

Manuscript/revision of manuscript: **M. L. Andersen**, D. Dahl-Jensen, J. L. Davis, G. Ekström, P. Elósegui, G. S. Hamilton, J. de Juan, S. A. Khan, T. B. Larsen, M. Nettles, L. A. Stearns, L. Stenseng, D. van As

M. L. Andersen planned and led the deployment of the automatic weather station, implemented the surface-energy-balance model, conducted the computer analysis of melt/velocity correlations, and wrote and revised the manuscript with input from and discussions with the co-authors.

Name (block letters):

Lars Stenseng

Signature:



Co-author statement

**Spatial and temporal melt variability at Helheim
Glacier, East Greenland, and its effect on ice dynamics**

Accepted by Journal of Geophysical Research – Earth Surface, September 2010

M. L. Andersen, T. B. Larsen, M. Nettles, P. Elósegui, D. van As, G. S. Hamilton, L. A. Stearns, J. L. Davis, A. P. Ahlstrøm, J. de Juan, G. Ekström, L. Stenseng, S. A. Khan, R. Forsberg, D. Dahl-Jensen

Co-author names are alphabetically listed in the separate sections below.

Experiment design: **M.L. Andersen**, A. P. Ahlstrøm, J. L. Davis, G. Ekström, P. Elósegui, R. Forsberg, G. S. Hamilton, S. A. Khan, T. B. Larsen, M. Nettles, L. A. Stearns

Collection/analysis of field and observatory data: **M. L. Andersen**, A. P. Ahlstrøm, J. L. Davis, G. Ekström, P. Elósegui, R. Forsberg, G. S. Hamilton, J. de Juan, S. A. Khan, M. Nettles, L. A. Stearns, L. Stenseng

Development of energy balance model and analysis: **M.L. Andersen**, D. van As

Manuscript/revision of manuscript: **M. L. Andersen**, D. Dahl-Jensen, J. L. Davis, G. Ekström, P. Elósegui, G. S. Hamilton, J. de Juan, S. A. Khan, T. B. Larsen, M. Nettles, L. A. Stearns, L. Stenseng, D. van As

M. L. Andersen planned and led the deployment of the automatic weather station, implemented the surface-energy-balance model, conducted the computer analysis of melt/velocity correlations, and wrote and revised the manuscript with input from and discussions with the co-authors.

Name (block letters):

SHFAQAT ABBAS KHAN

Signature:



Co-author statement

**Spatial and temporal melt variability at Helheim
Glacier, East Greenland, and its effect on ice dynamics**

Accepted by Journal of Geophysical Research – Earth Surface, September 2010

M. L. Andersen, T. B. Larsen, M. Nettles, P. Elósegui, D. van As, G. S. Hamilton, L. A. Stearns, J. L. Davis, A. P. Ahlstrøm, J. de Juan, G. Ekström, L. Stenseng, S. A. Khan, R. Forsberg, D. Dahl-Jensen

Co-author names are alphabetically listed in the separate sections below.

Experiment design: **M.L. Andersen**, A. P. Ahlstrøm, J. L. Davis, G. Ekström, P. Elósegui, R. Forsberg, G. S. Hamilton, S. A. Khan, T. B. Larsen, M. Nettles, L. A. Stearns


Collection/analysis of field and observatory data: **M. L. Andersen**, A. P. Ahlstrøm, J. L. Davis, G. Ekström, P. Elósegui, R. Forsberg, G. S. Hamilton, J. de Juan, S. A. Khan, M. Nettles, L. A. Stearns, L. Stenseng

Development of energy balance model and analysis: **M.L. Andersen**, D. van As

Manuscript/revision of manuscript: **M. L. Andersen**, D. Dahl-Jensen, J. L. Davis, G. Ekström, P. Elósegui, G. S. Hamilton, J. de Juan, S. A. Khan, T. B. Larsen, M. Nettles, L. A. Stearns, L. Stenseng, D. van As

M. L. Andersen planned and led the deployment of the automatic weather station, implemented the surface-energy-balance model, conducted the computer analysis of melt/velocity correlations, and wrote and revised the manuscript with input from and discussions with the co-authors.

Name (block letters): **DORTHE DAHL-JENSEN**

Signature: 

Appendix B

Co-author statements, Paper II

Co-author statement

Quantifying the influence of melt-water on velocity variations at a large Greenland outlet glacier

Submitted to Journal of Glaciology, September 2010

M. L. Andersen, M. Nettles, P. Elósegui, T. B. Larsen, G. S. Hamilton, L. A. Stearns

Co-author names are alphabetically listed in the separate sections below.

Experiment design: **M. L. Andersen**, M. Nettles

Collection/analysis of field and observatory data: **M. L. Andersen**, P. Elósegui, G. S. Hamilton, M. Nettles, L. A. Stearns

Manuscript/revision of manuscript: **M. L. Andersen**, P. Elósegui, G. S. Hamilton, T. B. Larsen, M. Nettles, L. A. Stearns

M. L. Andersen conducted the computer analysis of melt/velocity variability, and wrote and revised the manuscript with input from and discussions with the co-authors.

Name (block letters): MEREDITH NETTLES

Signature:



Co-author statement

Quantifying the influence of melt-water on velocity variations at a large Greenland outlet glacier

Submitted to Journal of Glaciology, September 2010

M. L. Andersen, M. Nettles, P. Elósegui, T. B. Larsen, G. S. Hamilton, L. A. Stearns

Co-author names are alphabetically listed in the separate sections below.

Experiment design: **M. L. Andersen**, M. Nettles

Collection/analysis of field and observatory data: **M. L. Andersen**, P. Elósegui, G. S. Hamilton, M. Nettles, L. A. Stearns

Manuscript/revision of manuscript: **M. L. Andersen**, P. Elósegui, G. S. Hamilton, T. B. Larsen, M. Nettles, L. A. Stearns

M. L. Andersen conducted the computer analysis of melt/velocity variability, and wrote and revised the manuscript with input from and discussions with the co-authors.

Name (block letters): PEDRO ELOSEGUI

Signature:

A handwritten signature in black ink, appearing to read 'Pedro Elósegui', with a horizontal line at the end.

Co-author statement

Quantifying the influence of melt-water on velocity variations at a large Greenland outlet glacier

Submitted to Journal of Glaciology, September 2010

M. L. Andersen, M. Nettles, P. Elósegui, T. B. Larsen, G. S. Hamilton, L. A. Stearns

Co-author names are alphabetically listed in the separate sections below.

Experiment design: **M. L. Andersen**, M. Nettles

Collection/analysis of field and observatory data: **M. L. Andersen**, P. Elósegui, G. S. Hamilton, M. Nettles, L. A. Stearns

Manuscript/revision of manuscript: **M. L. Andersen**, P. Elósegui, G. S. Hamilton, T. B. Larsen, M. Nettles, L. A. Stearns

M. L. Andersen conducted the computer analysis of melt/velocity variability, and wrote and revised the manuscript with input from and discussions with the co-authors.

Name (block letters): **TINE B. LARSEN**

Signature: 

Co-author statement

Quantifying the influence of melt-water on velocity variations at a large Greenland outlet glacier

Submitted to Journal of Glaciology, September 2010

M. L. Andersen, M. Nettles, P. Elósegui, T. B. Larsen, G. S. Hamilton, L. A. Stearns

Co-author names are alphabetically listed in the separate sections below.

Experiment design: **M. L. Andersen**, M. Nettles

Collection/analysis of field and observatory data: **M. L. Andersen**, P. Elósegui, G. S. Hamilton, M. Nettles, L. A. Stearns

Manuscript/revision of manuscript: **M. L. Andersen**, P. Elósegui, G. S. Hamilton, T. B. Larsen, M. Nettles, L. A. Stearns

M. L. Andersen conducted the computer analysis of melt/velocity variability, and wrote and revised the manuscript with input from and discussions with the co-authors.

Name (block letters): **Leigh A. Stearns**

Signature:

A handwritten signature in black ink that reads "Leigh A. Stearns". The signature is written in a cursive style with a large, prominent 'L' and 'S'.

Co-author statement

Quantifying the influence of melt-water on velocity variations at a large Greenland outlet glacier

Submitted to Journal of Glaciology, September 2010

M. L. Andersen, M. Nettles, P. Elósegui, T. B. Larsen, G. S. Hamilton, L. A. Stearns

Co-author names are alphabetically listed in the separate sections below.

Experiment design: **M. L. Andersen**, M. Nettles

Collection/analysis of field and observatory data: **M. L. Andersen**, P. Elósegui, G. S. Hamilton, M. Nettles, L. A. Stearns

Manuscript/revision of manuscript: **M. L. Andersen**, P. Elósegui, G. S. Hamilton, T. B. Larsen, M. Nettles, L. A. Stearns

M. L. Andersen conducted the computer analysis of melt/velocity variability, and wrote and revised the manuscript with input from and discussions with the co-authors.

Name (block letters):

Signature:



Appendix C

Co-author statements, Paper III

Co-author statement

Detection and spectral characterization of calving related seismic signals, Helheim Glacier, South East Greenland

In preparation, September 2010

Morten L. Andersen, T. B. Larsen, M. Nettles

Co-author names are alphabetically listed in the separate sections below.

Experiment design: **M. L. Andersen**, T. B. Larsen


Collection/analysis of field and observatory data: **M. L. Andersen**, M. Nettles

Analysis: **M. L. Andersen**

Manuscript/revision of manuscript: **Morten L. Andersen**, T. B. Larsen, M. Nettles

M. L. Andersen devised and implemented the detection algorithm, and wrote and revised the manuscript with input from and discussions with the co-authors.

Name (block letters): **TINE B. LARSEN**

Signature: 

Co-author statement

Detection and spectral characterization of calving related seismic signals, Helheim Glacier, South East Greenland

In preparation, September 2010

Morten L. Andersen, T. B. Larsen, M. Nettles

Co-author names are alphabetically listed in the separate sections below.

Experiment design: **M. L. Andersen**, T. B. Larsen, M. Nettles

Collection/analysis of field and observatory data: **M. L. Andersen**, M. Nettles

Analysis: **M. L. Andersen**

Manuscript/revision of manuscript: **Morten L. Andersen**, T. B. Larsen, M. Nettles

M. L. Andersen devised and implemented the detection algorithm, and wrote and revised the manuscript with input from and discussions with the co-authors.

Name (block letters): **Meredith Nettles**

Signature: 